IMPROVEMENT OF CORONA-PREIONIZED TEA-CO_2 LASER AND APPLICATION TO NON-DESTRUCTIVE AND REMOTE INSPECTION

Keiji Nakamura

(1)

IMPROVEMENT OF CORONA-PREIONIZED TEA-CO_2 LASER AND APPLICATION TO NON-DESTRUCTIVE AND REMOTE INSPECTION

Keiji Nakamura

CONTENTS

CHAPTER 1 INTRODUCTION

1-1. Features and Roles of Pulsed CO_2 Lasers

Since Mainmann succeeded in the oscillation of a ruby laser in 1960[1-1], the various lasers have been developed as an ideal optical source with an excellent spatiotemporal coherency, as shown in Fig.1-1. Even now, the various investigations from many approaches have been carried out vigorously to get a more high-performance and compact laser device.

The first laser action of CO_2 molecules was demonstrated by Patel in 1964[1-2], and the first laser had the continuous output power of only a few milli-watts. Nowadays continuous lasers are built with output powers of more than 20kW[1-3]. For pulsed systems, it started in 1968 with a few joules[1-4]. These developments, especially stimulated by the big laser-fusion projects, have led to huge systems in the range of 100kJ. The technologies for not only the big output power but also the output control, which is stability, beam divergence, mode structure, pulse shape, spectral purity etc., were investigated.

A CO_2 laser has the following features generally:

(1)An optical large energy is obtained with a comparatively simple device.

(2)An electrical energy is conversed into an optical energy with

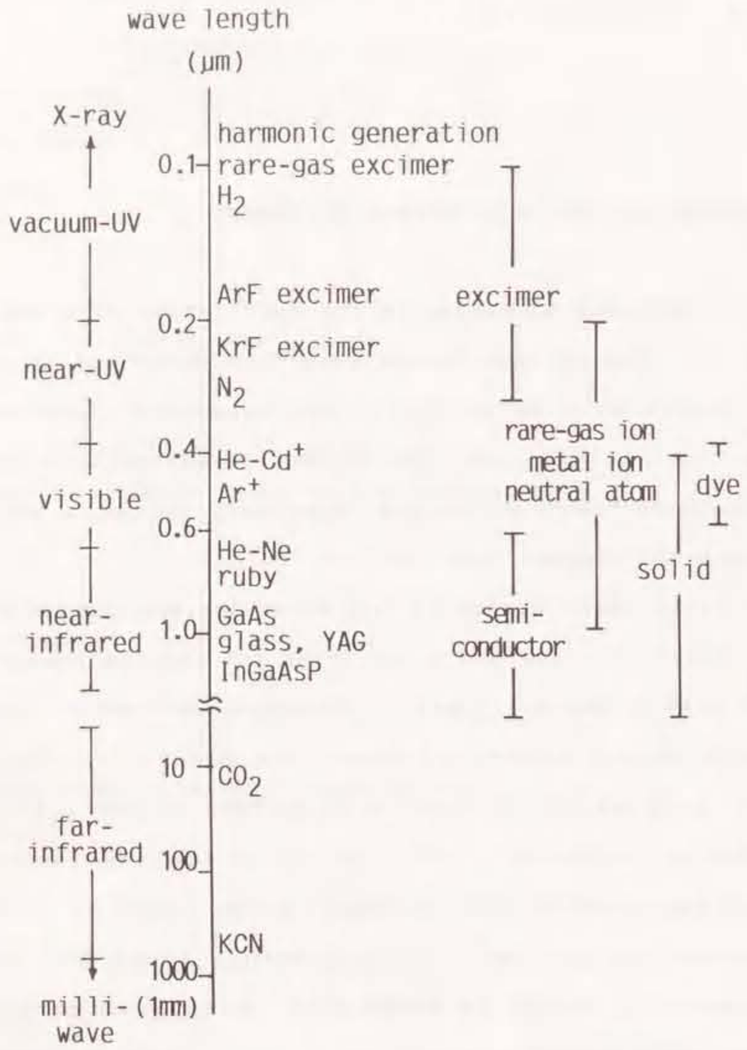

Fig.1-1.Oscillation wavelength of various lasers.

the high efficiency of 10～ 20%.

(3)The propagation loss in air due to absorption is small because the wavelength of the laser beam 10.6μm is within the optical window of atmosphere.

(4)The cost on investment and maintenance is relatively cheap.

The attentions of many researchers and engineers have been focussed on the above high potentialities, particularly much higher efficiency than other laser systems, and CO_2 lasers have been applied to various fields as optical and thermal sources.

The large energy and the high efficiency of pulsed CO_2 lasers have been very attractive for nuclear fusion[1-5], and the biggest CO_2 laser system known as "ANTARES" was built in 1983 at Los Alamos Laboratory. A small pellet with a few tenths of a millimeter is irradiated with an energy pulse of 100kJ. In Japan, the CO_2 laser system in the range of 10kJ was also built at Osaka University. However, the laser beam with a short wavelength is advantageous for laser fusion because both the absorption coefficient and the cut-off density of the laser-produced plasma are increased with the decrease of the wavelength. Therefore Nd glass lasers and excimer lasers have been also developed as a fusion driver, and it will be concluded in future which laser system is the most suitable.

A pulsed CO_2 laser is also useful for fusion plasma diagnostics, too[1-6][1-7]. The CO_2 laser is applied to an optical source of the interferometer or to an optical pumping source of far-infrared lasers using CH_3OH, HCN, CH_3I etc.. The electron line density of $10^{13-14}cm^{-2}$ can be precisely measured in

these systems. Further, ion temperature and electron density fluctuation etc. can be also measured using laser scattering techniques.

Another useful application of a pulsed CO_2 laser is in the field of isotope separation. There are the successful reports of the isotope separation for B, C, S and others with the irradiation of CO_2 laser beam, while the uranium concentration has recently attracted special interest[1-8]. The molecules of UF_6 have the absorption spectrum with the enough isotope shift in the range of 16μm , so a intensive tunable laser in the 16μm band is necessary to concentrate $^{235}UF_6$. A para-hydrogen Raman laser pumped by CO_2 laser beam satisfies such a demand. It has been reported that the maximum conversion efficiency of the CO_2 laser beam reaches 80% for the Raman laser[1-9].

Moreover, a pulsed CO_2 laser has been applied to the field of material processing, especially to marking. The laser processing has advantages of the superior control of the beam power, the absence of mechanical contact with the work piece, and the sharp focusing of the laser beam in the interesting region. The applied energy is restricted in such a small point that undesired deformation or decomposition of material can be avoided. Ablation, melting of thin metal layers, and vaporization without thermal effect for the material are possible. The 10μm wavelength of the CO_2 laser is better absorbed and preferable to the near-infrared radiation of the solid-state lasers, i.e. YAG laser(λ =1.06μm).

1-2. Lasing Process of CO_2 Laser

The CO_2 molecule is a linear symmetric molecule with an axis of symmetry along the nuclei and a plane of symmetry perpendicular to this axis. As shown in Fig.1-2(a), the CO_2 molecule has the vibrational motions v_1, v_2 and v_3 which represent the symmetric stretch mode, the bending mode and asymmetric stretch mode, respectively. The quantum numbers of those modes are presented by n_1, n_2 and n_3, respectively. In the vibration v_1, the C atom remains stationary, and the vibrations v_2 and v_3 have the property in common that during the motion the distance between the O atoms remains unchanged. In the case where the vibrational motion is only described by unperturbed harmonic oscillator, these vibrations are associated with different wave numbers ω_1, ω_2 and ω_3 and the vibrational state is indicated with the symbol (n_1 n_2 n_3):

ω_1=1351.2cm^{-1}, ω_2=672.2cm^{-1}, ω_3=2396.4cm^{-1}

Figure 1-2(b) shows the schematic diagram of the pertinent vibrational levels of the CO_2 molecule. The life time, about 10μs, of the (001) state as the upper laser level is much longer than that of the (020) or (100) states as the lower laser levels, a few hundred nano-seconds. Therefore a discharge excitation of the CO_2 molecule results in the production of the population

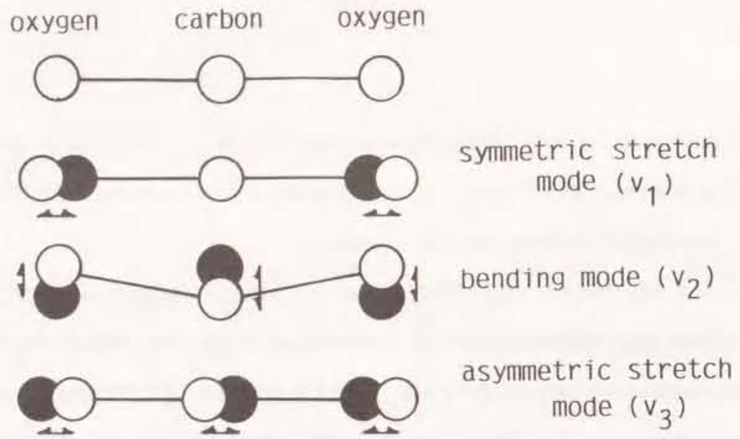

(a)

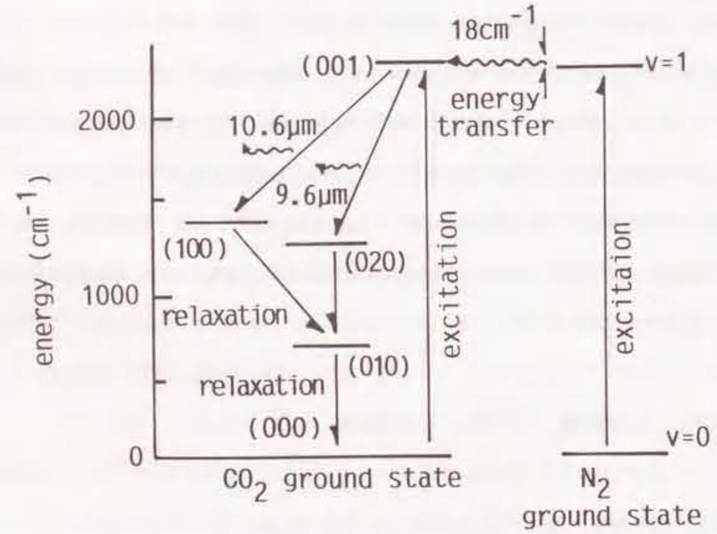

(b) (c)

Fig.1-2.(a)The upper figure shows the vibrational motion of CO_2 molecule. The lower figures show the pertinent vibrational levels of (b)CO_2 and (c)N_2.

inversion between the upper level (001) and the lower levels (020) and (100), and the stimulated emission occurs on one or more lines between vibrational levels.

1-3. High-Power and Efficient Operation of CO_2 Laser

For discharge-pumped CO_2 lasers, the various techniques lead to the large energy extraction and the efficient lasing. The countermeasures for high-power and efficient laser operations are as follows.

(1)Production of population inversion in a great degree

The population inversion is produced in a great degree by the selective excitation to the upper level (001) and by the fast relaxations of the lower levels (020) and (100).

a)Adjustment of the reduced electric field E/P in discharge volume

The excitation cross-section of the upper level (001) due to the electron collision has a maximum value when the electrons have the energy of about 1eV. The calculated results of the electron distribution function[1-10] indicate that the reduced field E/P of 6~ 7V/cm/torr is optimum to produce such electrons.

b)Increase of laser gas pressure

The increase of the partial pressure of CO_2 results in

the increase of the density of the radiation media. Further both the excitation to the upper level and the relaxation of the lower level due to the molecular collision are expected to increase with the total pressure of the laser gas.

c)Addition of some other gases of N_2, Xe, He etc. to CO_2 gas

An electric discharge in nitrogen leads to a very effective formation of vibrationally excited N_2 molecules up to 50% of all N_2 molecules[1-11]. The (001) level of CO_2 is only $\Delta E \fallingdotseq 18cm^{-1}$ higher than the vibrational level $v=1$ of N_2 as shown in Figs.1-2(b) and (c). In the presence of CO_2, the vibrational energy of N_2 is easily transferred to the (001) level of CO_2 because of the close resonance between the N_2 vibration and the vibration v_3 of CO_2, and the number of the CO_2 molecules excited to the upper level is increased.

The addition of Xe of a low concentration results in the increase of the laser output mainly due to the change of the electron energy distribution[1-12]-[1-14]. The number of electrons with energy of lower than 4eV is increased whereas the number of those with larger energies is decreased[1-14]. This change of the electron energy distribution has a favorable effect on the vibrational excitation of CO_2 and N_2.

The addition of He is effective for the cooling of the laser gas as well as the relaxation of the lower level. The thermal conductivity of He is about six times as large as that of CO_2 and N_2, therefore the rise of the laser gas temperature is suppressed. Because the more relaxation

effect for the lower laser level is obtained by He than by CO_2 or N_2[1-15], the addition of He also leads to the decrease of the molecular density of the lower laser level. Further, He has a favorable influence that the gas discharge become more homogeneous, especially for high-pressure pulsed laser systems.

(2)Suppression of glow-to-arc transition

The diffusible discharge such as a glow discharge is desirable to excite the CO_2 molecules in the discharge volume homogeneously. However, under the condition of the excess of a certain critical value for the input energy in the discharge volume, the glow discharge changes to an arc discharge during the main discharge, where the discharge current passes at one special point on the electrodes. This phenomenon is well known as a glow-to-arc transition. The occurrence of a glow-to-arc transition leads to the decrease in the laser output because of the rapid reduction of E/P and the rise of the gas temperature near the arc discharge channel. The following various techniques to suppress the glow-to-arc transition have been reported.

a)Design of electrode surface.

The uniformity of the electric field on the surface of the electrode is necessary to make a homogeneous glow discharge all over the surface of the electrodes as well as to suppress the glow-to-arc transition. For pulsed laser systems, although Rogowski profile has been used, the more uniform field can be obtained using the profiles proposed by

Chang[1-16] and Ernst[1-17].

b)Circulation of laser gas with disturbance by turbulent flow

The discharge products cause the glow-to-arc transition during the main discharge. Therefore the laser gas is circulated to remove the discharge products from the discharge area as well as to cool the gas through heat exchanger. The discharge is stabilized by aerodynamic turbulences in the gas flow to disturb the gas layer stayed near the wall, and the effective gas cooling is possible.

c)Preionization of discharge volume to supply many primary electrons.

Prior to the main discharge, the primary electrons are sufficiently produced in the discharge volume to suppress the glow-to-arc transition due to the inhomogeneous propagation of an individual electron avalanche.

d)Mixture of fractional additives with low ionization energy.

When a fractional gas with a low ionization energy is added to the laser gas, the preionization effect is more intensified and the discharge plasma becomes more conductive.

(3)Production of glow discharge with large volume.

A large volume of glow discharge using a long laser tube with a large diameter leads to the increase in the laser output energy in proportion to the active volume.

(4)Efficient injection of stored energy into discharge volume

The energy in the storage capacitor is efficiently injected into the discharge volume using the excitation circuit with PFN (Pulse Forming Network) or PFL (Pulse Forming Line) to make a impedance matching between the excitation circuit and the discharge plasma.

1-4. Development of Device Technology for Pulsed CO_2 Laser

In early reseaches, a modest laser pulse with the order of only a few killo-watts was generated by a pulse discharge excitation using an ordinary CW laser device[1-18]-[1-20]. In addition, Hill[1-4] achieved the output energy of 5J with a peak power of 200kW using large-scaled devices such as a 8-ft discharge tube and a transformer in the ranges of 200kV to 1MV. Thus the increases of the discharge tube length and the total gas pressure result in the increase of the energy extraction, whereas a high voltage power source is necessary using an axial discharge excitation.

Beaulieu proposed the transverse discharge excitation perpendicular to the laser axis using a relatively low voltage, and the homogeneous glow discharge was obtained at an atmospheric pressure[1-21]. This type of device has been called as a TEA laser. The anode of a plane electrode was separated by 2.5cm from the cathode of needle electrodes with ballast resistors. The laser output energy of 150mJ was obtained with the efficiency of

2.5%. Substituting capacitances for ballast resisters, the maximum laser output energy of 1.2J was also obtained with the efficiency of 6%[1-22]. Such a device has a disadvantage that the rise time of the discharge current is increased with the inductance around the discharge circuit due to the stabilizers of ballast resistors or capacitances. Therefore, when the glow discharge with a short duration was obtained without the stabilizer by reducing the inductance around the main discharge circuit, the efficiency of 15% was achieved[1-23].

On the other hand, Dumanchin et al. examined the new technique of preionizing the discharge volume prior to main discharge, and it was shown that the preionization is effective to make a glow discharge in a large volume compared with the above techniques[1-24][1-25]. Since then, the various preionizing sources have been developed such as corona discharge, spark discharge, electron beam and X-ray radiation.

(1)Corona preionization

The corona preionization is preferable for a sealed-off laser device because the energy for the preionization is so small that the laser gas is not very degraded due to few impurities produced from the preionizer[1-26]. For the device shown in Fig.1-3[1-27], the cathode has parallel grooves and a trigger electrode covered with a glass tube is put in each groove. The trigger electrodes are grounded with the anode through the capacitance C_s to avoid the breakdown of the glass tube due to the application of the over-voltage. When the

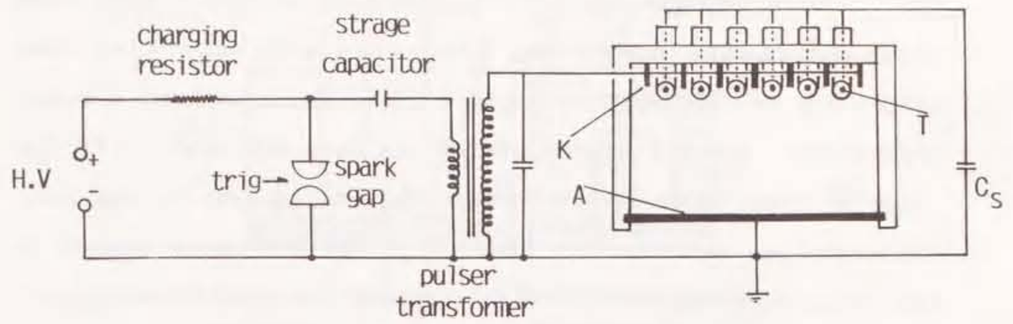

Fig.1-3.Schematic of electrical circuit.[1-27]

negative high voltage raised by the pulse transformer is applied to the cathode, the corona discharge occurs between the trigger electrode and the cathode through the glass tubes, and the homogeneous electron layer is formed on the surface of the cathode. The output energy density of 18J/l has been obtained at the operating frequency of 100Hz with the efficiency of 17%. Further using a PFN circuit without a pulse transformer, the efficiency of 24% has been achieved[1-28]. In these devices, although the efficient laser operation has been achieved, the input energy density in the discharge volume is less than 200J/l because of the weakness of corona preionization.

Yamabe et al.[1-29] have been reported that the extractable energy of a corona-preionized TEA-CO_2 laser can be increased by the superposition of a high-frequency corona discharge (HFCD) on a main discharge, although they examined the effect of HFCD only for the input energy density less than 200J/l. Ernst[1-30]-[1-33] achieved the input energy density over 200J/l with the efficiency of 18.5% both to intensify the effect of the corona preionization due to the rapid application of high voltage and to uniform the electric field on the cathode with Ernst profile[1-17]. Figure 1-4 shows the schematic diagram of the laser device reported by Ernst. The increase of the applied voltage was restricted rather by the occurrence of the surface discharge between the cathode and the preionizing electrode connected with the anode than by the instability of the main discharge due to the glow-to-arc transition. This device is unsuitable for the high-repetition-

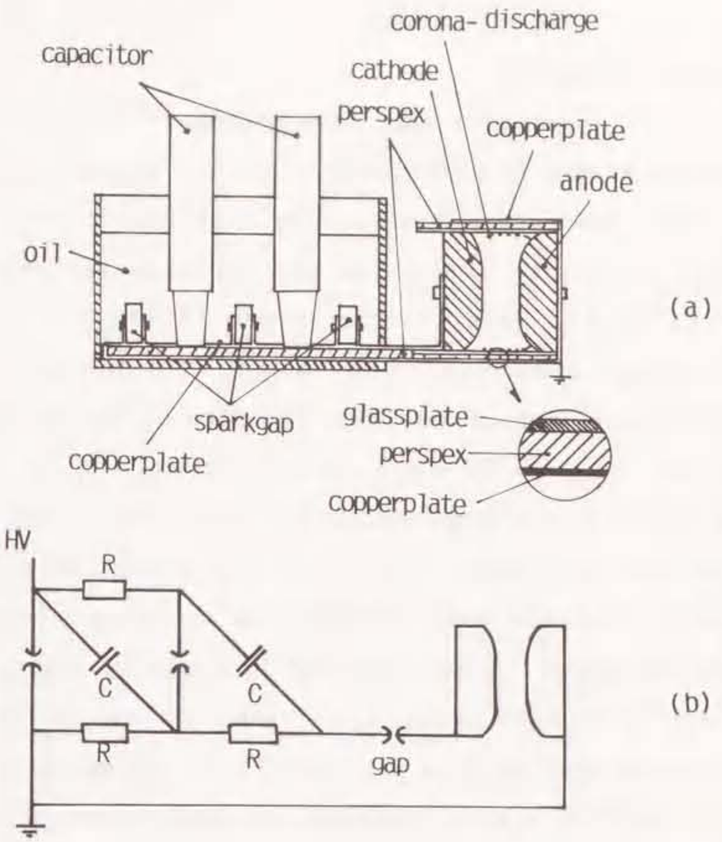

Fig.1-4.(a)Scheme of the construction of the system and detailes of side-wall construction of the laser.
(b)Electrical scheme of the laser system.[1-33]

rate operation because the corona preionizer obstructs the transverse gas flow perpendicular to the laser axis.

(2)Spark preionization

Spark discharges emit such strong UV radiation that the discharge volume is preionized in a great degree compared with the corona discharge. Consequently, the use of this technique results in the attainment of the input energy density over 300J/l. In the laser system shown in Fig.1-5[1-34], the sufficient preionization of the discharge volume is automatically carried out after the fire of the two-stage Marx generator by means of the auxiliary multiple spark discharges from point electrodes which are situated close behind a perforated mesh anode. Also, the preionization circuit are isolated from the main discharge circuit to preionize the larger discharge volume, and the preionizing spark electrode has a two dimensional array of 160 spark discharges distributed over an area of 600cm^2[1-35] as shown in Fig.1-6. In this system, a glow discharge has been obtained across the main electrodes separated by 30cm. Moreover, the UV radiation of spark discharges through the both mesh electrodes is effective to obtain a glow discharge in a large volume[1-36], [1-37]. Thus, the use of spark discharges is preferable for a large-volume preionization, however the degradation of the laser gas and the consumption of the preionizer due to the vaporization remain as a problem for a practical application.

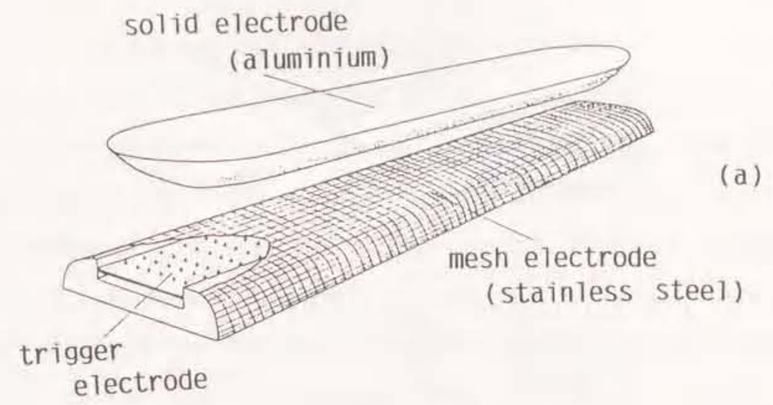

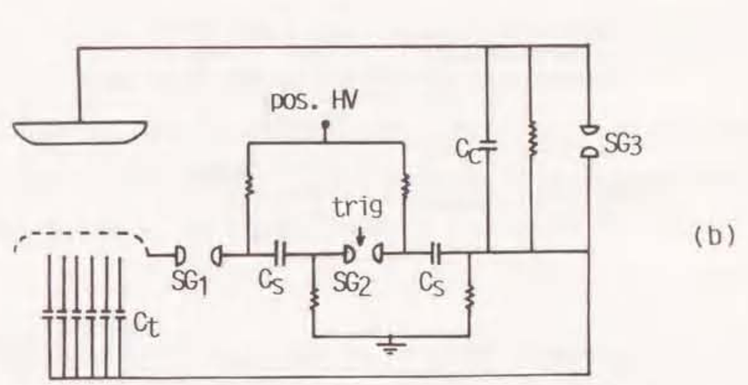

Fig.1-5.(a)Basic electrode structure of each discharge module.
(b)Schematic of Marx bank excitation circuit. C_S-storage capacitors, 0.1μF; C_t-trigger capacitors: $C_t \sim$160pF (5-cm system), $C_t \sim$100pF(7.5-cm system); C_c-cathode capacitor, 100pF; SG_1, SG_2, SG_3, pressurized nitrogen spark gaps.[1-34]

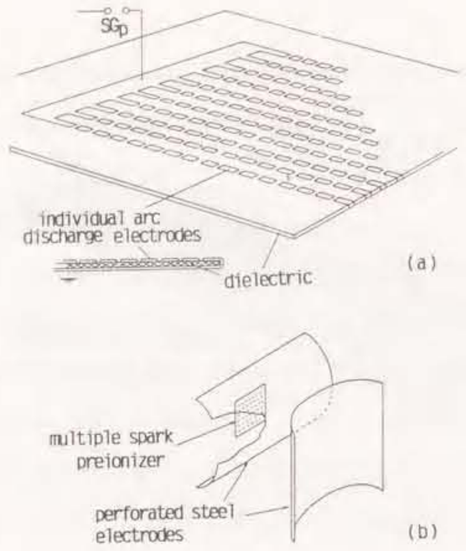

Fig.1-6.(a)Schematic diagram of the electrode configuration for the preionizer electrode.

(b)Schematic diagram of the situation of the preionizer electrode.

(c)Excitation circuits of the main discharge and of the preionizer. Legend: SG_1, SG_2, SG_3-high-pressure spark gaps for Marx bank; C_1, C_2, C_3, C_p-0.05 or 0.1μF low-inductance (20nH) capacitors; SG_D-high-pressure delay spark gap; SG_p-spark gap.[1-35]

(3)Electron-beam preionization

An electron-beam preionized TEA-CO_2 laser has been developed for a laser-fusion driver, and this technique was pioneered by Fenstermacher et al.[1-38], and later also by Daugherty et al.[1-39] and Basov et al.[1-40]. The electron beam controls the level of preionization and the conductivity of the discharge. Therefore an independently controlled main discharge volume provides the excitation of the vibrational levels in the laser process. Since the electric field of the main discharge in the conductive plasma can be chosen independently, this field can be adjusted for optimum excitation rates into the vibration levels. However, even under the best condition, the total efficiency of about 10% is lower compared with using the corona preionization. It is also difficult to operate the laser system at a high repetition rate because the metallic thin film as an electron-beam window is heated due to thermal losses.

(4)X-ray preionization

X-ray radiation has attracted an attention as a preionizing source because the mass penetration depth of X-ray is much greater than that of energetic electrons or UV photons. Further sealed-off operation at a high repetition rate is possible because of no degradation of laser gas due to X-ray radiation. The principles of X-ray preionization has been improved by Jayaram et al.[1-41]. In their system, the X-ray exposure in the active volume was 1-2mR/pulse with a

duration of 100ns, and the input energy density up to 300J/l/atm was obtained. Their experimental results indicated that the X-ray preionization results in the more energy extraction and makes the decrease of the laser output energy in a sealed-off operation smaller than the UV preionization by 36 spark discharges. However, the X-ray preionization system is inconvenient because the high voltage source in the range of more than 100kV is necessary to generate X-ray radiation.

1-5. Fundamental Research on Discharge Physics and Excitation Circuit for Pulsed CO_2 Lasers

For high-pressure pulsed CO_2 lasers, both a homogeneous glow discharge and an efficient energy injection into the discharge volume are necessary to extract a large energy. To achieve an efficient laser operation, many reserchers have studied on discharge physics and various excitation circuits.

1-5-1. Studies on Discharge Physics

(1)Conditions of primary electron density

At first, Palmer has shown the condition of primary electron density to produce a glow discharge in an atmospheric gas[1-42]. In order to suppress a filamentary streamer formation, i.e. an

arc discharge, the electric field associated with the space charge of avalanche should be smoothed out. If the following condition is satisfied, the homogeneous electron layer is produced in the discharge volume by overlapping the head of the neighboring electron avalanche, and the space charge field is expected to become sufficiently uniform:

$$n_0^{-1/3} \leqq r_c, \qquad r_c=(\lambda z_{crit})^{1/2},$$

where n_0 is the primary electron density, r_c is the radius of the head of the avalanche, λ is the electron mean free path and z_{crit} is the critical distance to initiate streamer breakdown. Substituting the typical parameters of a TEA-CO_2 laser into the above equations, n_0 is estimated as more than $10^4 cm^{-3}$.

Levatter et al.[1-43] have given the radius of the avalanche head by the following equation, considering both the thermal diffusion of electrons and the space charge field:

$$r_c=0.955(2C_e z_{crit}\lambda/3u_e)^{1/2},$$

where C_e is the electron mean thermal velocity and u_e is the electron mean drift velocity. The effect of voltage rise time is also examined considering the preavalanche and avalanche phases. The developing distance x_0 of the electrons to start from the cathode depends on the voltage rise time in the preavalanche phase, and it has been suggested that the filamentary streamer formation is suppressed under the condition of $x_0<r_c$. This

condition considerably agreed with the experimental results for excimer lasers where the voltage is rapidly applied across the main electrodes.

Karnyshin et al.[1-44] have proposed the following conditions to obtain a glow discharge:

$$n_0 \geqq (3e\alpha E/32\varepsilon)^{3/2}, \qquad 2\pi n_0 e\alpha^{-1}\exp(\alpha d_0) \geqq E,$$

where e is the electronic charge, α is the first Townsend coefficient, E is the electric field, ε is the mean electron energy and d_0 is the length of discharge gap. The former is a relation for a mutual overlapping of the neighboring electron avalanche, the latter is a relation for the initiation of main discharge. These conditions considerably agreed with the experimental results using a gas mixture of $CO_2/N_2/He=1/1/8$.

(2)Computation of transport coefficients and discharge phenomena

Transport coefficients for a laser mixture gas were not only measured[1-45]-[1-48] but also calculated using the Boltzmann equation[1-10],[1-50],[1-51]. The good agreement between the calculated and observed values has been obtained for the pressure of several torr. However, it is necessary to compensate the coefficients for the pressure of more than one atmosphere[1-52].

Kline et al.[1-53] have computed the waveforms of discharge voltage and current for the mixture gas pressure of less than 400torr, considering the spatiotemporal development of discharge plasma. The calculated results considerably agreed with the

observed waveforms. Also, the calculation has predicted that the discharge formative time is primarily determined by the characteristics of external excitation circuit and that photoemission in the gas can be neglected when strong preionization is used.

Further Midorikawa et al.[1-52] have calculated the waveforms of discharge voltage and current as well as the dependence of the deposited energy on gas pressure for the gas pressure up to 10atm, correcting the transport coefficients calculated by Lowke et al.[1-10].

(3)Occurrence and development of discharge instability.

The discharge instability has been studied by Nighan et al. and so on[1-54]-[1-57]. The instability has been considered to be amplified with a positive feedback due to heating of gas, and the relationship between the developing velocity of instability and the deposited energy or the gas pressure has been examined, treating the instability as a small disturbance in the calculation model. Also, Marode et al.[1-58] have calculated the development of instability, considering the variations of the transport coefficients caused by the decrease of the gas pressure in the heated region due to the thermal diffusion. The instability due to the production of negative ions[1-55] and the dissociative attachment of CO_2[1-59] have been also reported other than the thermal instability described before.

(4)Change of gas components due to laser discharge

The production rates and the life time of the discharge products in the active media have been measured[1-60)-(1-65]. For a sealed-off TEA-CO_2 laser, CO_2 molecules are dissociated into CO and O_2, and the negative ions of CO_3^- or CO_4^-, which cause the laser discharge to be instabilized, are produced by the reaction between CO and O_2.

Hokazono et al.[1-66] have analyzed the dissociation of CO_2 and the production of CO, O_2, O_3, N_2O, NO_2 and NO due to the laser discharge, using the Boltzmann equations in addition to 175 of plasma kinetic rate equations. For the laser gas mixture $CO_2/N_2/He=1/1/5$, the dissociation of CO_2 is proportional only to the deposited energy density in the ratio of 3.0×10^{-3}(%1/J). The amounts of CO, O_2 etc. also are increased with the deposited energy density.

1-5-2. Optimization of Excitation Circuit

Cridland et al.[1-67] have studied on the influences of a excitation circuit configuration on an extractable energy and a total efficiency. It has been concluded that a charge-transfer circuit makes a more efficient laser operation possible than a LC-inversion circuit and that a charge-transfer circuit with a Marx generator results in increasing the laser output.

Sato et al.[1-68] have investigated the effect of the circuit parameters in the charge-transfer circuit shown in Fig.1-7 using an experimental planning method. For the waveform of the

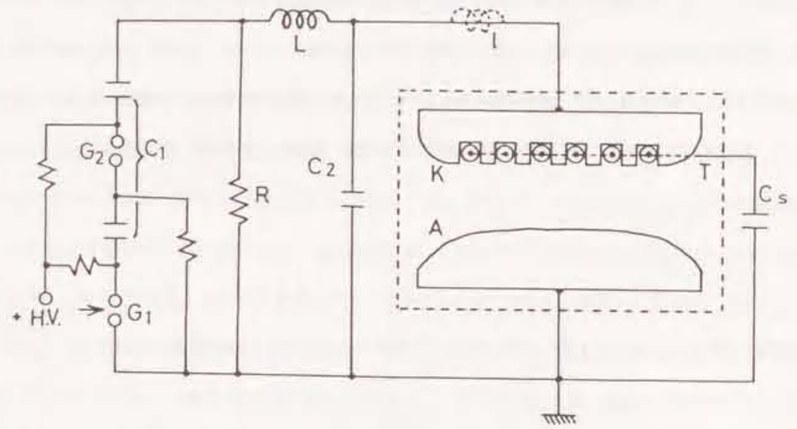

Fig.1-7. Schematic diagram of the laser apparatus and the discharge circuit.[1-68]

main discharge current, the continuous current is observed after the pulsive current. The laser output is increased in proportion to the amount of electrical charge of the continuous current. As the ratio of C_2/C_1 is decreased, it is difficult to obtain a glow discharge for a relatively high voltage of V_1 applied on the storage capacitor C_1, whereas the laser output and the total efficiency is increased for a relatively low voltage V_1. Although a glow discharge is apt to be obtained with the increase of the ratio C_2/C_1 even at a relatively higher voltage V_1, C_2/C_1 of about 1 is optimal value to maximize the laser output.

1-6. Present Situation of Non-Destructive Inspection

The non-destructive inspection has been developed and is very useful to ensure the quality of products. The inspections have been usually carried out using radioactivity, supersonic-wave etc.(1-69),(1-70).

The radioactive ray is irradiated to an article and the defects in the article are realized by the figure of the photograph. α-ray, β-ray, γ-ray and X-ray are properly used according to the transmittance of the article and the kind of the film. A copper or steel board of 20cm thick can be inspected using the radioactive ray emitted from ^{60}Co or X-ray with a high energy of 1~ 35MeV. However, the shape of the defects and the incident angle of the ray have much effect on the clearness of

the figure, so that it is difficult to detect small cracks under the condition of the incident angle over 15°. Moreover, strict treatments of radioactive sources are needed, i.e. the check of working safety zone, the custody of sources etc.

Supersonic wave is considerably propagated in a solid article, and is reflected on the discontinuous boundary such as a defect. The characteristics of the reflected and transmitted waves inform us the existence of defects. The recent development of small supersonic devices makes the inspection more convenient, and the wave in a frequency range of 2~ 5MHz is usually used in practice for the inspection. For the pulse reflection method, the depth of defects from the surface can be realized by processing the echo signal of the reflected pulses. For the pulse transmission method, although the information of the depth can not be obtained, the defects can be detected more simply only by measuring the transmittance of the pulse. However, the supersonic wave is unsuitable for a remote inspection because of the very low transmittance of supersonic wave into a solid material from air. Further, especially for the pulse reflection method, it is difficult to recognize the echo signal reflected on the defects inside the article which has a complicated shape.

A laser beam has recently attracted an attention as a new media for non-destructive inspection because of more convenience of a laser device than radioactive sources. Also, a laser beam which has both a good directivity and a long interferable length is preferable for a remote inspection. The two different types of laser inspection have been reported(1-71),(1-72).

One is the detection of the ultrasonic vibration generated by a high-power pulsed laser with a laser interferometer[1-73],[1-74]. One example shows in Fig.1-8. A laser pulse from a Nd:YAG Q-switched laser, having typically the energy of 15mJ in 30ns pulse duration, is focussed onto the aluminum block with a f≒15cm convex lens to form a surface plasma. The aluminum block has an artificial slot typically 0.75mm deep and 0.25mm wide. The longitudinal, shear and Rayleigh pulses with a frequency components up to 15MHz are transmitted through the slot, and the depth of slot can be estimated by the time difference between the shear pulse and the Rayleigh pulse.

The other is the detection of the change of the periodical vibration with the irradiating frequency of the incident laser beam[1-75]-[1-78]. One example shows in Fig.1-9. A chopper wheel modulates the intensity of an argon laser beam, which is focused onto a specimen's surface, generating a temperature variation and a periodical spherical heat flow into the material. The specimen is mounted onto a steping-motor-driven and computer-controlled table which can be moved in X and Y directions with a position accuracy of 1μm. A computer-controlled piezo element (PZT) moves the reference mirror in order to adjust the interferometer. The interference signal detected by photodiode is fed into a lock-in amplifier to measure the amplitude and the phase of the specimen's vibration. The drilled holes of 0.8mm diameter in an aluminum block can be detected due to a phase decay of 5 degrees.

However there are the following problems in these techniques in a practical application. For the former method, not only the

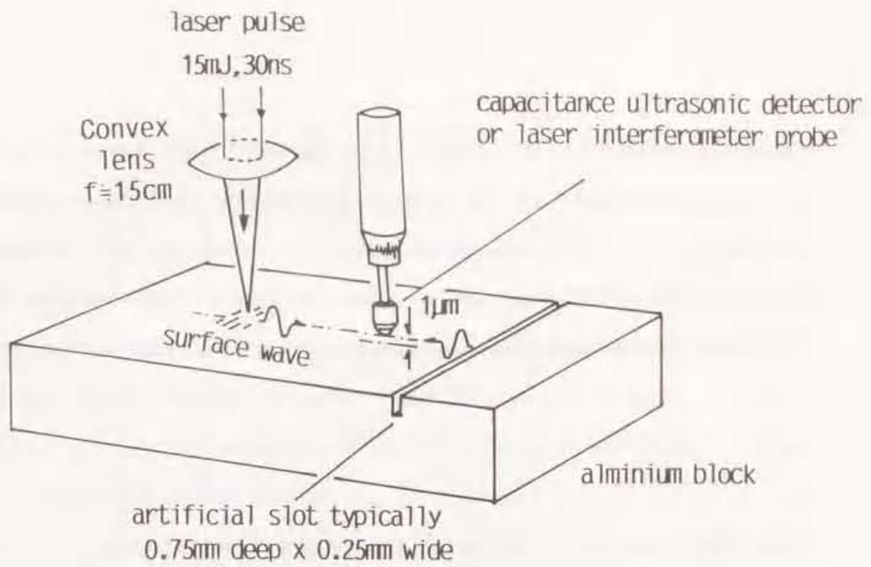

Fig.1-8.Experimental arrangement.[1-73]

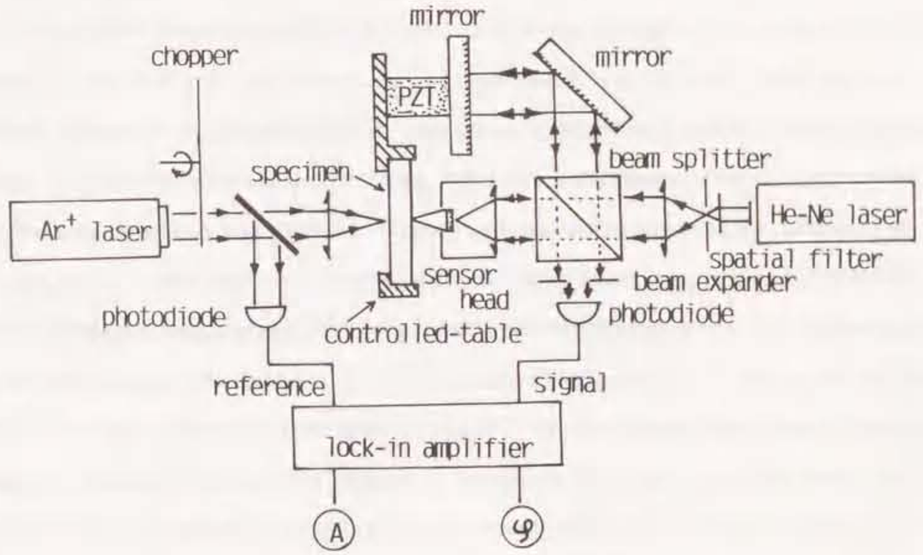

Fig.1-9.Experimental arrangement using a sensor head.[1-75]

interferometer with a very high upper limit frequency over 15MHz is necessary but it is difficult to realize the signals due to the defects in the article with a complicated shape. For the latter method the use of a lock-in amplifier and the scanning of the laser beam lead to the prolongation of the working time.

1-7. Purposes and Composition of the Dissertation

1-7-1. Purposes of the Dissertation

A corona-preionized TEA-CO_2 laser has a relatively simple structure and a good ability for efficiency and lifetime in a sealed-off operation. However it is inferior to TEA-CO_2 lasers with the other preionization for high energy of laser output because of the weakness of the preionization. Therefore it is desirable to enlarge the extractable energy of corona-preionized TEA-CO_2 lasers to make use of the superior features. One of the purposes of this study is to increase the input and output energy densities of a corona-preionized TEA-CO_2 laser with the Dumanchin's electrode configuration by intensifying the corona preionization. In order to attain this object, a high-frequency corona discharge (called as HFCD) is superposed on the main discharge as reported by Yamabe et al.[1-29], and it is examined how effect on the discharge condition and the optical energy extraction the HFCD has. Further the new circuit called as SC-HFCD circuit is devised

to save the energy for the HFCD operation. In the SC-HFCD circuit, the residual energy not to be injected into the discharge volume is collected and recycled as the energy source of the HFCD in the next laser operation. Therefore it is probable not only to save the energy for the HFCD operation but also to miniturize the laser device because another power supply for the HFCD operation is not necessary. The results are included in the former half of this dissertation.

Another purpose of this study are to apply the TEA-CO_2 laser to a vibrational source of electric suspension insulators and to develope a new inspection method to distinguish a cracked insulator detecting the natural vibration, whose frequency components and decay constant change due to the cracks in the insulator. Although various informations of the cracks can be realized by the techniques described in 1-6, it is sufficiently useful in some application to find only whether some cracks are in the solid sample or not. The characteristics of the vibration generated by a pulsed CO_2 laser beam are measured, and the mechanism of the vibration is investigated. Moreover the author has studied on the possibility that the existence of a crack can be found by performing Fast Fourier Transfer (FFT) to the vibrational signal detected with a laser interferometer or by hearing the vibrational signal. The results are included in the latter half of this dissertation.

1-7-2. Composition of the Dissertation

This dissertation is composed of the following 6 chapters.

Chapter 1 is the introduction of this dissertation. The survey of the progress and the remaining problem for discharge-pumped pulsed CO_2 lasers and non-destructive inspection is described. The motivation and the purpose of this study are also described.

In chapter 2, the characteristics of the main discharge and the laser output in a corona-preionized TEA-CO_2 laser with a HFCD circuit are described. It is shown that the laser output is increased by the HFCD circuit due to the suppression of the glow-to-arc transition and that some conditions of the HFCD current are required to be satisfied in order to increase the laser output.

In chapter 3, the performance of the TEA-CO_2 laser with the SC-HFCD circuit is described. It is examined whether the HFCD can be superposed on the main discharge using the SC-HFCD circuit, after both the main discharge circuit and the ratio of the laser gas mixture (CO_2/N_2/He) are optimized to operate the SC-HFCD circuit without the remarkable decrease of the laser output. It is shown that the SC-HFCD circuit is effective to increase the laser output and that the output voltage of the SC-HFCD circuit is predicted by the calculation using the equivalent circuit.

In chapter 4, the vibrational characteristics of an electric suspension insulator with the irradiation of a pulsed CO_2 laser beam on the surface of the insulator are described. It is observed that the insulator is vibrated in the natural mode with

the passing of time after the irradiation of the laser beam. The variation of the vibrational amplitude with the change of the irradiation intensity can be approximately explained by calculating the force applied on the surface of the insulator.

In chapter 5, the non-destructive and remote inspection system for an electric suspension insulator using a pulsed TEA-CO_2 laser to vibrate the insulator and a laser interferometer to detect the vibration remotely is described. It is shown that the crack in the insulator is found by performing FFT to the detected vibrational signal or by hearing the signal.

In chapter 6, the content of this dissertation is summarized and the significance of the present work is also given.

In each chapter, references are listed cumulatively at the end of the chapter.

References

1-1)T.H.Maiman : "Stimulated optical radiation in ruby", Nature 187(1960) 493.

1-2)C.K.N.Patel : "Interpretation of CO_2 optical maser experiments", Phys. Rev. Lett. 12(1964) 588.

1-3)H.Sugawara, K.Kuwabara, S.Takemori, A.Wada and K.Sasaki : In Gas Flow and Chemical Lasers, Sixth Intern. Symp., Jerusalem, 8-12 Sept. 1986, Springer Proc. Phys. vol.15(Springer, Berlin, Heidelberg 1987) p265.

1-4)A.E.Hill : "Multijoule pulses from CO_2 lasers", Appl. Phys. Lett., 12(1968) 324.

1-5)IEEE J. Quantum Electron., Special Issue on Lasers for Fusion, QE-17, No.9.

1-6)E.Sindoni and C.Wharton : Diagnostics for Fusion Experiments (Pargamon, Oxford, 1979)

1-7)N.C.Luhmann Jr. and W.A.Peebles : "Instrumentation for magnetically confined fusion plasma diagnostics", Rev. Sci. Instrum. 55(1986) 279.

1-8)T.Arisawa and Y.Naruse : "Uranium enrichment by laser method", J. Atom Energ. Soc. Jpn. 22(1980) 79, in Japanese.

1-9)H.Tshiro, K.Midorikawa, K.Nagasaki, K.Toyoda and S.Namba : "A CO_2-laser-pumped para-H_2 Raman laser", Rev. Laser Eng. 13(1985) 292, in Japanese.

1-10)J.J.Lowke, A.V.Phelps and B.W.Irwin : "Predicted electron transport coefficients and operating characteristics of CO_2-N_2-He laser mixtures", J. Appl. Phys. 44(1973) 4664.

1-11)W.F.Krupke and W.R.Sooy : "Properties of an unstable confocal resonator CO_2 laser system", IEEE J. Quantum Electron. QE-5(1969) 575.

1-12)P.O.Clark and J.Y.Wada : "The influence of Xenon on sealed-off CO_2 lasers", IEEE J. Quantum Electron. QE-4(1968) 263.

1-13)P.Bletzinger and A.Garscadden : "Influence of Xenon on CO_2 laser plasma", Appl. Phys. Lett. 12(1968) 289.

1-14)M.Z.Novgorodov, A.G.Sviridov, N.N.Sobolev : "Electron energy distribution in CO_2 laser discharges", IEEE J. Quantum Electron. QE-7(1971) 508.

1-15)W.Streifer : "Unstable optical resonators and waveguides", IEEE J. Quantum Electron. QE-4(1968) 229.

1-16)T.Y.Chang : "Improved uniform-field electrode profiles for TEA laser and high-voltage applications", Rev. Sci. Instrum. 44(1973) 405.

1-17)G.J.Ernst : "Uniform-field electrodes with minimum width", Opt. Commun. 49(1984) 275.

1-18)C.Frapard, M.Froulot and X.Ziegler : "High peak power pulsed 10μ CO_2 laser", Phys. Lett. 20(1966) 384.

1-19)P.K.Cheo : "Effects of CO_2, He and N_2 on the lifetimes of the 00^01 and 10^00 CO_2 laser levels and on pulsed gain at 10.6μ", J. Appl. Phys. 38(1967) 3563.

1-20)M.J.Weber and T.F.Deutsch : "Pulsed and steady-state infrared emission studies of CO_2 laser systems", IEEE J. Quantum Electron. QE-2(1966) 369.

1-21)A.J.Beaulieu : "Transversely excited atmospheric pressure CO_2 lasers", Appl. Phys. Lett. 16(1970) 504.

1-22)D.C.Johnson : "Excitation of an atmospheric-pressure CO_2-N_2-

He laser by capacitor discharges", IEEE J. Quantum Electron. QE-7(1971) 185.

1-23)K.A.Laurie and M.M.Hale : "A pin-electrode atmospheric-pressure CO_2 laser", IEEE J. Quantum Electron. QE-7(1971) 530.

1-24)R.Dumanchin and J.Rocca-Serra : "Augmentation de l' énergie et de la puissance fournie par unitè de volume dans un laser à CO_2 en règime pulsè", C. R. Acad. SC. Paris, t. 269(1969) 916-Sèrie B.

1-25)R.Dumanchin, J.C.Farcy, M.Michion and J.Rocca-Serra : "High power density pulsed molecular laser", Proc. 6th Quantum Electron. Conf., Kyoto, Japan(1970)

1-26)R.Marchetti, E.Penco and G.Salvetti : "Sealed, miniaturized, corona-preionized, high-repetition-rate TEA CO_2 laser using hydrogen buffered gas mixtures", IEEE J. Quantum Electron. QE-21(1985) 1766.

1-27)R.Dumanchin, M.Michion, J.C.Farcy, G.Boudinet and J.Rocca-Serra : "Extension of TEA CO_2 laser capabilities", IEEE J. Quantum Electron. QE-8(1972) 163.

1-28)Yu-Li Pan, A.F.Berniiardt and J.R.Simpson : "Construction and operation of a double-discharge TEA CO_2 laser", Rev. Sci. Instrum. 43(1972) 662.

1-29)C.Yamabe, H.Ishihara, H.Akiyama and K.Horii : "Improvement of laser output of TEA CO_2 laser by high frequency corona discharge", Rev. Laser Eng. 14(1986) 960.

1-30)G.J.Ernst : "Single-frequency, atmospheric pressure CO_2 laser", Rev. Sci. Instrum. 48(1977) 1281.

1-31)G.J.Ernst and A.G.Boer: "Construction and performance characteristics of a rapid discharge TEA CO_2 laser", Opt. Commun. 27(1978) 105.

1-32)G.J.Ernst and A.G.Boer: "A 5cm single-discharge CO_2 laser having high power output", Opt. Commun. 34(1980) 221.

1-33)G.J.Ernst : "A 10cm aperture, high quality TEA CO_2 laser", Opt. Commun. 44(1982) 125.

1-34)M.C.Richardson, A.J.Alcock, K.Leopold and P.Burtyn : "A 300-J multigigawatt CO_2 laser", IEEE J. Quantum Electron. QE-9(1973) 236.

1-35)M.C.Richardson, K.Leopold and A.J.Alcock : "Large Aperture CO_2 laser discharges", IEEE J. Quantum Electron. QE-9(1973) 934.

1-36)O.P.Judd and J.Y.Wada : "Investigations of a UV preionized electrical discharge and CO_2 laser", IEEE J. Quantum Electron. QE-10(1974) 12.

1-37)A.Girard : "Multiple preionization discharge TEA CO_2 laser", Rev. Sci. Instrum. 47(1976) 608.

1-38)C.A.Fenstermacher, M.H.Nutter, W.T.Leland and K.Boyer : "Electron-beam-controlled electrical discharge as a method of pumping large volumes of CO_2 laser media at high pressure", Appl. Phys. Lett. 20(1972) 56.

1-39)J.D.Daugherty, E.R.Pugh, D.H.Douglas-Hamilton : "A stable, scalable, high pressure gas discharge as applied to the CO_2 laser", Bull. Am. Phys. Soc. 17 399(1972).

1-40)N.G.Basov, E.M.Belenov, V.A.Danilychev, O.M.Kerimov, I.B.Kovsh and A.F.Suchkov : "Gas lasers at high pressure",

JETP Lett.14(1971) 285, in English.

1-41)K.Jayaram and A.J.Alcock : "X-ray preionization of self-sustained, transverse excitation CO_2 laser discharges", J. Appl. Phys. 58(1985) 1719.

1-42)A.J.Palmer : "A physical model on the initiation of atmospheric-pressure glow discharges", Appl. Phys. Lett. 25(1974) 138.

1-43)J.I.Levatter and S.Lin : "Necessary conditions for the homogeneous formation of pulsed avalanche discharges at high gas pressures", J. Appl. Phys. 51(1980) 210.

1-44)V.N.Karnyushin, A.N.Malov and R.I.Soloukin : "Influence of preionization conditions on the development of a homogeneous discharge in gases", Sov. J. Quantum. Electron. 8(1978) 319.

1-45)C.S.Lakshminarasimha, J.Lucas, J.L.Moruzzi and I.J.Spalding : "Electron swarm parameters in CO_2 laser gas mixtures", J. Phys. D: Appl. Phys. 9(1976) 1727.

1-46)D.K.Davies : "Ionization and attachment coefficients in CO_2:N_2:He and pure CO_2", J. Appl. Phys. 49(1978) 127.

1-47)R.A.Sierra, H.L.Brooks and K.J.Nygaard : "Electron drift velocities in N_2, CO_2 and (N_2+CO_2) laser mixtures", Appl. Phys. Lett. 35(1979) 764.

1-48)R.A.Sierra, H.L.Brooks, A.J.Sommerer, S.R.Foltyn and K.J.Nygaard : "Effective swarm parameters and transport coefficients in CO_2 laser mixtures", J. Phys. D: Appl. Phys. 14(1981) 1791.

1-49)M.C.Cornell, I.M.Littlewood, H.L.Brooks and K.J.Nygaard : "Electron drift velocities in gas mixtures of He, N_2 and CO_2", J. Appl. Phys. 54(1983) 1723.

1-50)W.L.Nighan : "Electron energy distributions and collision rates in electrically excited N_2, CO and CO_2", Phys. Rev. A 2(1970) 1989.

1-51)Y.Sakai, S.Kaneko, H.Tagashira and S.Sakamoto : "A Boltzmann equation analysis of electron swarm parameters in CO_2 laser mixtures", J. Phys. D: Appl. Phys. 12(1979) 23.

1-52)K.Midorikawa, K.Wakabayashi, K.Nakamura, M.Obara and T.Fujioka : "Discharge parameters of a high pressure, ultraviolet-preionized, transversely excited CO_2 laser", J. Appl. Phys. 53(1982) 3410.

1-53)L.E.Kline and L.J.Denes : "Investigations of glow discharge formation with volume preionization", J. Appl. Phys. 46(1975) 1567.

1-54)W.L.Nighan and W.J.Wiegand : "Causes of arcing in cw CO_2 convection laser discharges", Appl. Phys. Lett. 25(1974) 633.

1-55)W.L.Nighan, W.J.Wiegand and R.A.Haas : "Ionization instability in CO_2 laser discharges", Appl. Phys. Lett. 22(1973) 579.

1-56)W.L.Nighan and W.J.Wiegand : "Influence of negative ion processes on steady-state properties and striations in molecular gas discharges", Phys. Rev. A 10(1974) 922.

1-57)J.H.Jacob and S.A.Mani : "Thermal instability in high-power laser discharges", Appl. Phys. Lett. 26(1975) 53.

1-58)E.Marode, F.Bastien and M.Bakker : "A model of the streamer-induced spark formation based on nutral dynamics", J. Appl.

Phys. 50(1979) 140.

1-60)P.W.Pace and M.Lacombe : "A sealed high-repetition-rate TEA CO_2 laser", IEEE J. Quantum Electron. QE-14(1978) 263.

1-61)C.Willis, W.J.Sarjeant and D.M.Wardlaw : "Initial rate of decomposition of CO_2 in volume discharges: An experimental study", J. Appl. Phys. 50(1979) 68.

1-62)W.J.Wiegand and W.L.Nighan : "Plasma chemistry of CO_2-N_2-He discharges", Appl. Phys. Lett. 22(1973) 583.

1-63)A.L.S.Smith and H.Shields : "Positive ion processes in the positive column of CO_2 laser electrical discharges", J. Chem. Phys. 67(1977) 1594.

1-64)Y.Wang and J.Liu : "Direct mass spectrometric diagnostics for a CO_2 gas laser", J. Appl. Phys. 59(1986) 1834.

1-65)H.Shields, A.L.S.Smith and B.Norris : "Negative ion effects in TEA CO_2 lasers", J. Phys. D: Appl. Phys. 9(1976) 1587.

1-66)H.Hokazono and H.Fujimoto : "Theoretical analysis of the CO_2 molecule decomposition and contaminants yield in transversely excited atmospheric CO_2 laser discharge" J. Appl. Phys. 62(1987) 1585.

1-67)J.V.Cridland and S.Howells : "The dependence of transversely excited atmospheric CO_2 laser performance on circuit configuration", J. Appl. Phys. 53(1982) 4016.

1-68)S.Sato, C.Yamabe and K.Horii : "An analysis of the laser output properties for a TEA CO_2 laser with the design of experiments", Trans. IEE Jpn. 100-A(1980) 657, in Japanese.

1-69)Nihon Hihakai Kensa Kyokai : Hihakaikensa Binran (Nikkan Kogyo Shinbun-sha, 1978), in Japanese.

1-70)Nihon Hihakai Kensa Kyokai : Hoshu Kensa Binran (Nikkan Kogyo Shinbun-sha, 1980), in Japanese.

1-71)A.C.Tam : "Applications of Photoacoustic sensing techniques", Rev. Mod. Phys. 58(1986) 381.

1-72)D.A.Hutchins : "Mechanisms of pulsed photoacoustic generation", Can. J. Phys. 64(1986) 1247.

1-73)J.A.Cooper, R.A.Crosbie, R.J.Dewhurst, A.D.W.Mckie and S.B.Palmer : "Surface acoustic wave interactions with cracks and slots: A non-contacting study using lasers", IEEE Trans. Ultrason. Ferroelect. and Freq. Cont. UFFC-33(1986) 462.

1-74)R.J.Dewhurst, D.A.Hutchins and S.B.Palmer : "Quantitative measurements of laser-generated acoustic waveforms", J. Appl. Phys. 53(1982) 4064.

1-75)P.Hess and J.Pelzl : Photo Acoustic and Photo Thermal Phenomena p400 (Springer Series in Optical Sciences vol.58, Springer-Verlag, Berlin, Heidelberg, New York, London, Paris, Tokyo)

1-76)K.Hane, T.Kanie and S.Hattori : "Photothermoelastic probing for a clamped plate sample", Appl. Opt. 27(1988) 386.

1-77)I.Tomeno and H.Ohzu : "Photoacoustic signal from subsurface defects in ceramics", Jpn. J. Appl. Phys. 24(1985) 1445.

1-78)P.Cielo : " Pulsed photothermal evaluation of layered materials", J. Appl. Phys. 56(1984) 230.

CHAPTER 2 IMPROVEMENT OF CORONA-PREIONIZED TEA-CO_2 LASER BY MEANS OF HIGH FREQUENCY CORONA DISCHARGE

2-1. Introduction

The corona-preionized TEA-CO_2 laser, proposed by Dumanchin et al.[2-1], has a simple and compact structure, and is preferable for a sealed-off operation, because the laser mixture gas is not degraded due to few impurities produced by corona discharge[2-2]. Furthermore, only less than 1% of the energy for the main discharge is consumed to preionize the discharge volume, while the electrons produced on the surface of the cathode by the corona discharge are effectively used for the formation of glow discharge. However, the input energy density in the discharge volume has been reduced to less than 200J/l because of the weakness of the corona preionization compared with the other preionization, i.e. spark discharges, X-ray radiation etc.. Therefore, it is expected that the increase of the corona preionization intensity leads to the development of a high-power and long-life laser device.

In this chapter, the superposition of high frequency corona discharge (called as HFCD) on the main discharge is described as a method to increase the intensity of the corona preionization[2-3][2-4]. The influences of the superposition of the HFCD on the laser output as well as on the main discharge are examined, changing the parameters in the HFCD circuit. The developing distance of the electrons starting from the surface of the cathode is calculated to examine the influence of the triggering time and the period of HFCD current. The calculation of the HFCD current using the equivalent circuit makes the effect of the parameters in the HFCD circuit clear, comparing with the observed HFCD current.

2-2. Experimental Apparatus and Procedure

The electrical circuit of the experimental apparatus is shown in Fig.2-1. The main electrodes, 50mm wide and 600mm long, are made of aluminum at a gap length of 30mm. The effective discharge volume is estimated to be 0.5(l). The anode is formed with the Chang profile[2-5] and the cathode has ten parallel grooves, 4.5mm wide and 3mm deep, on the surface along the laser axis. Many trapezoidal protrusions are distributed on the surface along the laser axis between each groove[2-3].

A trigger electrode covered with a pyrex glass tube is put in each groove. The outer diameter and the thickness of the glass tube are 4mm and 1.2mm, respectively.

The electrical discharge circuit with the pulse forming network (PFN) is composed of the capacitances C_1(=60nF), C_2(=52nF), the inductances L_1(=22.4μH), L_2($\sim$ 100nH), and the

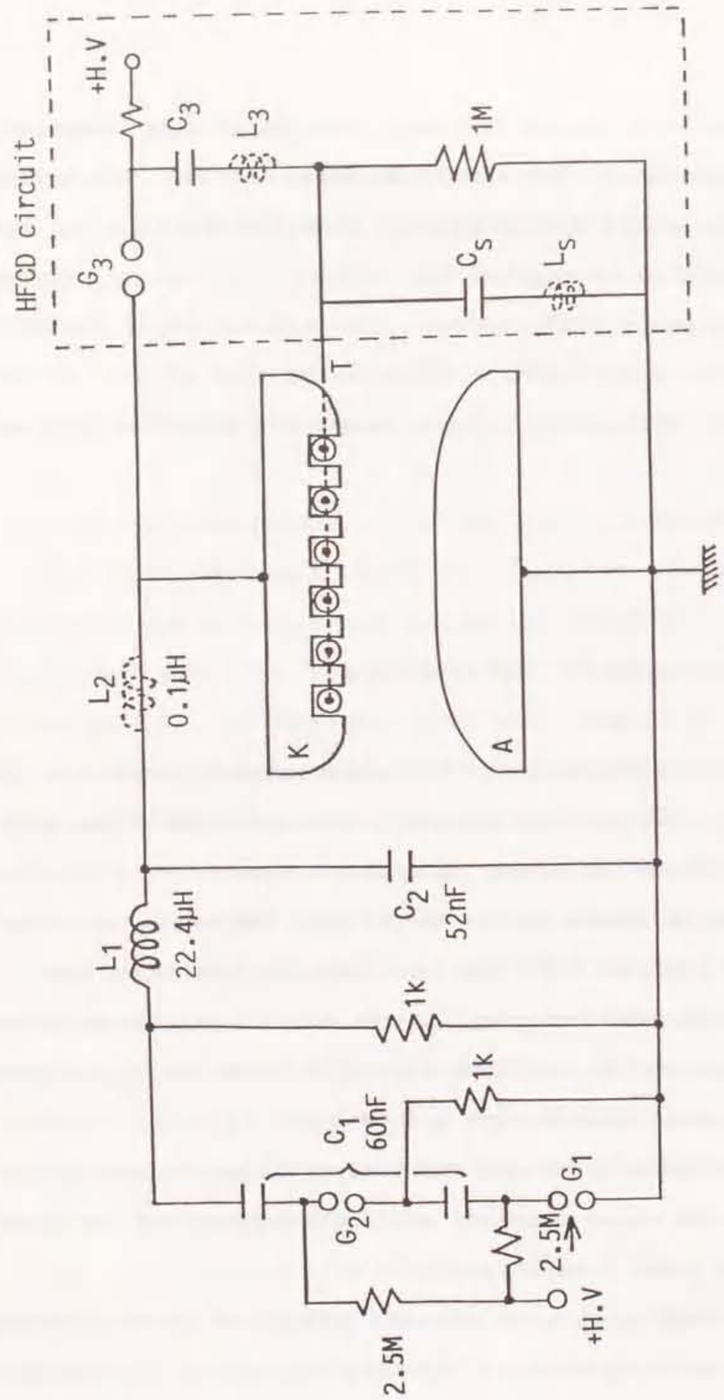

Fig.2-1.Schematic diagram of experimental apparatus and electrical circuit.

gaps G_1, G_2 pressurized with nitrogen gas. The HFCD circuit is enclosed by the broken line in Fig.2-1, and the operating sequence of these circuits is described in 2-3-1 in detail. The minimums of the inductances L_3 and L_S are 1.7μH and 2.5μH, respectively, due to the geometrical structure of the laser device.

A $CO_2/N_2/He$ mixture gas in the ratio 1:1:5(l/min) is flowed along the laser axis at an atmospheric pressure. The optical resonator consists of a gold-coated reflector with a 10m radius of curvature and a germanium flat coupler with a reflection coefficient of 51%. The length of the resonator is about 1m.

The laser beam is partially reflected on the surface of the NaCl Brewster window, and the waveform of the laser output pulse is measured by detecting the reflected beam with a gold-doped germanium detector cooled by liquid nitrogen. The waveforms of the voltage V between the main electrodes and the main discharge current I_m are measured with a R-C divider and a search coil, respectively, while the waveform of the current at the trigger electrode, I_t, is measured with a Rogowski coil. The glow-to-arc transition rate is measured by timing the rapid reduction of V due to the arcing for the thirty discharges at the repetition rate of 0.1Hz. The laser output is also measured with a calorimeter.

2-3. Experimental Results

2-3-1. Effect of Triggering Time of HFCD Current

The waveforms of the voltage V, the main discharge current I_m, the laser power and the trigger current I_t are shown in Fig.2-2 when V_1=60kV, V_3=20kV, C_3=40nF, C_s=850pF, L_3=1.7μH and L_s=2.5μH, where V_1 and V_3 are the voltages applied on the capacitances C_1 and C_3, respectively. The breakdown voltage between the main electrodes and the peak value of I_m are about 55kV and 3.5kA, respectively. After triggering the gap G_1, the electrical charge stored in C_1 is transferred to C_2, and the voltage V is applied on the main electrodes. Then the trigger current passes through the capacitance C_s before the spark of G_3. If the voltage V exceeds a critical value, the gap G_3 is automatically fired and the HFCD current flows by L-C oscillation at the trigger electrode through C_3 and L_3 after the spark of G_3. The peak value of the HFCD current ($\fallingdotseq$ 700A) is so large that the main discharge volume is intensively preionized by the HFCD current. The time $t_{G3\text{-}BD}$ between the spark of G_3 and the main discharge indicates the delay time of the main discharge after the preionization, as shown in Fig.2-2. The delay time $t_{G3\text{-}BD}$ is controlled by the pressure of nitrogen gas sealed in G_3. The laser oscillation with two peaks is observed after the main discharge initiation. The first peak is due to the excitation of the CO_2 molecules by electron collision, whereas the second peak is due to the energy transfer from the vibrationally excited N_2 molecules to the CO_2 molecules.

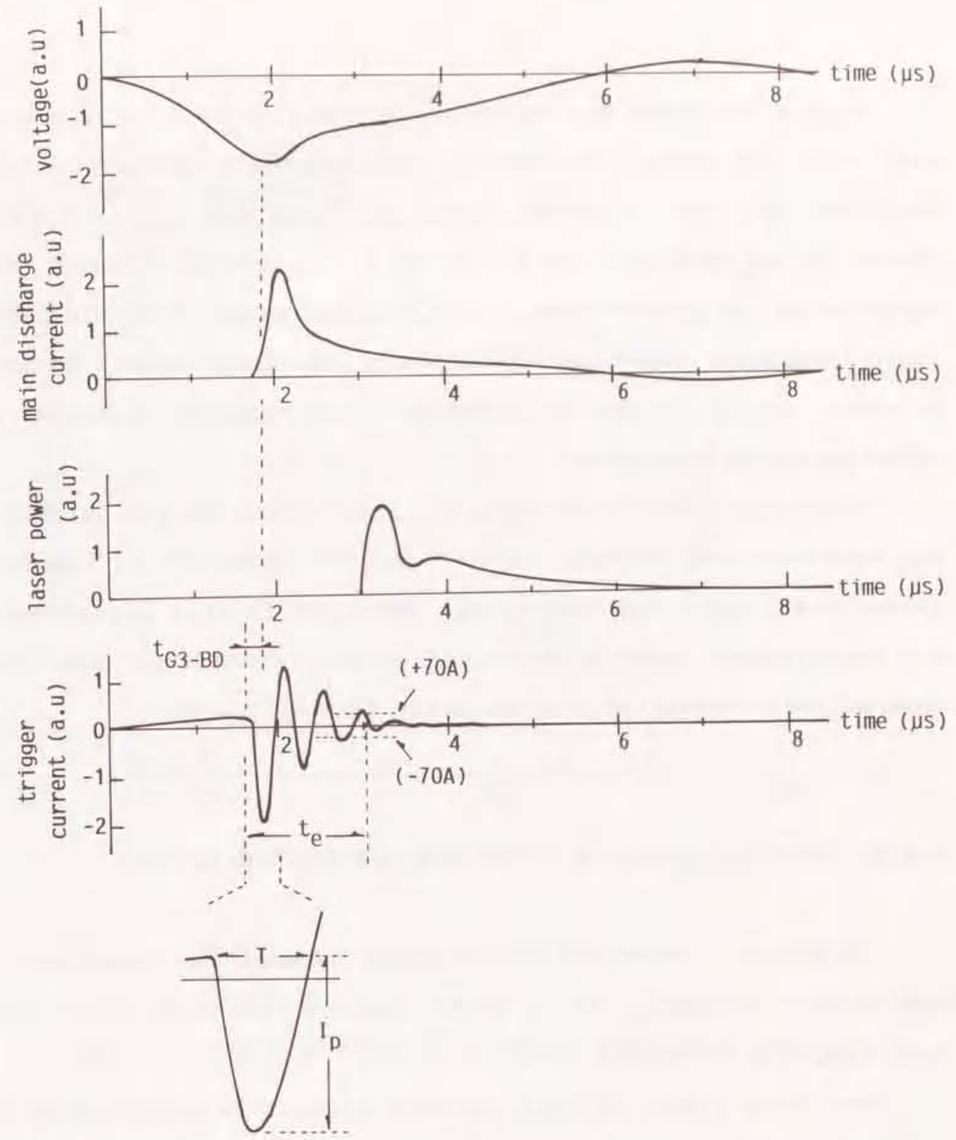

Fig.2-2.Temporal characteristics of voltage across the main electrodes, main discharge current, laser output power and trigger current. The definitions of delay time $t_{G3\text{-}BD}$, peak value I_p, half-period T and duration t_e are also shown in the bottom figure.

Figure 2-3 shows the variation of the glow-to-arc transition rate with the delay time $t_{G3\text{-}BD}$. The operating parameters are V_1=58.8kV, V_3=20kV, C_3=40nF, C_s=850pF, L_3=1.7μH and L_s=2.5μH. There is an optimal value of $t_{G3\text{-}BD}$, 220ns~ 240ns, for suppressing the glow-to-arc transition, and an arc-free discharge (zero transition rate) is maintained at the input energy density of about 205J/l. A similar tendency is reproducibly observed at other operating parameters.

The delay time of the main discharge from the preionization has been reported in refs.2-6, 2-7 and 2-8, however the reported values are longer than the values obtained in this experiment. All experimental results described below are obtained under the most suitable condition for the delay time of $t_{G3\text{-}BD}$.

2-3-2. Characteristics of Laser Output with HFCD Circuit

Figure 2-4 shows the relationship between the laser output and V_1 as a parameter of V_3 in the case of C_3=40nF, L_3=1.7μH, L_s=2.5μH, and C_s=850pF.

The laser output without the HFCD circuit is saturated at V_1 of about 51.3kV and gradually is decreased for V_1>51.3kV because of the occurrence of the glow-to-arc transition, while that with the HFCD circuit is saturated at V_1 higher than 51.3kV because of the suppression of the glow-to-arc transition due to the increase of the peak value of the HFCD current with V_3. Arc-free discharges are produced for the input energy density up to about

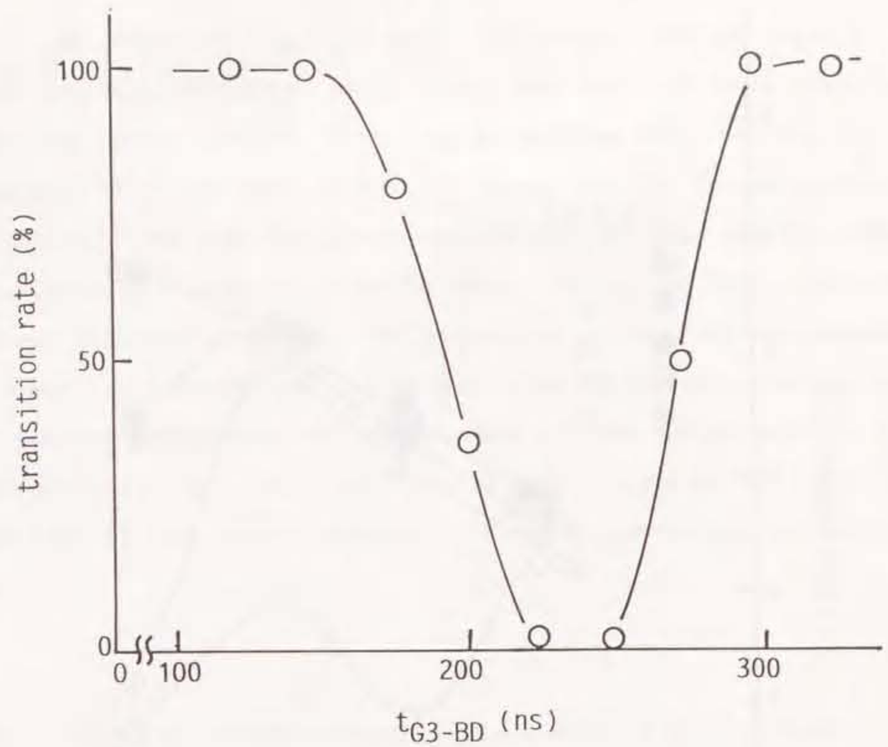

Fig.2-3.Transition rate as a function of delay time $t_{G3\text{-}BD}$.

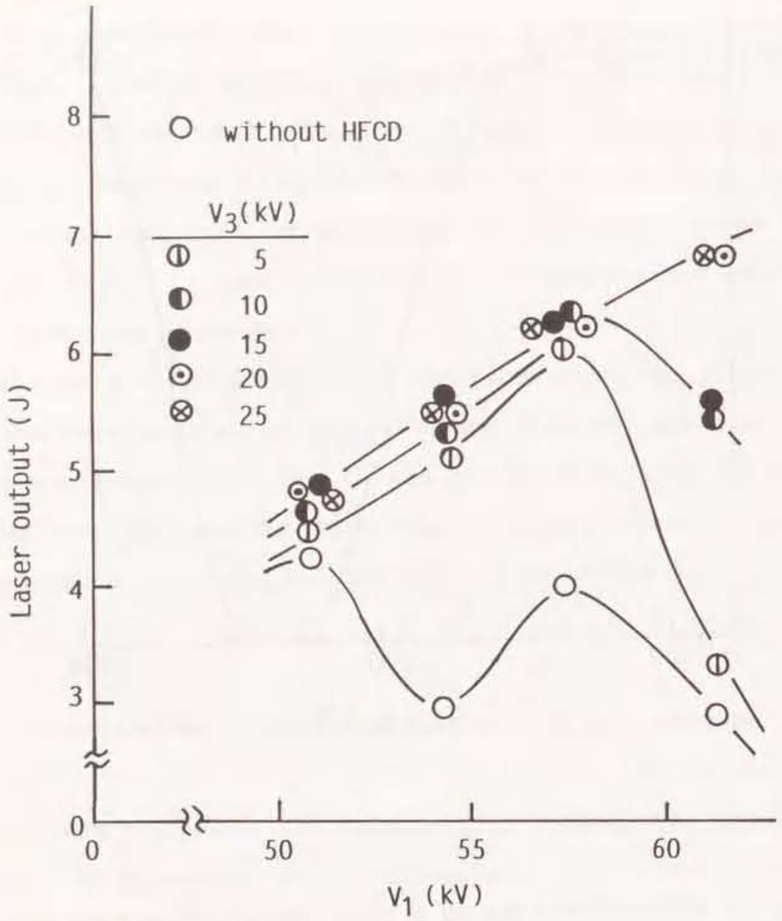

Fig.2-4.Relationship between laser output and voltage V_1 as a parameter of voltage V_3.

205J/l for V_3>20kV, where the output energy density is about 13J/l, as shown in Fig.2-3, while the output energy density of about 14J/l is obtained at a transition rate of less than 10% when the input energy density is 220J/l at V_1=60kV. It is suggested that the HFCD circuit is effective for the increase of the laser output for the input energy density over 200J/l, where the glow-to-arc transition would occur during the main discharge without the HFCD circuit. The waveforms of the voltage between the main electrodes and the main discharge current prior to the glow-to-arc transition are independent of the parameters in the HFCD circuit, so that the laser output depends only on the stability of the main discharge, i.e. the glow-to-arc transition rate.

2-3-3. Effect of Parameters of C_3, C_s and L_3 in HFCD Circuit

Figure 2-5 shows the relationship between the capacitance C_3 and the laser output, where V_1=60kV, V_3=20kV, C_s=850pF, L_3=1.7μH and L_3=2.5μH. The laser output is saturated at a certain value of C_3.

Figure 2-6 shows the relationship between the inductance L_3 and the laser output as a parameter of V_3, where V_1=60kV, C_3=40nF, C_s=850pF and L_s=2.5μH. The laser output is decreased with the increase of L_3, and it is found that the reduction of L_3 results in the increase of the laser output.

Figure 2-7 shows the relationship between the capacitance C_s

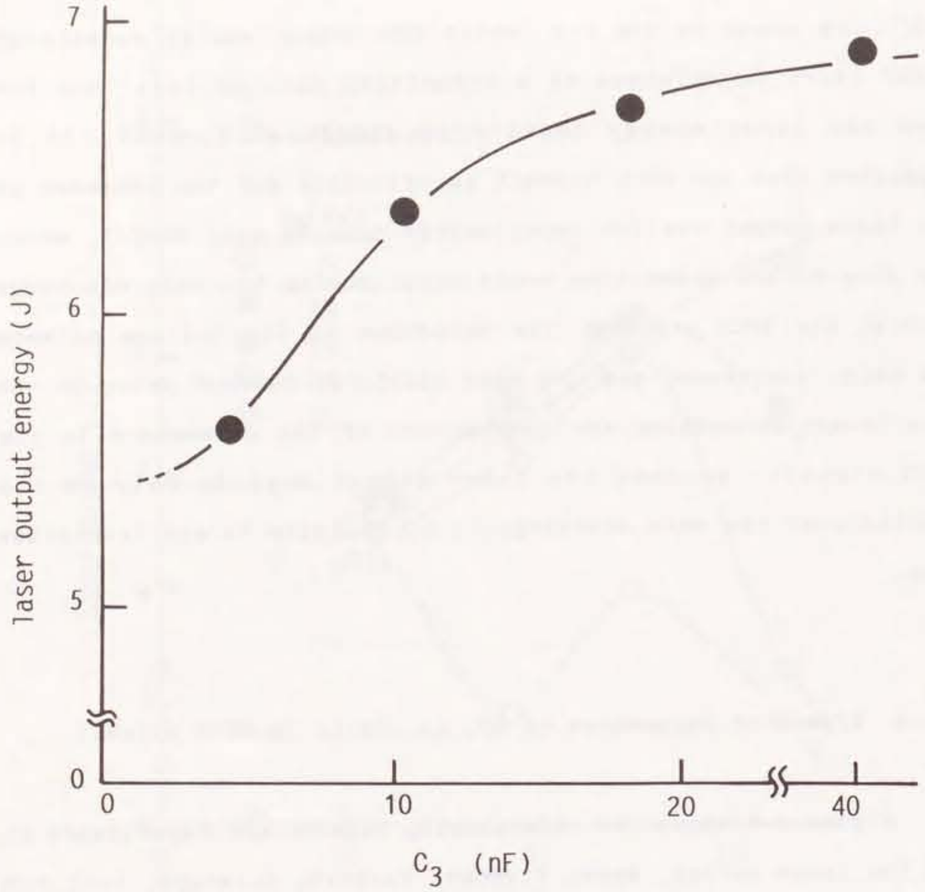

Fig.2-5.Variation of laser output with capacitance C_3.

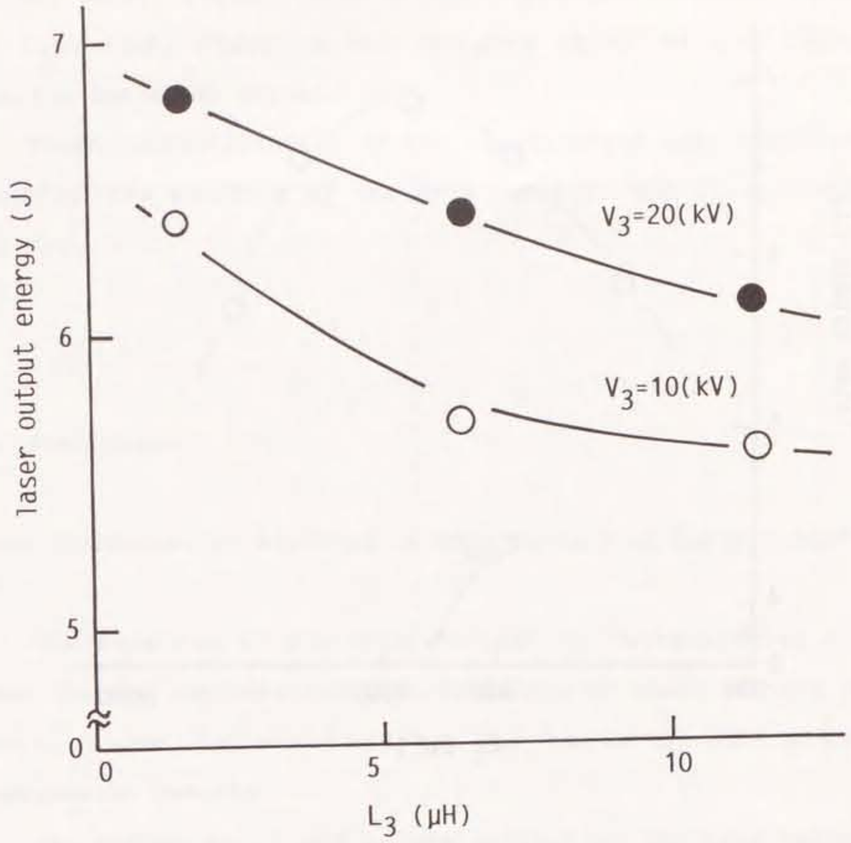

Fig.2-6.Variation of laser output with inductance L_3 as a parameter of voltage V_3.

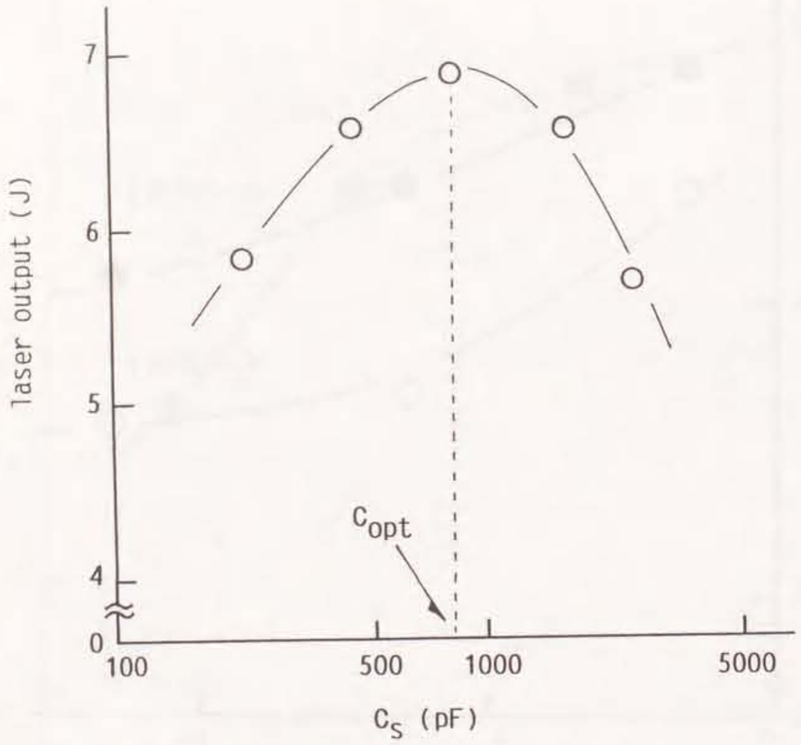

Fig.2-7.Variation of laser output with capacitance C_s.

and the laser output, where V_1=60kV, V_3=20kV, C_3=40nF, L_3=1.7μH and L_s=2.5μH. There is the optimal value of C_s, C_{opt}, to maximize the laser output.

These characteristics of the laser output are considered to depend on the waveform of the HFCD current, and it is discussed in 2-4-1.

2-4. Discussion

2-4-1. Influence of Waveform of HFCD Current on Laser Output

The waveform of the HFCD current is characterized by peak value, period and duration. The influence of these factors on the laser output is examined on the basis of the previous experimental results.

The values I_p, T and t_e are defined as the peak value, the half-period and the duration of the HFCD current, respectively, as shown in Fig.2-2. In this experiment, t_e is the time required for the amplitude of the HFCD current to decrease down to 70A after the spark of G_3. Figure 2-8 shows the dependence of t_e on C_3 at V_1=60kV, V_3=20kV, C_s=850pF, L_3=1.7μH and L_s=2.5μH, where both I_p and T do not change appreciably with C_3. The variation of t_e with C_3 considerably corresponds to that of the laser output shown in Fig.2-5. It is found that t_e of 1$\sim$ 1.5μs at the saturation point of the laser output considerably agrees with the

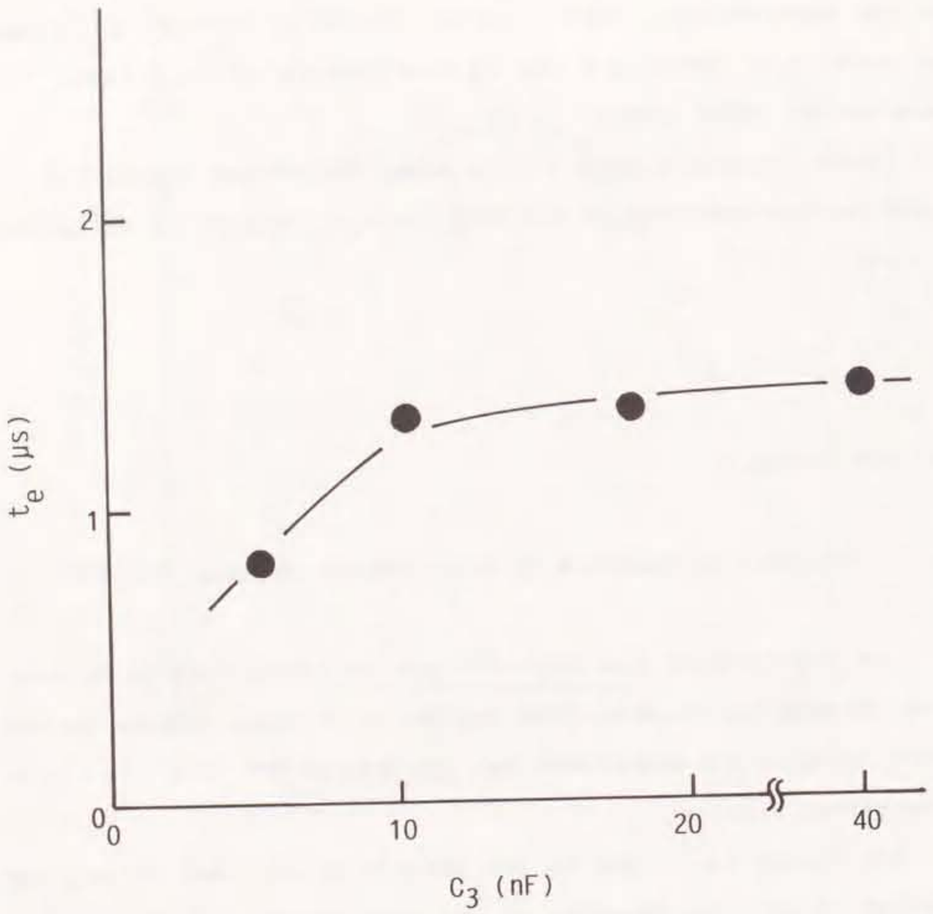

Fig.2-8.Dependence of duration t_e on capacitance C_3.

pulse width of the main discharge current from the peaking capacitance C_2. Therefore it seems to be important to produce the electrons on the surface of the cathode while the main discharge current flows from C_2 at least.

Figure 2-9 shows the contour lines of the laser output E_L with the changes of I_P and T using the experimental results shown in Figs.2-4 and 2-6, where t_e is more than 1μs. As shown in Fig.2-9, the laser output is increased as I_P becomes higher or T becomes shorter with the increase of V_3 and with the decrease of L_3. Therefore short T and high I_P are very important, and it is necessary both to increase V_3 and to reduce L_3 in order to increase the laser output.

Figure 2-10 shows the observed variations of (a)I_P, T and (b)t_e with C_s in comparison with the calculated results described in 2-4-3. The period T is so large for $C_s > C_{opt}$, while t_e is less than 1μs for $C_s < C_{opt}$. Therefore, there is the optimal value of C_s, C_{opt}, to maximize the laser output as shown in Fig.2-7.

2-4-2. Mechanism of Suppression of Glow-to-Arc Transition with HFCD Operation

Both the adjustment of $t_{G3\text{-}BD}$ and the shortness of T other than the highness of I_P lead to the stabilization of the main discharge due to the suppression of the glow-to-arc transition and to the increase in the laser output as described before. It is very important to ionize the whole discharge volume

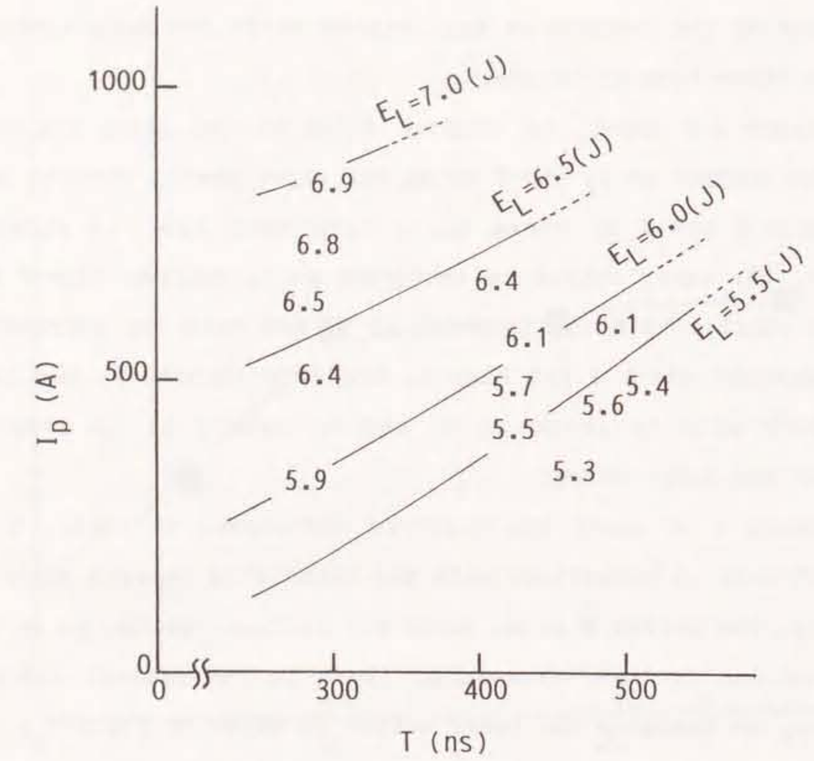

Fig.2-9.Contour lines of laser output as functions of peak value I_P and half-period T.

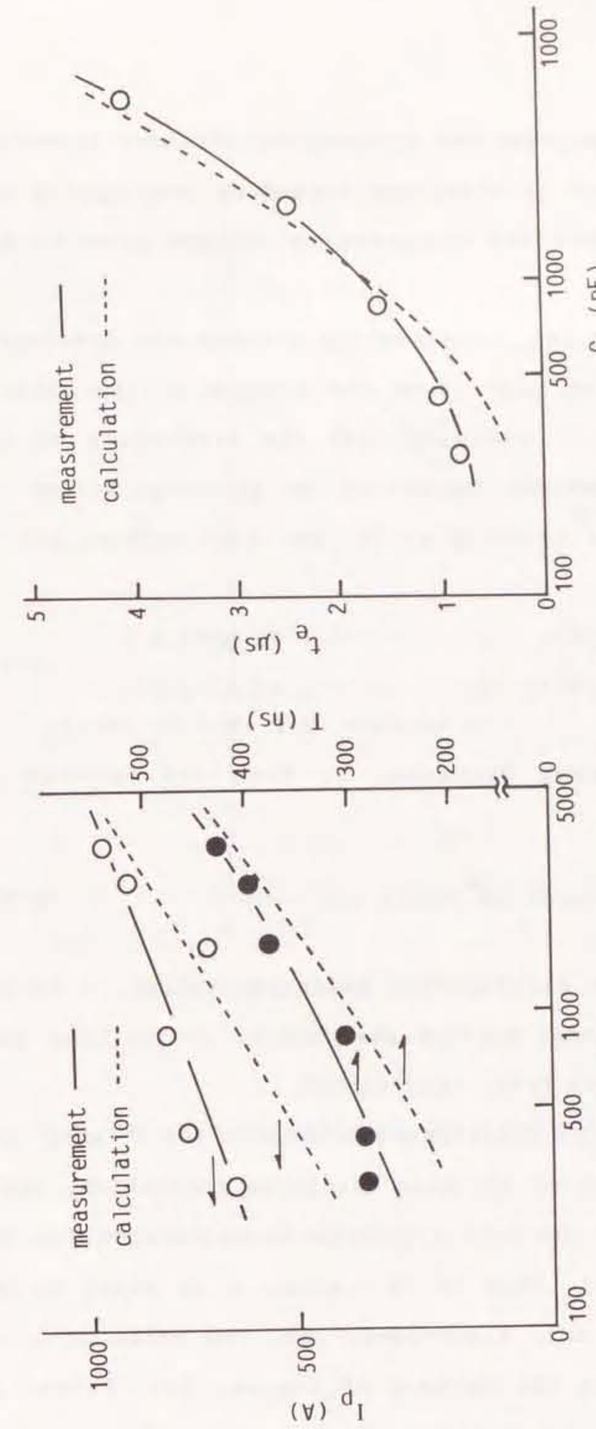

Fig.2-10.(a)Measured and calculated relationships between capacitance C_S and peak value I_P or half-period T.
(b)Measured and calculated relationship between capacitance C_S and duration t_e.

homogeneously and to suppress the filamentary streamer formation with a homogeneous layer of electrons formed by overlapping the electron avalanches for the suppression of the glow-to-arc transition[2-9][2-10].

Here are estimated the relationships between the developing distance of the electron layer from the surface of the cathode and $t_{G3\text{-}BD}$ as well as T. Assuming that the distortion of the electric field by the spatial charges in the discharge volume can be neglected, the drift velocity v_d in the laser mixture gas is given by[2-11]

$$v_d = \begin{cases} 1.4\cdot10^6\cdot(E/P) & \cdots\cdots (\ 0 \leqq E/P \leqq 2\ ) \\ 4.5\cdot10^5\cdot(E/P)+2\cdot10^6 & \cdots\cdots (\ 2 \leqq E/P \leqq 20) \end{cases} \quad (2\text{-}1)$$

(v_d in cm/s, E/P in V/cm·Torr)

Therefore the developing distance, x, from the cathode is approximately given by

$$x = \int_{t_1}^{t} v_d \, dt \qquad (x \text{ in cm}) \quad , \qquad (2\text{-}2)$$

where E is the electric field in the discharge volume, P is the total pressure of the laser mixture gas, and t_1 is the time when the electron layer starts from the cathode.

Figure 2-11 shows the relationship between x and t_1 when t is 1.9μs, which is the time of the main discharge initiation, where the change in E before the main discharge is calculated for the circuit shown in Fig.2-1. When t_1 is 1.66μs, x is equal to the gap length between the main electrodes, 3cm. The value of $t-t_1$, 240ns, is very close to the optimum of $t_{G3\text{-}BD}$, 220~ 240ns, in Fig.2-3. Therefore it is considered that the efficient and

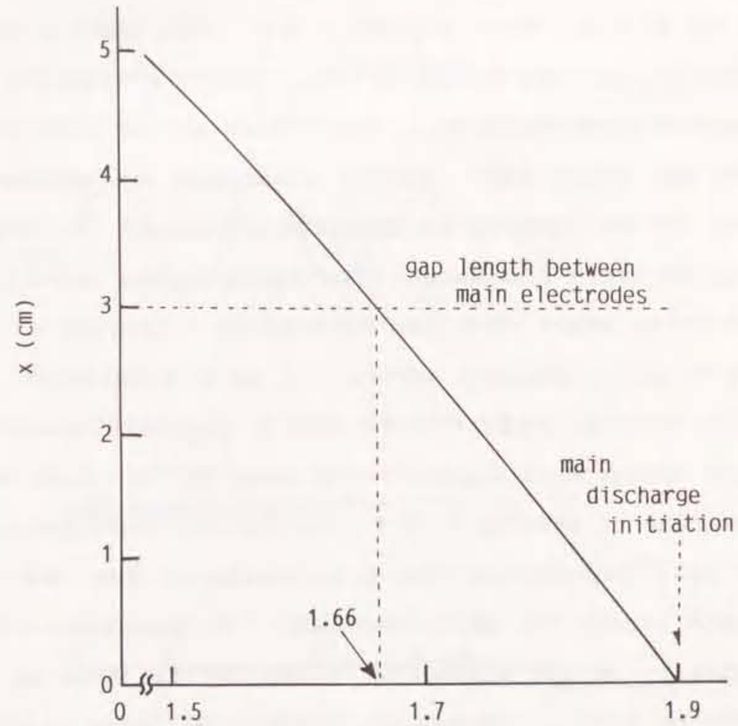

Fig.2-11.Relationship between developing distance x and time t_1.

homogeneous electron layer reaches the anode and that the whole of the discharge volume is sufficiently ionized at the optimal value of $t_{G3\text{-}BD}$. Most electrons are consequently distributed throughout the discharge volume, and the transition to the homogeneous glow discharge occurs there at the same time.

On the other hand, if the electrons are produced on the surface of the cathode in both polarities of the HFCD current during the main discharge, the homogeneous electron layers successively start from the cathode at intervals of the half-period T and propagate across the main electrodes along the electric field. Figure 2-12 shows the developments of the electron homogeneous layers represented by "e" from the cathode to the anode at intervals of T like a streak-mode photograph. The value $t_{K\text{-}A}$ represents the time required for the layers to propagate across the main electrodes. No homogeneous layers are periodically in the discharge volume for the time of $T-t_{K\text{-}A}$ in the case of $T>t_{K\text{-}A}$, whereas one homogeneous layer is always there at least in the case of $T\leqq t_{K\text{-}A}$. The homogeneous layers suppress the formation of filamentary streamer and maintain the glow discharge due to the uniformity of the electric field on the layers. The glow-to-arc transition is considered to occur when there are no layers in the discharge volume during the main discharge. Therefore it is important that there is one homogeneous layer at least in the discharge volume to suppress the glow-to-arc transition, and it is necessary to produce the layers frequently on the surface of the cathode.

When E in eq.(2-1) is the average electric field in the

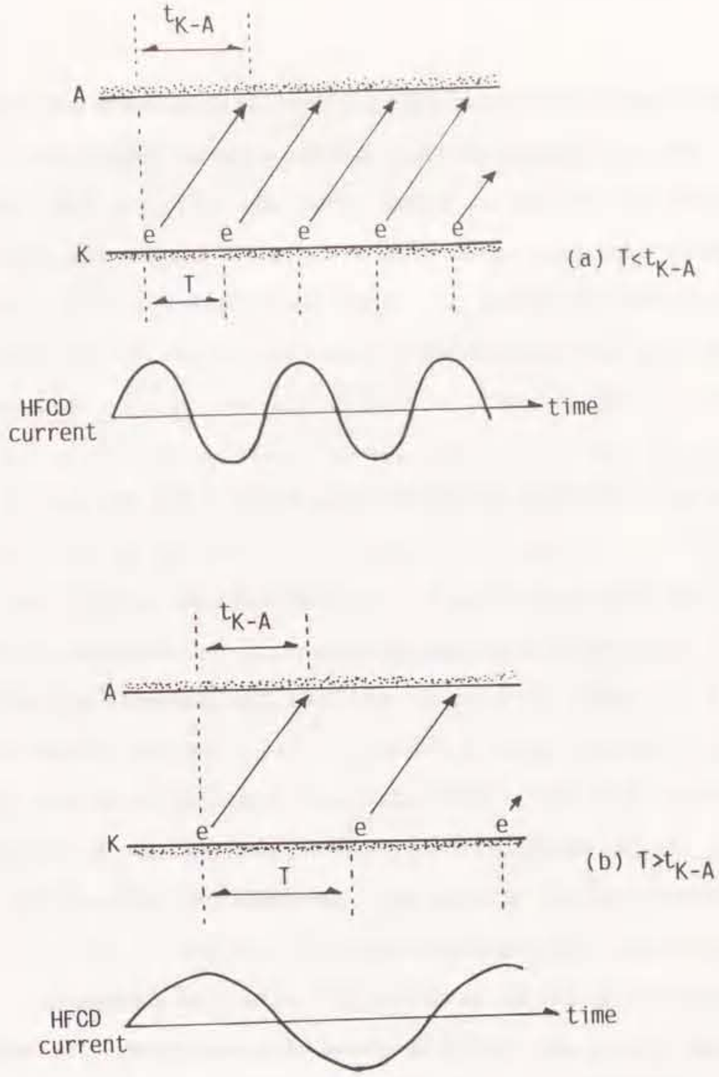

Fig.2-12. Schematic successive propagations of homogeneous electron layers at intervals of T (a)for $T>T_{K\text{-}A}$ and (b)for $T<T_{K\text{-}A}$. The value $T_{K\text{-}A}$ represents the time required for the layer to propagate across the main electrodes. The symbol "e" represents a homogeneous electron layer.

discharge volume for 1μs after the initiation of the main discharge, it is estimated that the electrons starting from the cathode reach the anode at 300ns. The shorter the half-period T between the first and next layers is down to 300ns, the larger the laser output becomes as shown in Fig.2-9. This result is consistent with the above model.

2-4-3. Analysis of HFCD Current using Equivalent Circuit

In order to increase the laser output according to the results of the previous experiments, it is necessary for the waveform of the HFCD current to satisfy the following conditions; the increase of the peak value (for I_P), the decrease of half-period (for T) and the prolongation of duration (>1μs for t_e). Therefore, it is useful to calculate the waveform of the HFCD current and to suggest the optimal parameters in the HFCD circuit for the increase of the laser output.

The HFCD current is considered to be the transient current for charging C_S and C_g from the charged capacitance C_3, where the following conditions are assumed to simplify the calculation.

1)The impedance of the main discharge circuit, including the discharge volume, is negligible compared with the impedance of C_S.

2)The voltage across the main electrodes is assumed to be constantly equal to the breakdown voltage V_{BD} after the spark of G_3.

3)The impedance of the corona discharge between the cathode and the trigger electrode is given by the constant resistance of R_g.

The equivalent circuit of the HFCD circuit is shown in Fig.2-13, where V_{BD} is the breakdown voltage of the main discharge, R_S is the resistance of the electrical line, C_g is the capacitance of the glass tube, L_g is the inductance at the trigger electrode. It is so difficult to resolve the waveform of the HFCD current analytically that it is computed numerically.

Figures 2-10 shows the calculated values of I_P, T and t_e as a function of C_S. The relatively good agreement between the observed and calculated values is obtained at L_3=1.7μH, L_S=2.5μH, L_g=90nH, R_g=21Ω and R_S=3Ω .

Figure 2-14 shows the calculated contour lines of I_P, T and t_e as functions of L_S and L_3 at C_S=3400pF, C_3=40nF and V_3=20kV. The duration t_e is decreased with the decrease of L_3 because of no oscillation due to over-damping, while I_P is decreased with the increase of L_3 because the HFCD current is more apt to flow into C_S. Therefore there is the optimal relation between L_3 and L_S in the HFCD current flow according to the condition for the increase of the laser output. The measurement of I_P, T and t_e is performed at the values of L_3 and L_S shown by the circle (○) in Fig.2-14, because L_3 and L_S are limited to $\geqq$ 1.7μH and $\geqq$ 2.5μH, respectively, due to the structure of the laser device. If L_3 and L_S can be reduced in accordance with the shaded portion in Fig.2-14, the conditions of I_P>1kA, T<250ns, t_e>1μs will be satisfied. Consequently, it is expected that greater laser output would be

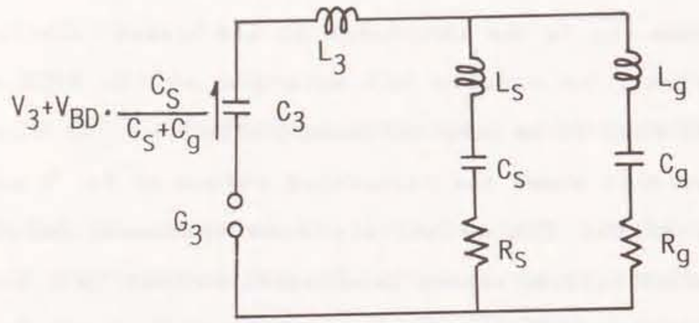

Fig.2-13.Equivalent circuit for calculation.

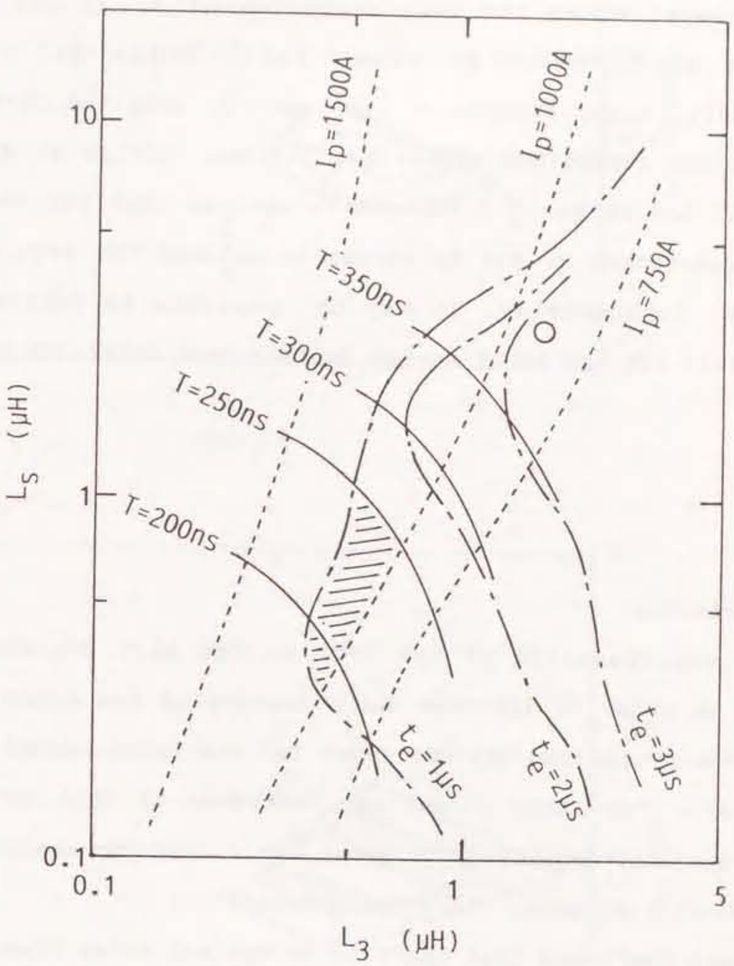

Fig.2-14.Calculated contour lines of peak value I_p, half-period T and duration t_e as functions of inductances L_s and L_3. The circle(○) represents the values of L_3 and L_s measuring I_p, T and t_e.

obtained without the glow-to-arc transition than that in thisexperiment where the best condition of I_p, T and t_e are obtained at C_s=850pF as about 800A, 300ns and 1.5μs, respectively. Also, Figures 2-15(a) and (b) show the part which satisfies the conditions of I_p>1kA, T<250ns, t_e>1μs at R_g=11Ω , 16Ω , 21Ω and at R_s=1Ω , 3Ω . It is obvious that the reduction of the resistances R_s and R_g serves to enlarge the area of such condition. Consequently, it may be possible to increase the laser output for the input energy density over 220J/l in a future study.

2-5. Conclusion

The superposition of the HFCD on the main discharge was examined in order to increase the intensity of the preionization in a corona-preionized TEA-CO_2 laser for the input energy density over 200J/l. The laser output was increased by this method for the input energy density up to about 220J/l and the maximum laser output density of about 14J/l was obtained.

It was confirmed that there is an optimal delay time between the spark of the gap G_3 and the initiation of the main discharge to suppress the glow-to-arc transition. When the HFCD current was characterized by the peak value (I_p), the half period (T) and the duration (t_e), both higher I_p and shorter T were necessary to increase the laser output, while t_e was required to be more than about 1μs. The calculation of the waveform of the HFCD current

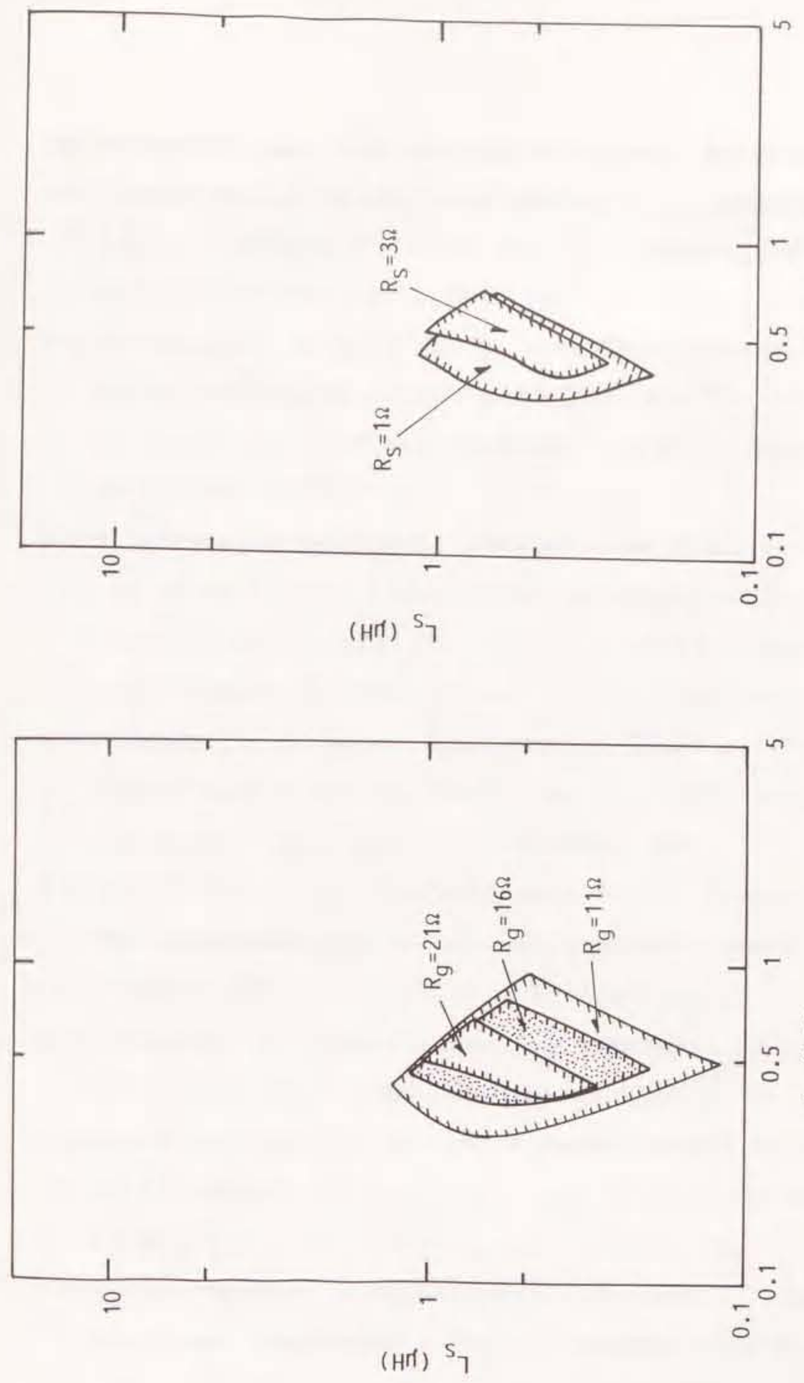

Fig.2-15.Calculated region of inductances L_s and L_3 under the condition of I_p>1000A, T<250ns, t_e>1μs as parameters of resistances (a)R_g and (b)R_s.

using the equivalent circuit suggested that the reduction of resistance and inductance in the HFCD circuit might result in increasing the laser output.

References

2-1)R.Dumanchin, M.Michion, J.C.Farcy, G.Boudinet and J.Rocca-Serra : "Extension of TEA CO_2 laser capabilities", IEEE J. Quantum Electron. QE-8(1972) 163.

2-2)R.Marchetti, E.Penco and G.Salvetti : "Sealed, miniaturized, corona-preionized, high-repetition-rate TEA CO_2 laser using hydrogen buffered gas mixtures", IEEE J. Quantum Electron. QE-21(1985) 1766.

2-3)H.Akiyama, T.Takamatsu, C.Yamabe and K.Horii : "Suppression of glow-to-arc transition in atmospheric pressure gas discharge of TEA CO_2 laser by high frequency corona discharges", J. Phys. E: Sci. Instrum. 17(1984) 1014.

2-4)C.Yamabe, H.Ishihara, H.Akiyama and K.Horii : "Improvement of laser output of TEA CO_2 laser by high frequency corona discharge", Rev. Laser Eng. 14(1986) 960.

2-5)T.Y.Chang : "Improved uniform-field electrode profiles for TEA laser and high-voltage applications", Rev. Sci. Instrum. 44(1973) 405.

2-6)H.Shields, J.Giannelli and A.L.S.Smith : "X-ray preionized CO_2 laser", Appl. Phys. B 37(1985) 219.

2-7)M.C.Richardson, A.J.Alcock, K.Leopold and P.Burtyn : "A 300-J multigigawatt CO_2 laser", IEEE J. Quantum Electron. QE-9(1973) 236.

2-8)M.C.Richardson, K.Leopold and A.J.Alcock : "Large Aperture CO_2 laser discharges", IEEE J. Quantum Electron. QE-9(1973) 934.

2-9)A.J.Palmer : "A physical model on the initiation of

atmospheric-pressure glow discharges", Appl. Phys. Lett. 25(1974) 138.

2-10)J.I.Levatter and S.Lin : "Necessary conditions for the homogeneous formation of pulsed avalanche discharges at high gas pressures", J. Appl. Phys. 51(1980) 210.

2-11)J.J.Lowke, A.V.Phelps and B.W.Irwin : "Predicted electron transport coefficients and operating characteristics of CO_2-N_2-He laser mixtures", J. Appl. Phys. 44(1973) 4664.

Chapter 3 DEVELOPMENT OF CORONA-PREIONIZED TEA-CO_2 LASER WITH HFCD CIRCUIT RECYCLING RESIDUAL ENERGY

3-1. Introduction

As described in chapter 2, the superposition of HFCD on the main discharge leads both to the keep of a glow discharge for the input energy density over 200J/l and to the increase in the laser output in a corona-preionized TEA-CO_2 laser. However, as the energy for the HFCD operation has to be supplied from another power source, there are problems of enlarging the size of laser device and reducing the total efficiency.

About 10% of the electric stored energy is converted to the laser beam energy, while the rest of the stored energy is lost by heating. Therefore, the heat exchanger is necessary to prevent the temperature of the laser mixture gas from rising in a closed-cycle device at a high-repetition-rate operation. In the experiment described in the previous chapter, it is observed that the voltage across the main electrodes remains for more than 6μs after the main discharge initiation, because the stored energy is not fully injected into the discharge volume. This residual and inefficient energy is considered to be converted to the loss by heating.

Here is described a new HFCD circuit in which the residual

energy not to be injected into discharge volume is collected and recycled as the energy for the HFCD in the next operation. It is called as SC-HFCD (i.e. Self-Charging HFCD) circuit. Using the SC-HFCD circuit, it is expected that the laser device becomes more compact and efficient because of the innecessity of another power source to supply the energy for the HFCD operation. After the PFN circuit is optimized to operate the SC-HFCD circuit without the decrease of laser output, the characteristics of the laser output with the SC-HFCD circuit are examined. Both the collection of the residual energy and the consumption of the energy due to the HFCD operation in the SC-HFCD circuit are also examined, and the output voltage in the SC-HFCD circuit is investigated by the calculation using the equivalent circuit described in 2-4-3.

3-2. Experimental Apparatus and Procedure

Figure 3-1 shows the electrical circuit of the laser device with the SC-HFCD circuit. The same apparatus as the previous chapter except the SC-HFCD circuit is used. The SC-HFCD circuit enclosed by the broken line is composed of the capacitances C_{31} and C_{32} in the two-stage Marx bank, the collecting capacitance C_{30}, the diode D and the inductance L_d. The inductance L_d restricts the amplitude of the current through the diode D so as not to exceed the permitted value of surge current for the diode.

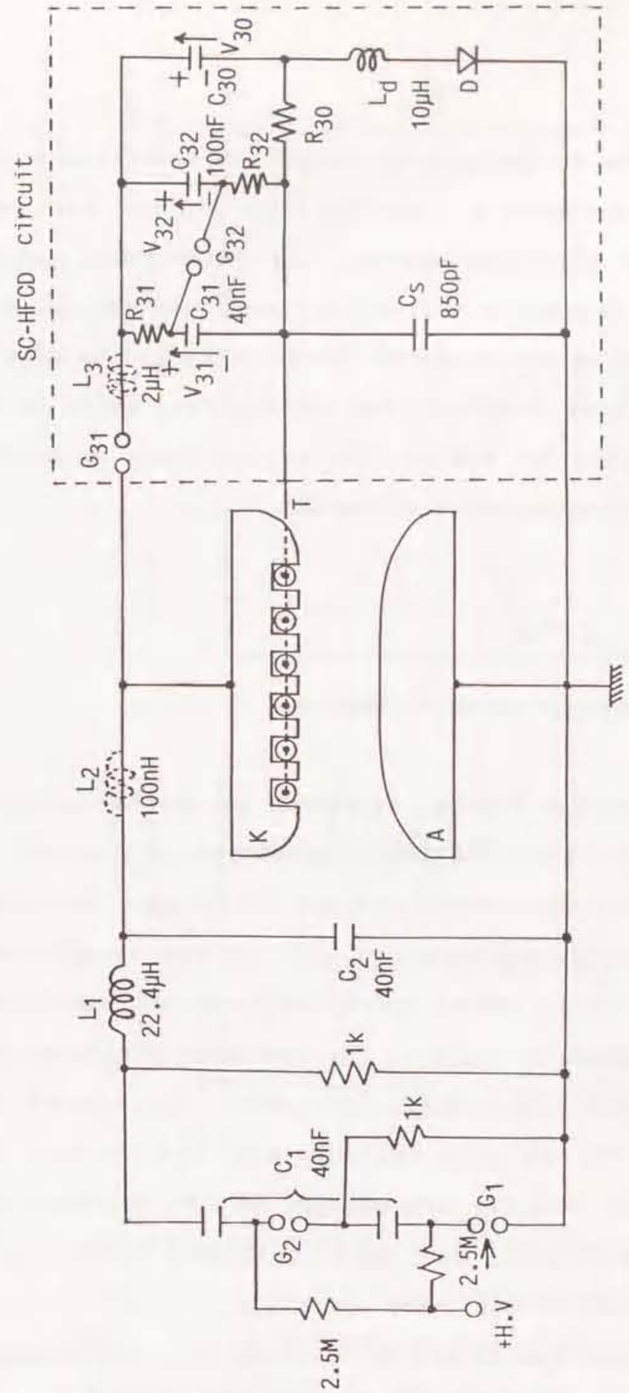

Fig.3-1.Schematic diagram of experimental apparatus and electrical circuit.

The operating sequence of the SC-HFCD circuit is described in 3-3 in detail. The waveforms of the voltage across the main electrodes, the main discharge current, the laser power and the current through the trigger electrode are measured in the same way as chapter 2. The waveform of the current through the diode D is measured with a shunt resistor. The voltage V_{C3}, which is the voltage applied on C_{30}, C_{31} and C_{32} before the laser operation, is measured with an electrostatic voltmeter.

3-3. Operating Sequence of SC-HFCD Circuit

Figure 3-2 shows the typical waveforms of (a)the voltage V across the main electrodes, (b)the main discharge current I_m, (c)the laser power, (d)the current through the trigger electrode, I_t, and (e)that through the diode D, I_d, in the steady-state operation described later, where the SC-HFCD circuit has a two-stage Marx bank as shown in Fig.3-1. The operating parameters are $L_1=10\mu H$, $C_1=C_2=40nF$, $C_{30}=75nF$, $C_{31}=40nF$, $C_{32}=100nF$ and $V_1=68.1kV$, where V_1 is the voltage applied on C_1. The capacitances C_{30}, C_{31} and C_{32} are charged at the voltages V_{30}, V_{31} and V_{32}, respectively, and these voltages remains at a certain voltage V_{C3} before the laser operation.

After the nitrogen-sealed gap G_1 is triggered, the voltage V is applied across the main electrodes and the trigger current passes through the capacitance C_s before the sparks of the main

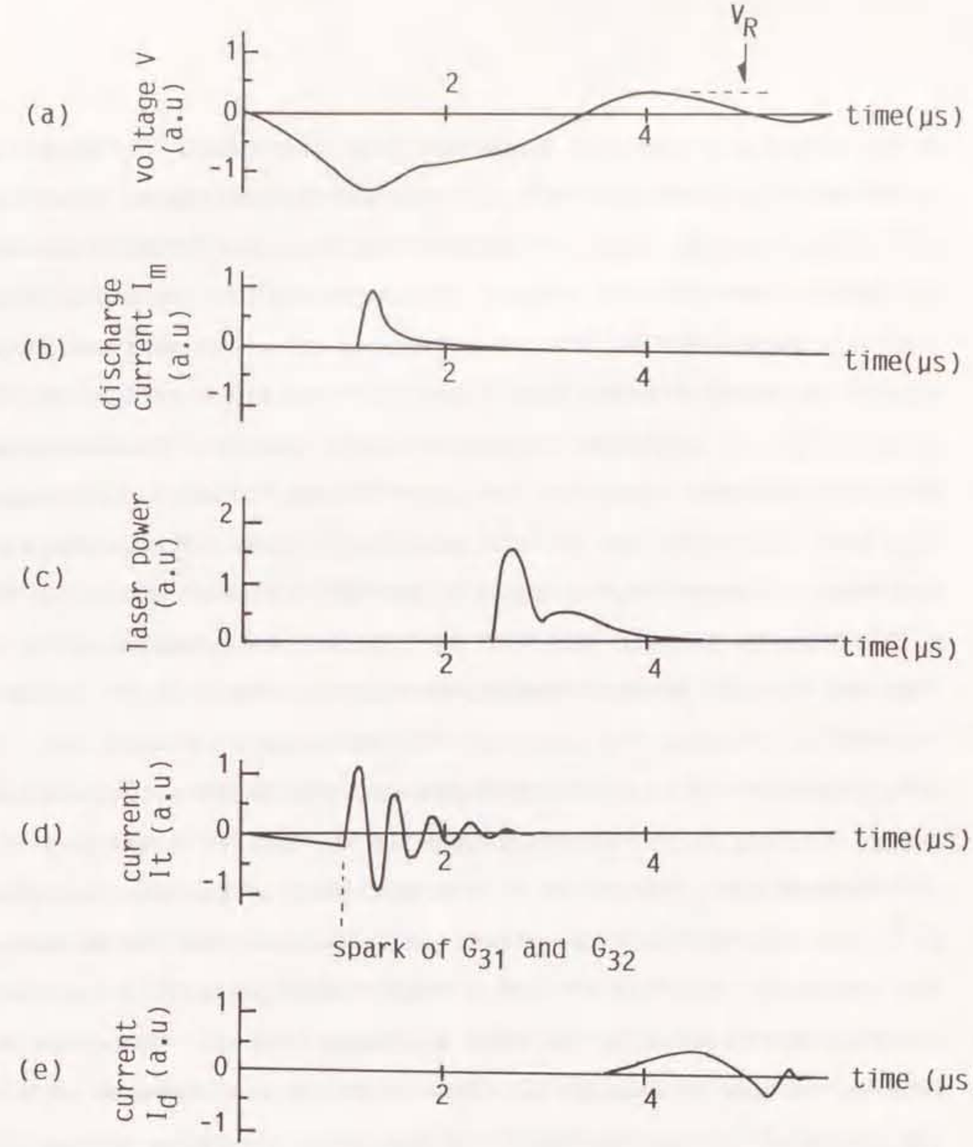

Fig.3-2.Temporal characteristics of (a)voltage across the main electrodes, V, (b)main discharge current, I_m, (c)laser power and (d)current on the trigger electrode, I_t, and (e)that on diode D, I_d, with the operation of SC-HFCD circuit.

electrodes gap and the gaps G_{31} and G_{32}. When V exceeds a critical value, the gaps G_{31} and G_{32} are automatically fired and the output voltage V_{out} of the Marx bank in the SC-HFCD circuit is applied between the trigger electrode and the cathode, where V_{out} is estimated as the value multiplying V_{C3} by the stage number of the Marx bank. The triggering time is controlled by the pressure of the nitrogen gas sealed in G_{31} and G_{32}. Consequently, the HFCD current flows by L-C oscillation through the trigger electrode, C_{31}, C_{32} and L_3. The discharge volume between the main electodes is mainly preionized by the HFCD current prior to the main discharge because the HFCD current has the higher peak value than the trigger current passing through C_s. The flow of the HFCD current also causes V_{31} and V_{32}, the voltages on C_{31} and C_{32}, to drop in proportion to Q_{out} which represents the amount of electrical charge flowing out of the Marx bank in the SC-HFCD circuit.

Before the polarity of V reverses, most of the energy stored on C_1 is injected into the discharge volume and the CO_2 molecules are excited, whereas 5~ 10% of the stored energy, E_R, is not injected and remains in the main discharge circuit. Therefore the reverse voltage V_R appears as shown in Fig.3-2(a) because of both the increase of the impedance in the main discharge volume and the L-C oscillation in the circuit of C_1-L_1-C_2. The residual energy E_R becomes usually the loss by heating of resistances. In this laser device with the SC-HFCD circuit, a part of E_R is collected and recycled as the energy for the HFCD in the next operation in the following way.

The voltages of V_{30}, V_{31} and V_{32} before the laser operation

are equal to V_{C3}. When a glow discharge is produced in the main discharge volume, V is gradually decreased after the main discharge initiation and is increased again up to V_R in the opposite polarity as shown in Fig.3-2(a). Consequently, when V_R is larger than V_{C3}, the charging current flows to C_{30} in the circuit of G_{31}-C_{30}-L_d-D with the electromotive force of V_R-V_{C3} due to the application of the forward voltage on the diode D, and the amount of electrical charge, Q_{in}, is supplied to C_{30}. Then the voltage V_{30} is the value higher than V_{C3} because of collecting the residual energy, whereas the voltages V_{31} and V_{32} are the values lower than V_{C3} because of passing the HFCD current. After the recovery of the insulation in the gaps G_{31} and G_{32}, C_{31} and C_{32} in the Marx bank are slowly charged from C_{30} through the several mega-ohm resistances R_{30}, R_{31} and R_{32}. The voltages V_{30}, V_{31} and V_{32} accordingly settle at a certain value V_{C3}' lower than V_R. If the amount of electrical charge consumed for the HFCD operation is equal to that supplied to C_{30} from PFN while the reverse voltage appears, V_{C3}' is equal to V_{C3}. Then the voltages V_{30}, V_{31} and V_{32} can be maintained at V_{C3} between shots, and the successive laser operation is possible without the change of V_{30}, V_{31} and V_{32}. It is called as the steady-state operation. Thus the residual energy collected in C_{30} is distributed to C_{31} and C_{32}, and is recycled as the energy for the HFCD in the next laser operation.

When V_1 is a relatively large value, a glow discharge is not produced in the first laser operation where V_{30}, V_{31} and V_{32} are zero, because the main discharge volume is preionized only by the

trigger current through C_s. However, when V_1 is a relatively low value, a glow discharge is produced even without the HFCD operation, and C_{30}, C_{31} and C_{32} are charged if the reverse voltage V_R appears. Then it is possible to superpose the HFCD on the main discharge because C_{31} and C_{32} are charged, and a glow discharge is produced evenwhen V_1 is increased slightly. As the reverse voltage V_R is increased with V_1 as described in 3-4-1, V_{30}, V_{31} and V_{32} are increased and a glow discharge is maintained even at the higher V_1. Therefore, repeating such a procedure, the steady-state operation is obtained even at a relatively high voltage of V_1.

3-4. Experimental Results

3-4-1. Determination of PFN Parameters and Laser Mixture Gas for SC-HFCD Circuit

Under the condition that the reverse voltage V_R is so small, the SC-HFCD circuit can not be operated because it is difficult to collect the residual energy due to the small electromotive force in the circuit of G_{31}-C_3-L_d-D. Therefore, it is necessary to determine the conditions of the PFN parameters and the laser mixture gas so as to enlarge V_R without the decrease of the laser output.

The following parameters are determined in the laser device without the SC-HFCD circuit.

(1) PFN parameters of C_1, C_2 and L_1

Sato et al.[3-1] has reported that the ratio C_2/C_1 of about one and C_1 over 20nF are preferable to obtain large laser output. Therefore, the combinations (C_1,C_2) of (40nF,40nF) and (60nF,52nF) as well as L_1 between 1μH and 22.4μH are examined in this experiment.

(2) Ratio of N_2, CO_2 and He in the laser mixture gas

As shown in Fig.3-3, the optimal ratio of N_2/CO_2 in the laser mixture gas is 1:1, and this mixture ratio has been popularly used[3-2]-[3-5]. Therefore the optimal ratio of He is examined at atmospheric pressure, changing the flow rate of He to other gases at a constant flow rate of N_2/CO_2= 1/1(l/min).

Figure 3-4 shows the relationship between the input energy density and the laser output as parameters of (C_1,C_2) and the flow rate of He at L_1=10μH. When the flow rate of He is 3(l/min) at (C_1,C_2)=(40nF,40nF) or 4(l/min) at (C_1,C_2)=(60nF,52nF), the laser output has a maximum value at the input energy density of 220J/l.

Figure 3-5 shows the variation of the reverse voltage V_R with the input energy density as parameters of (C_1,C_2) and the flow rate of He. The voltage V_R at (C_1,C_2)=(40nF,40nF) becomes so large as compared with that at (C_1,C_2)=(60nF,52nF). On the other hand, V_R is increased with the input energy density. This characteristic of V_R is favorable to the suppression of the glow-to-arc transition as described in 3-4-3.

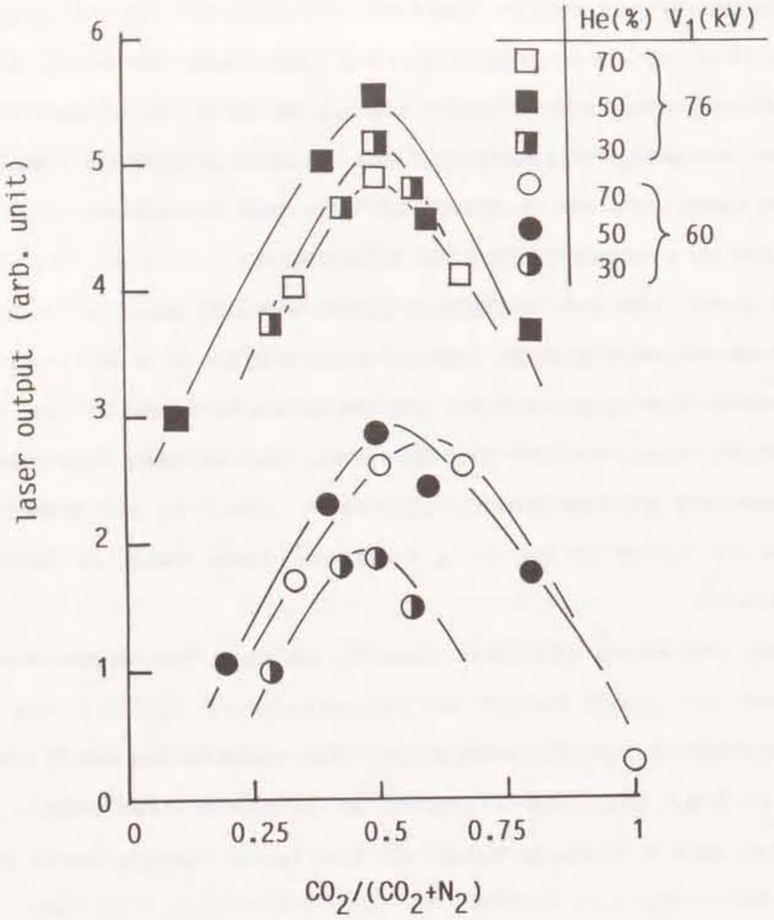

Fig.3-3.Variation of laser output as a function of CO_2/N_2 mixture ratio as parameters of voltage V_1 and mixture ratio of He.

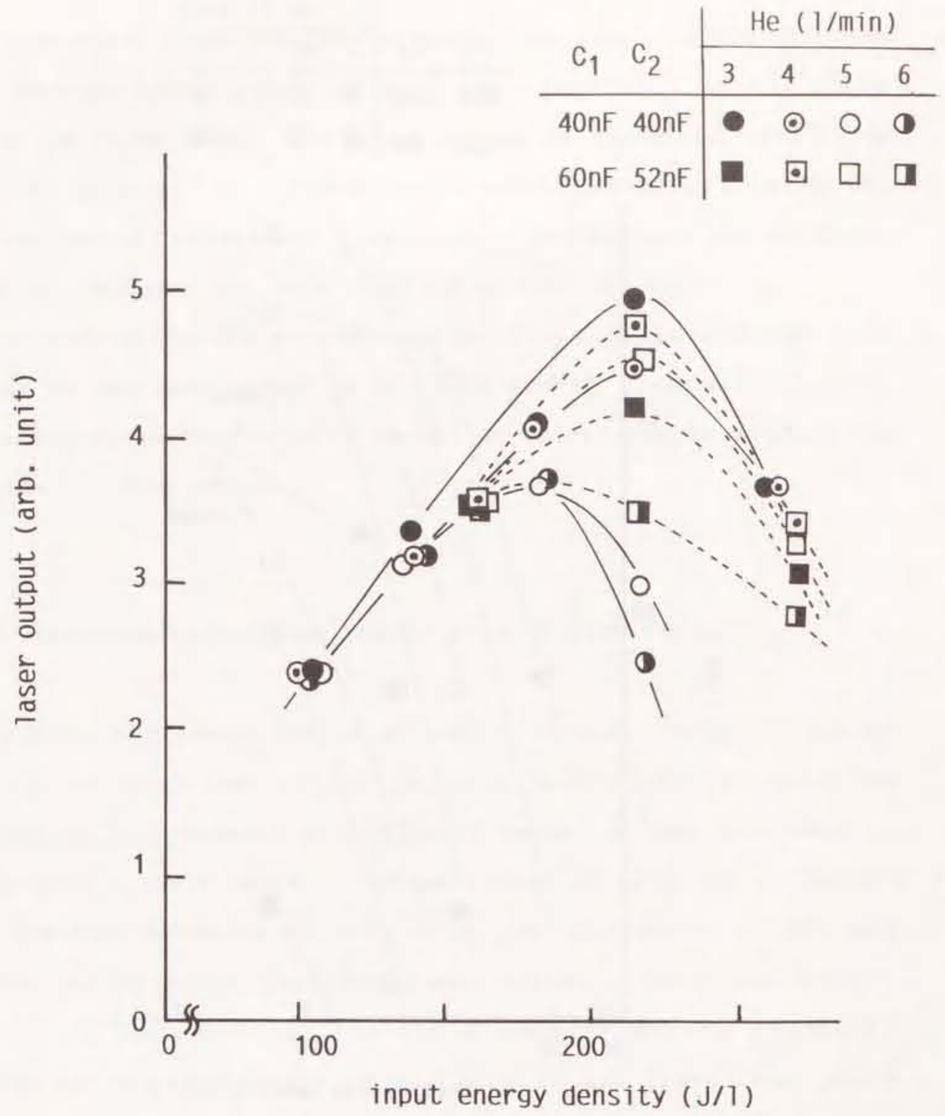

Fig.3-4.Relationship between input energy density and laser output as parameters of flow rate of He and combination (C_1,C_2) at $L_1=10\mu H$.

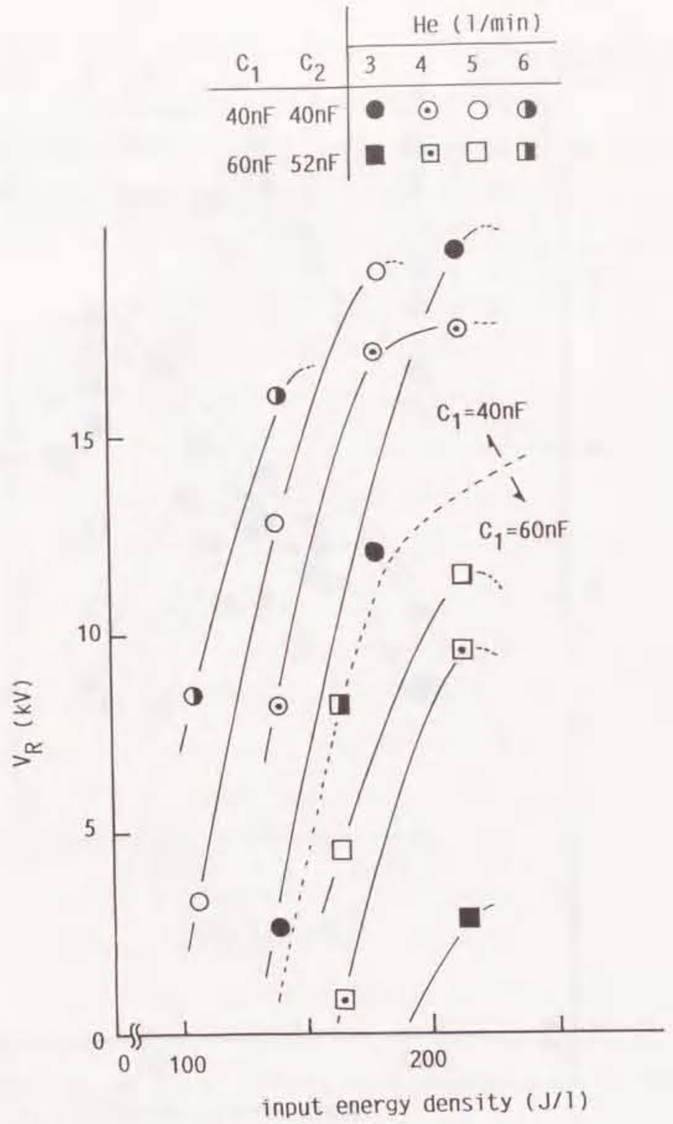

Fig.3-5. Variation of reverse voltage V_R with input energy density as parameters of combination (C_1,C_2) and flow rate of He at $L_1=10\mu H$.

Figure 3-6 shows the variation of the laser output with the input energy density up to 200J/l as a parameter of L_1, where (C_1,C_2) is (40nF,40nF). The laser output is increased with L_1 up to 10μH, whereas the glow-to-arc transition described in the previous chapter causes the laser output to decrease for $L_1>10\mu H$. A similar tendency has been reported by Sato et al.[3-1].

According to the above results, (C_1,C_2), L_1 and the flow rate of He are determined to be (40nF,40nF), 10μH and 3(l/min), respectively, as the suitable condition to enlarge V_R without the decrease of laser output.

3-4-2. Improvement of Laser Output with SC-HFCD Circuit

Figure 3-7 shows the relationship between the input energy density and the laser output in the steady-state operation at $C_{30}=75nF$ as a parameter of the stage number of the Marx bank in the SC-HFCD circuit. When the stage number is equal to 1, the SC-HFCD circuit is operated both with the shortening of R_{31} and without the spark of G_{32}. The laser output without the SC-HFCD circuit is saturated at the input energy density of 230J/l because of the occurrence of the glow-to-arc transition, while the laser output with the SC-HFCD circuit is increased for the input energy density over 230J/l. Using the SC-HFCD circuit with a two-stage Marx bank, the maximum laser output of 8.75J is obtained at the input energy density of 250J/l, and the arc-free condition is maintained for the input energy density up to

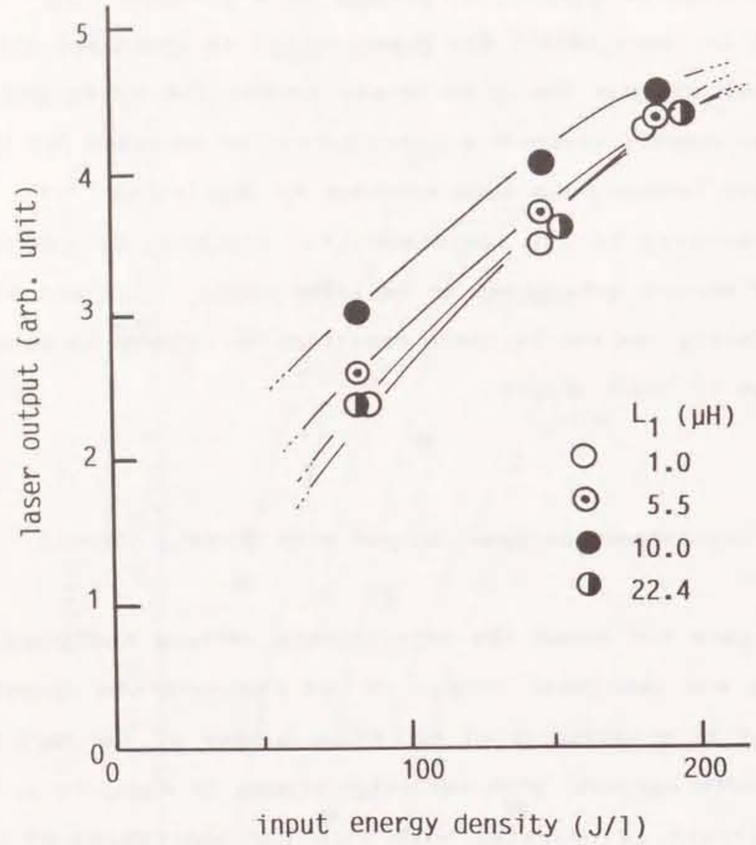

Fig.3-6.Variation of laser output with input energy density as a parameter of L_1.

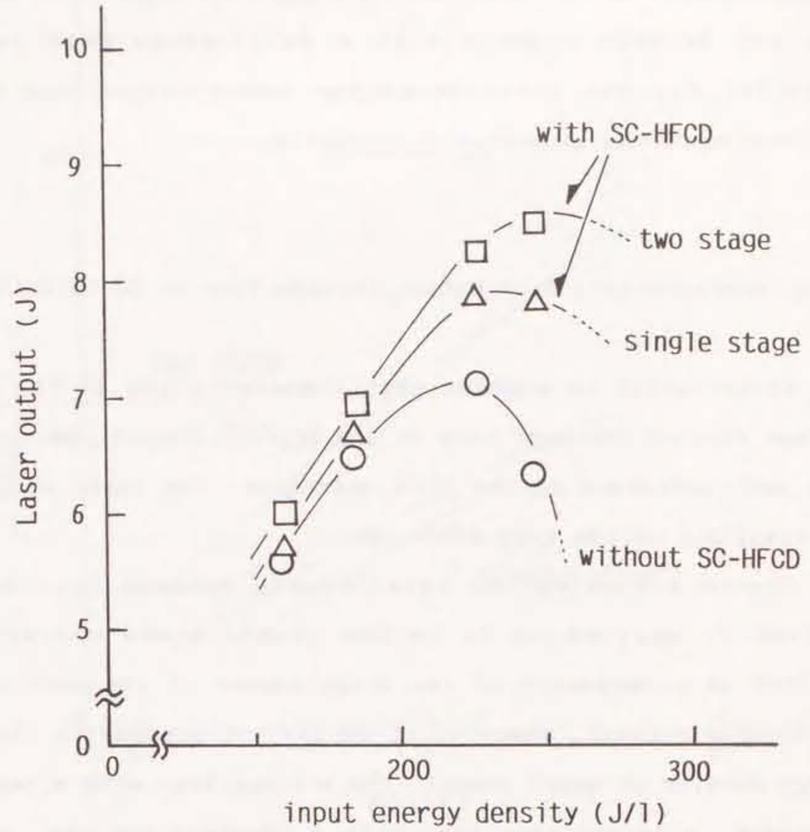

Fig.3-7.Relationship between input energy density and laser output as a parameter of stage number of Marx bank in SC-HFCD circuit.

230J/l. The laser output of 8.75J corresponds to the output energy density of 17.5J/l. It is suggested from these results that the SC-HFCD circuit with a multi-stage Marx bank is effective for the increase of the laser output due to the suppression of the glow-to-arc transition.

3-4-3. Characteristics of Output Voltage V_{out} of SC-HFCD Circuit

It is useful to examine the characteristics of the output voltage V_{out} of the Marx bank in the SC-HFCD circuit because V_{out} have much influence on the HFCD operation, the laser output and the stability of the main discharge.

Figure 3-8 shows the relationship between V_{out} and the voltage V_1 applied on C_1 in the steady-state operation at C_{30}=75nF as a parameter of the stage number of the Marx bank in the SC-HFCD circuit, where V_1 of 68.1kV corresponds to the input energy density of about 186J/l. The voltage V_{out} with a two-stage Marx bank is larger than that with a single-stage one, and the laser output is increased with the stage number as shown in Fig.3-7. On the other hand, V_{out} is increased with V_1 because of the increase of the reverse voltage V_R. This tendency in V_{out} is favorable to suppress the glow-to-arc transition, because it is necessary for the HFCD current to have a higher peak value as the input energy density is increased. The characteristics of V_{out} are discussed in 3-6, using the equivalent circuit.

After the charging current flows into C_{30} through the diode

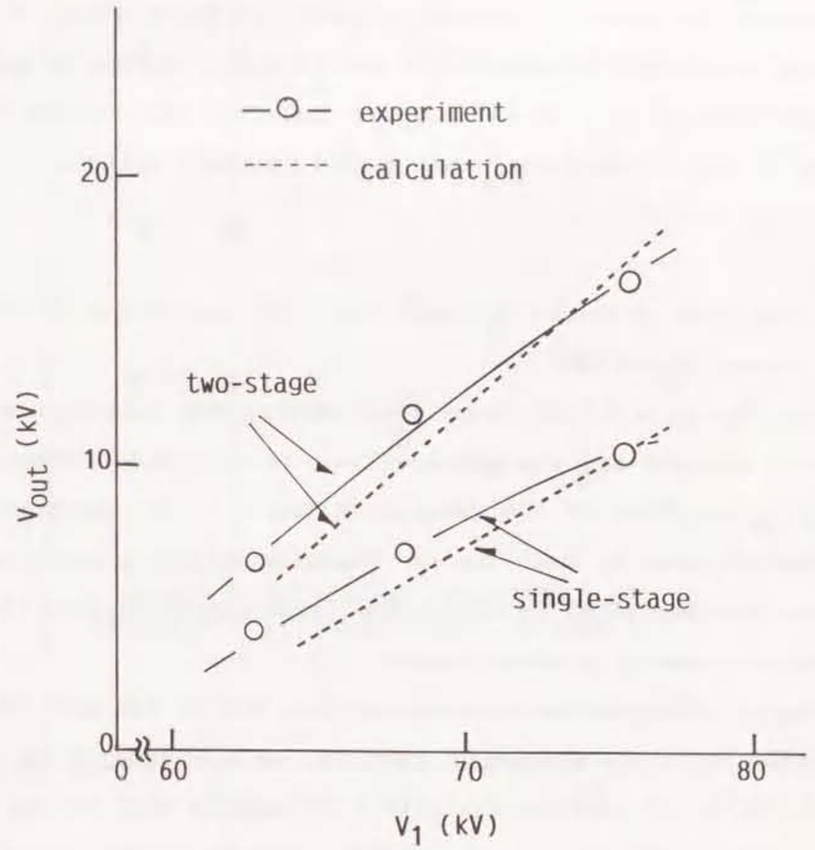

Fig.3-8. Dependence of output voltage V_{out} on applied voltage V_1 as a parameter of stage number of Marx bank in SC-HFCD circuit.

D, the recovery current of the diode is observed in the polarity opposite to the charging current as shown in Fig.3-2(e). As the amount of electrical charge due to the recovery current is not so small, it causes V_{out} to be reduced. Therefore the voltage V_{out} will be larger if the diode D has a good recovery ability.

3-4-4. Decrease of Output Voltage V_{out} with Occurrence of Glow-to-Arc Transition

When the glow-to-arc transition occurs, the capacitance C_{30} cannot be charged and the voltage V_{out} is decreased because of the rapid reduction of the reverse voltage. It is important to make the decrease of V_{out} due to the glow-to-arc transition as small as possible so as to insure the laser operation even if the glow-to-arc transition should occur.

Figure 3-9 shows the decrease of V_{out} due to the glow-to-arc transition with the number of shot, i, as a parameter of C_{30}, where V_1 is 68.1kV and the control of triggering time of the HFCD current due to the change of the gas pressure in G_{31} makes the glow-to-arc transition rate be 100% artificially after C_{30}, C_{31} and C_{32} are sufficiently charged in the steady-state operation until i_0 using the SC-HFCD circuit. The voltage V_{out} is gradually decreased with i, and is maintained at a relatively high value with the increase of C_{30} even if the several glow-to-arc transitions occur successively. Therefore it is required to increase C_{30} in order to insure the laser operation against the glow-to-arc transition because the keep of V_{out} at a high value

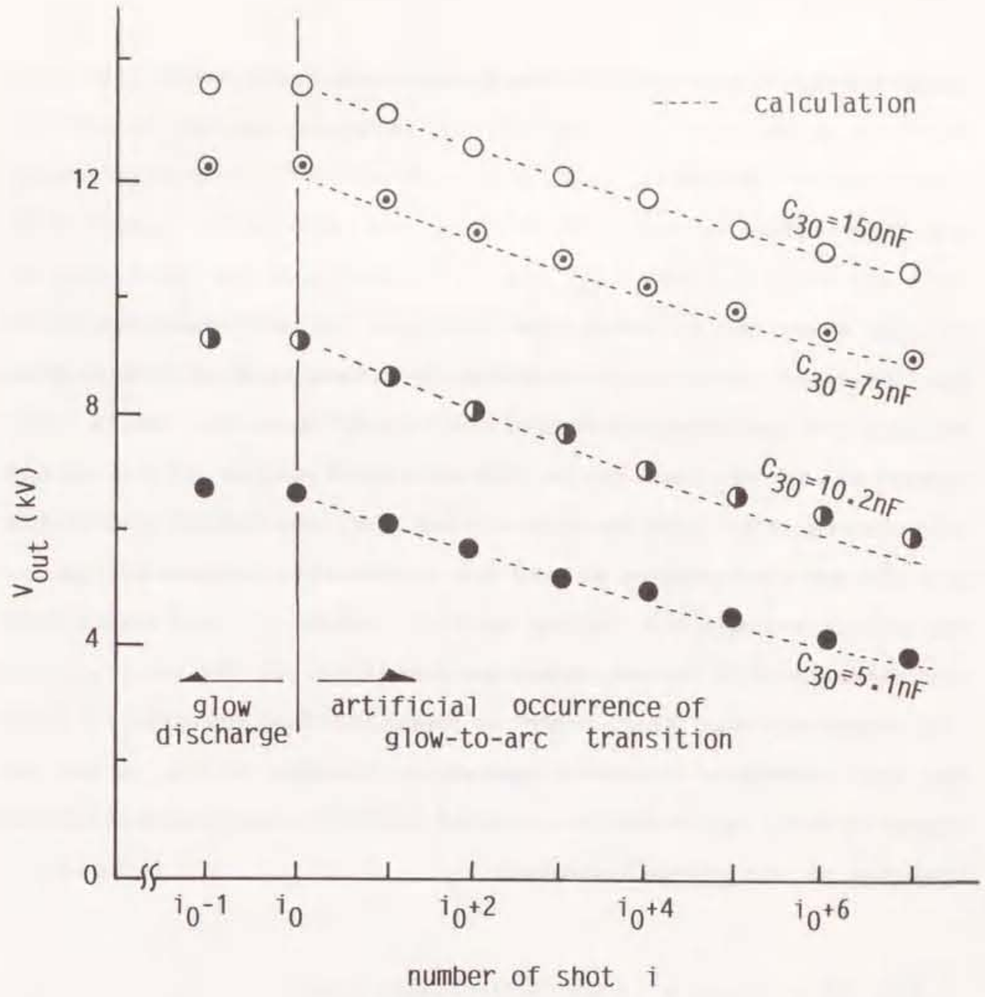

Fig.3-9. Decrease of output voltage V_{out} due to glow-to-arc transition with number of shot, i, as a parameter of C_{30}.

leads to the suppression of the glow-to-arc transition.

3-5. Discussion

As described in 2-4-3, the HFCD current is considered to be the transient charging current from the Marx bank in the SC-HFCD circuit to the parallel-connected capacitances C_s and C_g (the capacitance of the glass tubes which cover the trigger electrodes) under the condition that the impedances of the PFN and the main discharge plasma are negligible compared with C_s. The output voltage V_{out} of the SC-HFCD circuit is here calculated and compared with the experimental results.

Assuming that V_{C3}, which is equal to the voltages on C_{30}, C_{31} and C_{32} before the laser operation, changes to V_{C3}' after the laser operation, V_{C3}' is related with V_{C3} by the following equation on the charge conservation:

$$\sum_{i=0}^{n} C_{3i} \cdot V_{C3}' = \sum_{i=0}^{n} C_{3i} \cdot V_{C3} - n \cdot Q_{out}(V_{C3}) + Q_{in}(V_1, V_{C3}) \quad , \qquad (3\text{-}1)$$

$$V_{out} = n \cdot V_{C3} \quad , \qquad (3\text{-}2)$$

where n is the stage number of the Marx bank in the SC-HFCD circuit (n=1 or 2 in this experiment), C_{3i} at i=0 is the electrostatic capacity of the capacitance C_{30} to collect the residual energy and C_{3i} for $i \geq 1$ is that of i-th stage

capacitance in the Marx bank. The value Q_{in} is the amount of electrical charge supplied to C_{30} while the reverse voltage appears, and the value Q_{out} is that flowing out of each capacitance in the Marx bank by the HFCD current. The value Q_{in} is considered as functions of V_1 and V_{C3}, and it is obvious from the other experimental results shown in Fig.3-10 that Q_{in} is decreased linearly with the increase of V_{C3}.

It is assumed that the conductivity of G_{31} and G_{32} is sufficiently maintained until the voltage across the main electrodes disappears. The amount of electrical charge Q_{out} can be approximately expressed by the following equation as a function of V_{C3}, estimating the amount of electrical charge flowing from the series-connected capacitances in the Marx bank, which correspond to C_3 charged at the voltage $n \cdot V_{C3}$ in Fig.2-13, to the parallel-connected capacitances of C_s and C_g (the capacitance of the glass tubes which cover the trigger electrodes):

$$Q_{out}(V_{C3}) = \frac{n \cdot V_{C3} \cdot (C_s + C_g) \cdot (1/\sum_{i=1}^{n}(1/C_{3i}))}{C_s + C_g + 1/\sum_{i=1}^{n}(1/C_{3i})} \quad , \qquad (3\text{-}3)$$

In the steady-state operation, eq.(3-1) can be transformed to the following equation because V_{C3}' equals to V_{C3}:

$$Q_{in}(V_{C3}) = n \cdot Q_{out}(V_{C3}) \quad . \qquad (3\text{-}4)$$

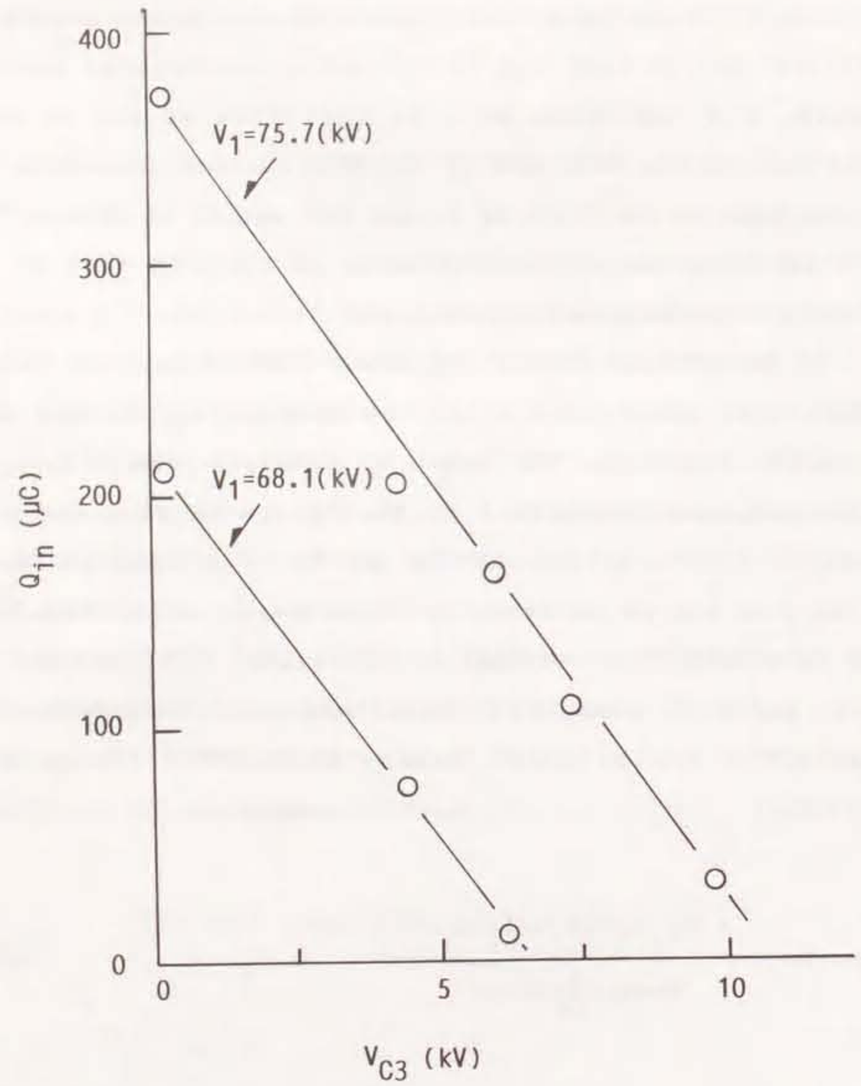

Fig.3-10.Relationship between voltage V_{C3} and amount of electrical charge Q_{in} as a parameter of applied voltage V_1.

Resolving eq.(3-4) for V_{C3}, the calculated variation of V_{out} expressed by eq.(3-2) in the steady-state operation is shown in Fig.3-8 with the observed value. It is obvious that the comparatively good agreement between the observed and calculated values is obtained.

On the other hand, the decrease of V_{out} due to the glow-to-arc transition is calculated, where the residual energy is not collected because the reverse voltage V_R do not appear. Therefore eq.(3-2) can be transformed to the following equation, substituting zero and eq.(3-3) for Q_{in} and Q_{out}, respectively:

$$V_{C3}' = V_{C3} \cdot \left[1 - \frac{n^2 \cdot (C_s+C_g) \cdot 1/\sum_{i=1}^{n}(1/C_{3i})}{(C_s+C_g+1/\sum_{i=1}^{n}(1/C_{3i})) \cdot \sum_{i=0}^{n} C_{3i}} \right] , \qquad (3\text{-}5)$$

Letting the successive occurrence times of the glow-to-arc transition be m, V_{C3}' can be expressed by the following geometrical progression:

$$V_{C3} = V_{C30} \cdot \left[1 - \frac{n^2 \cdot (C_s+C_g) \cdot 1/\sum_{i=1}^{n}(1/C_{3i})}{(C_s+C_g+1/\sum_{i=1}^{n}(1/C_{3i})) \cdot \sum_{i=0}^{n} C_{3i}} \right]^{m-1} , \qquad (3\text{-}6)$$

where V_{C30} is the initial value of V_{C3}. Substituting eq.(3-6) for eq.(3-2), the calculated variation of V_{out} at n=2 is shown with broken lines in Fig.3-9. The considerably good agreement between the observed and calculated values is obviously obtained. From

the above results, the characteristics of V_{out} can be predicted if Q_{in} and the initial value V_{C30} are known.

Next, the energy saved by the SC-HFCD circuit is estimated. If the capacitances in the n-stage Marx bank are charged with another transformer, the energy E_{HFCD} supplied for one HFCD operation is expressed by the following equation:

$$E_{HFCD} = 2\cdot\left[\sum_{i=1}^{n}\frac{V_{C3}^2\cdot C_{3i}}{2} - \frac{Q_{out}^2}{2(C_s+C_g)} - \sum_{i=1}^{n}\frac{(V_{C3}\cdot C_{3i}-Q_{out})^2}{2C_{3i}}\right] \quad . \qquad (3\text{-}7)$$

In practice, the hysterisis loss and the iron loss in the transformer are added to E_{HFCD}. Eliminating V_{C3} and Q_{out} in eq.(3-7) by eq.(3-2) and (3-3), the relation between E_{HFCD} and V_{out} is shown in Fig.3-11, where n=2. At V_1=75.8kV where V_{out} is about 16kV as shown in Fig.3-8, the energy E_{HFCD} is 0.7J, while the energy stored on C_1 is about 115J. Therefore it is estimated that the electric energy is saved by the order of 1 percent of the stored energy using the SC-HFCD circuit.

Although the energy is saved by only ~ 1% with the SC-HFCD circuit in this experiment, the more energy might be saved when the capacitance of the glass tube or the stage number of the Marx bank is increased to intensify the corona preionization.

3-6. Conclusion

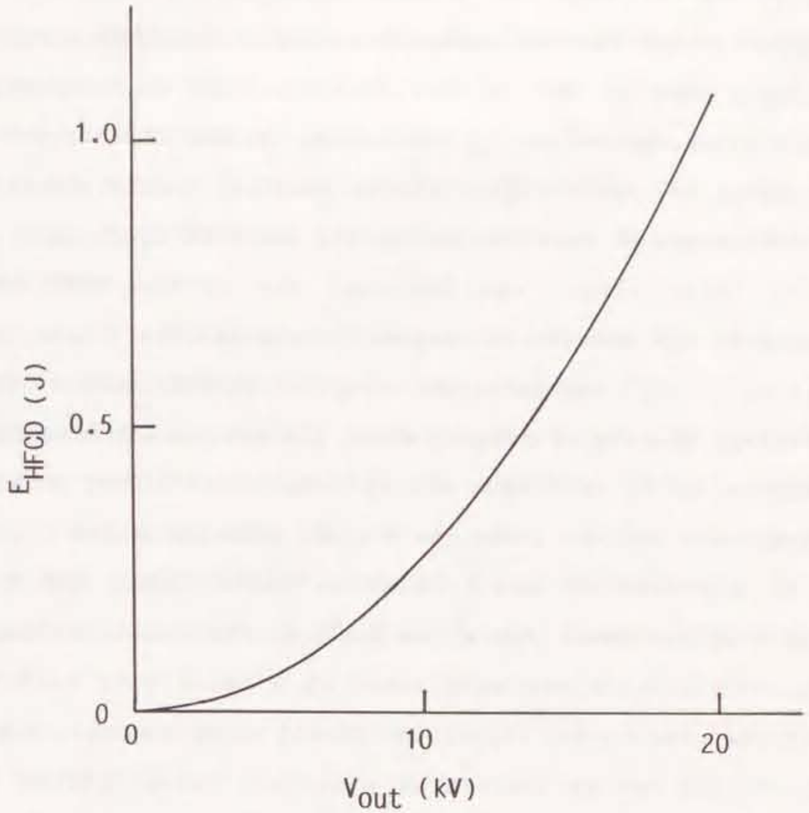

Fig.3-11.Relationship between output voltage V_{out} and energy for a HFCD operation, E_{HFCD}.

A new HFCD circuit called as SC-HFCD circuit has been devised, and the HFCD was able to be superposed on the main discharge without another energy source for the HFCD circuit by recycling a part of the residual energy not to be injected into the main discharge volume as the energy of the HFCD in the next laser operation. Accordingly, it was possible to miniaturize the laser device and to save the energy for the HFCD operation.

The laser output was improved due to the HFCD effect similarly to the results in chapter 2. The maximum output energy density of 17.5J/l was obtained using the SC-HFCD circuit at the input energy density of 250J/l, while the arc-free discharges can be produced up to the input energy density of 230J/l after the PFN parameters and the laser gas mixture were optimized.

The increase of the collecting capacitance led to the insurance of the laser operation because the output voltage of the SC-HFCD circuit was maintained at a relatively high value even if the glow-to-arc transition should occur successively. The output voltage was maintained at a certain value between laser operations under the condition that the amount of electrical charge flowing into the SC-HFCD circuit was equal to that flowing out of the SC-HFCD circuit.

References

3-1)S.Sato, C.Yamabe and K.Horii : "An analysis of the laser output properties for a TEA CO_2 laser with the design of experiments", Trans. IEE Jpn. 100-A(1980) 657, in Japanese.

3-2)R.Marchetti, E.Penco and G.Salvetti : "Sealed, miniaturized, corona-preionized, high-repetition-rate TEA- CO_2 laser using hydrogen buffered gas mixtures", IEEE J. Quantum Electron. QE-21(1985) 1766.

3-3)G.J.Ernst : "A 10cm aperture, high quality TEA CO_2 laser", Opt. Commun. 44(1982) 125.

3-4)O.P.Judd and J.Y.Wada : "Investigations of a UV preionized electrical discharge and CO_2 laser", IEEE J. Quantum Electron. QE-10(1974) 12.

3-5)P.E.Dyer and D.N.Raouf : "Axial X-ray preionization of a 10 atmosphere pressure TE CO_2 laser", Opt. Commun. 53(1985) 36.

CHAPTER 4 GENERATION OF ACOUSTIC VIBRATION IN ELECTRIC SUSPENSION INSULATOR WITH IRRADIATION OF PULSED CO_2 LASER BEAM

4-1. Introduction

It is well known that, irradiating a pulsed laser beam onto the surface of a substance, the acoustic vibration of the substance is generated by thermal shock due to the heating of laser beam or reaction of a laser-produced plasma etc.[4-1][4-2]. Moreover, the conversion efficiency from the optical energy to the vibrational energy depends on the irradiation intensity of the laser beam on the substance. When the substance is intensively irradiated with a pulsed laser beam, the efficient conversion to the acoustic vibration is obtained by the laser produced plasma[4-3]. On the other hand, the acoustic vibration due to thermal shock is generated with a considerably low efficiency by irradiating a relatively weak laser beam on the substance[4-1].

In this chapter, it is investigated how the irradiation intensity of a pulsed CO_2 laser beam influences on the vibration of an electric suspension insulator. Also, the principle of vibration is inferred from the figure of the time-integrated (still) photographs on the surface of the insulator with the

irradiation of the CO_2 laser beam, and the consistency of the inferred principle is examined in comparison with the experimental results.

4-2. Experimental Apparatus and Procedure

Figure 4-1 shows the schematic diagram of the experimental apparatus. A pulsed laser beam from a TEA-CO_2 laser, focused by a convex germanium lens whose focal length is about 10cm, is irradiated onto the surface of an electric suspension insulator without a crack. The insulator is made of ceramics with the diameter of about 26cm. The irradiation intensity on the surface of the insulator varies both with the laser beam energy in the range of 2.4~ 5.9 joules and with the distance between the convex germanium lens and the surface of the insulator, d, as shown in Fig.4-1. The diameter and the pulse width of the CO_2 laser beam are about 3cm and 400nsec, respectively.

The vibration of the insulator is measured both with a He-Ne laser interferometer and with an acceleration sensor touched on the surface of the insulator. The He-Ne laser beam is divided to two beams by a beam splitter. One beam is irradiated and reflected on the surface of the insulator, and is used through the slide glass as an objective beam of the laser interferometer. Another beam as a reference beam is reflected on the slide glass after passing through the beam expander and the ND filter so that

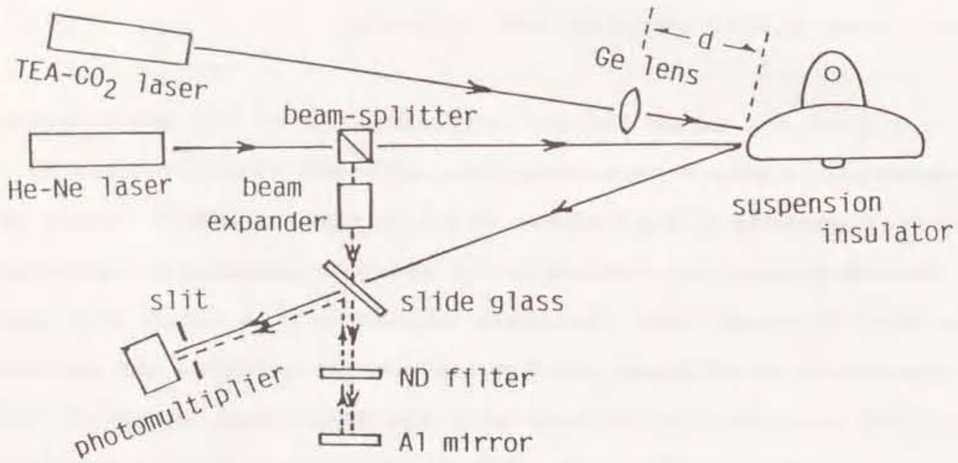

Fig.4-1.Schematic diagram of experimental apparatus.

the divergence and the intensity of the reference beam could correspond to those of the objective beam. Overlapping with the objective beam, the reflected reference beam propagates to a photomultiplier through a slit to detect the change of the interference pattern due to the vibration of the insulator. The acceleration sensor has the minimum measurable acceleration of about 10G and the upper-limit frequency of about 15kHz, while the laser interferometer has the minimum measurable displacement of about 10nm and the upper-limit frequency of about 10kHz.

The amplified signals of the photomultiplier and the acceleration sensor are recorded with the storage oscilloscope so as to analyze the frequency components of the signals by performing Fast Fourier Transform (known as FFT).

4-3. Experimental Results

4-3-1. Phenomena on Surface of Electric Insulator with Irradiation of Laser Beam

Figure 4-2 shows the time-integrated photographs of the phenomena on the surface of the insulator irradiated with the CO_2 laser beam as a parameter of d in the range of 3.5～10.5cm, where the laser beam energy is about 3 joules. Immediately after the irradiation, the surface slightly shines at d=3.5cm as shown in Fig.4-2(a). However, the increase of d results in heating the

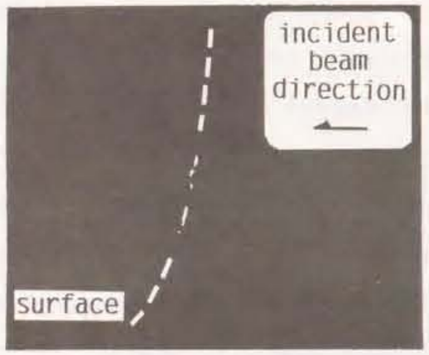

(a) d=3.5cm

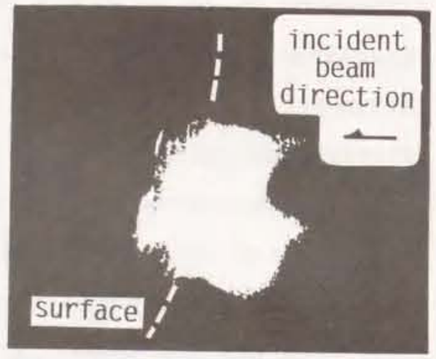

(b) d=8.2cm

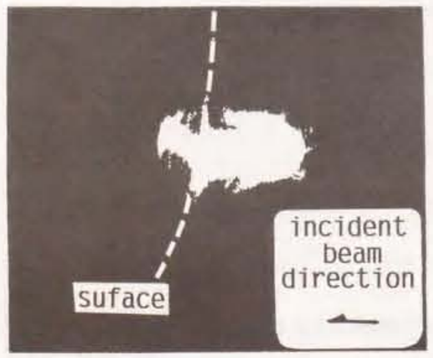

(c) d=9.5cm

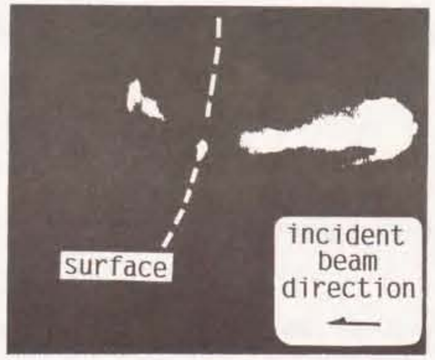

(d) d=10.5cm

Fig.4-2.Phenomena on surface of insulator (a) at d=3.5cm, (b) at d=8.2cm, (c) d=9.5cm and (d) d=10.5cm.

surface more locally and strongly, and the plasma spouts from the whole of the spot area at d=8.2cm as shown in Fig.4-2(b). The intensive air breakdown plasma is observed besides the spouting plasma at d=9.5cm as shown in Fig.4-2(c). Furthermore, in the case of d=10.5cm, the air breakdown plasma can be more clearly observed whereas the spouting plasma is seldom observed as shown in Fig.4-2(d), where the focal point of the germanium lens is in front of the surface of the insulator.

The air in front of the insulator is weakly ionized by the strong UV radiation from the spot area with the intensive irradiation of the pulsed laser beam, and the explosive increase of the electrons in the low-ionized plasma due to inverse bremsstrahlung results in the air breakdown.

4-3-2. Temporal Variation of Laser-Induced Acoustic Vibration of Electric Suspension Insulator

Figure 4-3 shows the temporal waveforms of the signals of the acceleration sensor and the photomultiplier for the electric suspension insulator at d=8.2cm and 5.9J of the laser beam energy. These signals continues for more than 100msec at several kiro-hertz after the irradiation of the laser beam.

Figure 4-4 shows the relative temporal variations of the frequency spectrums for the signals of the acceleration sensor and the photomultiplier during the time of 1-31msec, 70-100msec, 150-180msec, 230-260msec after the irradiation of the laser beam.

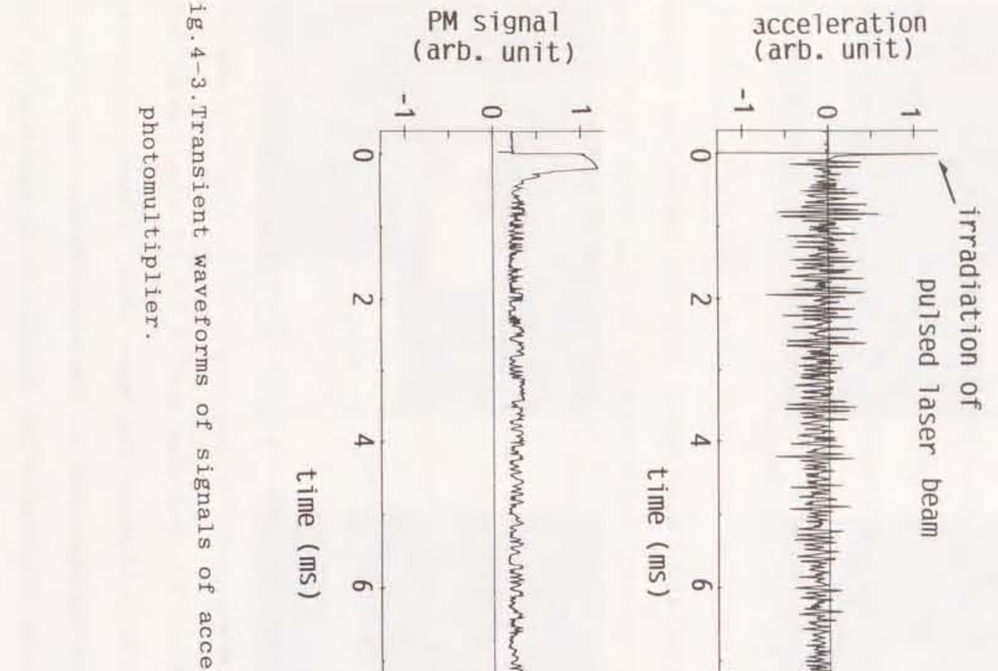

Fig.4-3.Transient waveforms of signals of acceleration sensor and photomultiplier.

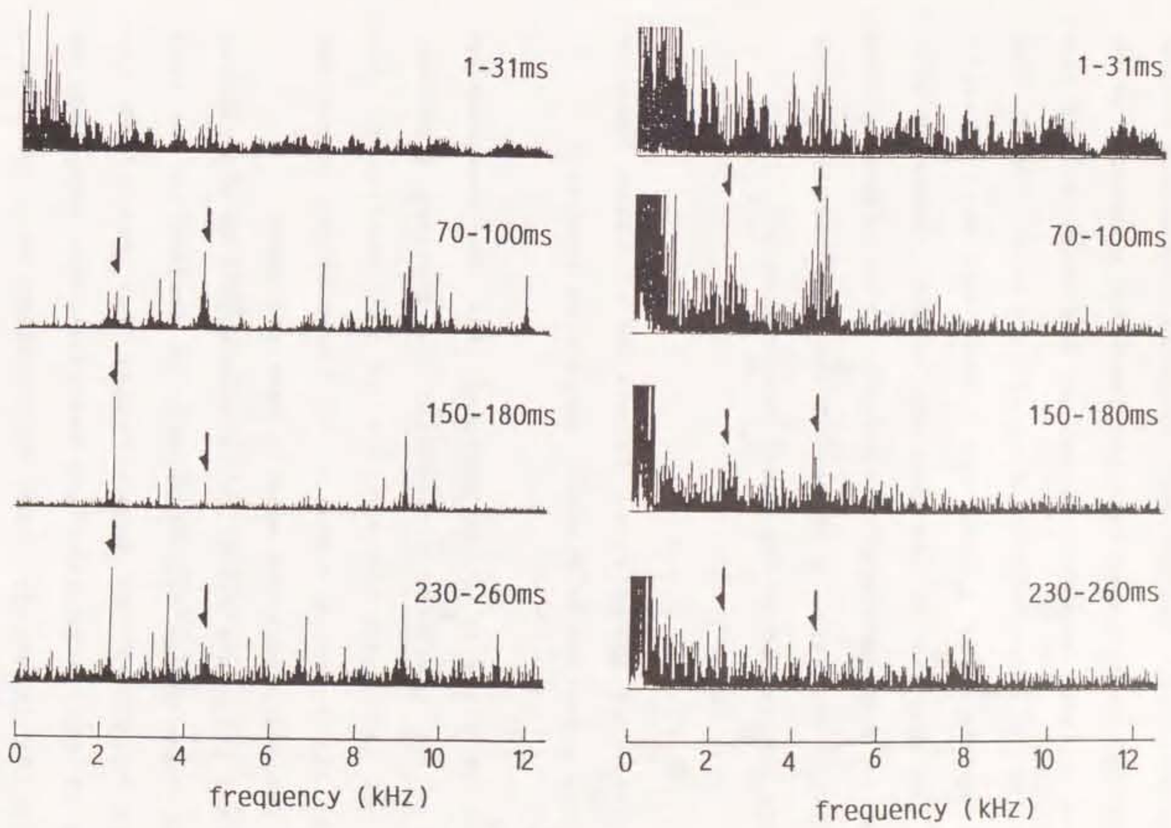

Fig.4-4.Temporal relative variations of frequency spectrums for signals of (a)acceleration sensor and (b)photomultiplier.

These signals obviously includes many frequency components during 1-31msec. However, it is found that the insulator continues to be vibrated in a natural mode to depend on the material and the shape of the insulator with the passing of time after 70msec. The frequency components of 2.2kHz and 4.4kHz are more clearly observed in the spectrum of the photomultiplier, comparing with the spectrum of the acceleration sensor. After 230msec, the natural vibration decays to a degree of the amplitude less than the detectable limitation of the laser interferometer.

4-3-3. Influence of Irradiation Intensity of Laser Beam on Acoustic Vibration of Electric Suspension Insulator

As shown in Fig.4-2, it is observed that the phenomena on the surface of the insulator varies with the distance d between the germanium lens and the surface of the insulator. The dependence of the acoustic vibration on the distance d and the irradiation intensity of laser beam is examined here.

Figure 4-5 shows the variation of a_{rms} with d as a parameter of the laser beam energy E_L, where a_{rms} is defined as the root mean square value of the acceleration for 2ms after the irradiation of the laser beam and indicates the amplitude of vibration in the insulator. The acceleration a_{rms} shows the maximum value at $d=d_{opt}$(8～ 9cm), and the variation of a_{rms} consists of the following three regions.

1)region 1:the acceleration a_{rms} is independent of d for $d<d_{th}$.

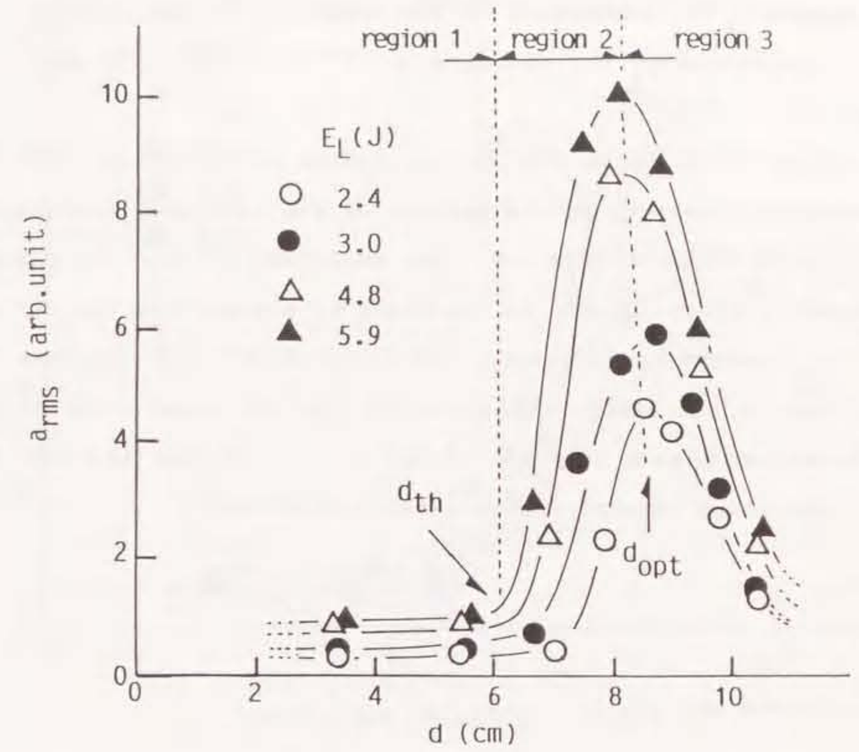

Fig.4-5.Variation of acceleration a_{rms} with distance d as a parameter of laser beam energy E_L.

2)region 2:the acceleration a_{rms} is increased with d for $d_{th}<d<d_{opt}$.
3)region 3:the acceleration a_{rms} is decreased with d for $d>d_{opt}$.
The phenomena on the surface of the insulator in the regions 1, 2 and 3 correspond to the photographs of Fig.4-2(a), (b) and (c), respectively.

Figure 4-6 shows the relationship between a_{rms} and the irradiation intensity on the surface of the insulator rearranging the results shown in Fig.4-5. The amplitude of a_{rms} is rapidly increased correspondingly to the spout of plasma from the surface for the irradiation intensity over about $2\times10^7 W/cm^2$, whereas the amplitude is decreased correspondingly to the generation of the air breakdown plasma in front of the surface of the insulator for the irradiation intensity over about $6.5\times10^7 W/cm^2$.

4-4. Discussion

The acceleration a_{rms} intensively depends on the irradiation intensity and the phenomena on the surface of the insulator as described in 4-3-3. It is suggested that the observed plasma and the generated heat on the surface are associated with the vibration of the insulator, and the following processes are considered as the principles of the vibration; 1)the thermal shock by heating of the laser beam, 2)the reaction of the particles spouting from the insulator, 3)the shock wave from the air breakdown plasma generated by the laser beam in front of the

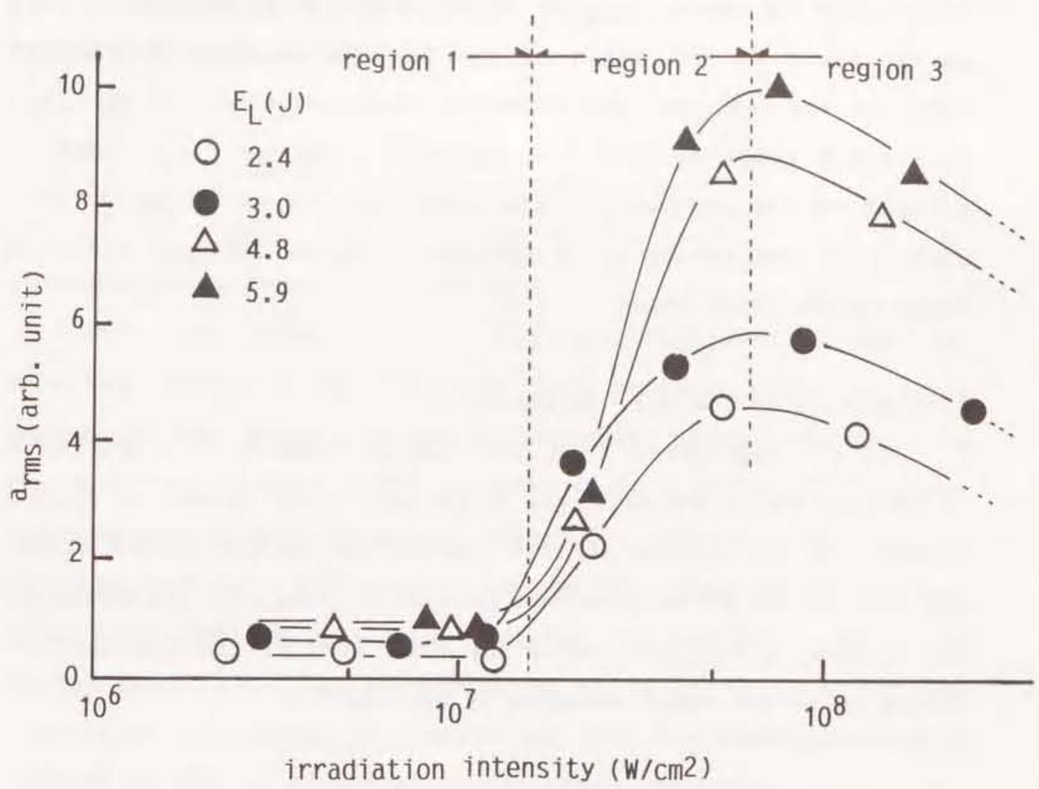

Fig.4-6.Variation of acceleration a_{rms} with irradiation intensity of laser beam as a parameter of laser beam energy E_L.

surface of the insulator. In this section, the principle of the vibration in each region shown in Figs.4-5 and 4-6 is investigated on the basis of the time-integrated photographs shown in Fig.4-2, and the observed characteristics of a_{rms} are relatively compared with the calculated forces F_1, F_2 and F_3 applied on the surface of the insulator in each region. The surface of the insulator is assumed to be an infinite plane to simplify the calculation.

(1)Deduction of force F_1 in region 1

It is considered that the thermal shock is a dominant vibration force because the laser-produced plasma is seldom observed on the surface in this region. The maximum of the stress applied on the surface of the insulator, σ_{max}, is expressed by the following equation under the condition of the free surface according to the paper reported by Gournay[4-4]:

$$\sigma_{max} = \frac{v\beta M}{2\rho C} I_0 \quad , \tag{4-1}$$

where v is the velocity of thermal-wave propagation, β is the coefficient of linear thermal expansion, M is the molecular weight, ρ is the density, C is the specific heat per mole and I_0 is the irradiation intensity on the surface. The irradiation intensity I_0 and the wave velocity v are expressed by the equations, $I_0=E_L/\tau S$ and $v=(\varepsilon/\rho)^{1/2}$, respectively, where E_L is the laser beam energy, τ is the pulse duration of the laser beam, S

is the irradiated area and ε is the modulus of elasticity. Multiplying σ_{max} by S, the force F_1 applied on the surface in the region 1 is expressed by

$$F_1 = \sigma_{max} \cdot S = \frac{\beta M \varepsilon^{1/2} E_L}{2C\rho^{3/2}\tau} \quad . \tag{4-2}$$

(2)Deduction of force F_2 in region 2

It is considered that the reaction of the particles spouting from the surface of the insulator is a dominant vibration force because of the observation of the intensive plasma spouting from the spot area in this region. However it is necessary to consider the transform of the laser beam energy not only to accelerate the spouting particles but also to change the phase of the surface material of the insulator, i.e. melting and vaporizing. According to the paper reported by Shimomura et al.[4-5], most of the irradiated beam energy is transformed into the kinetic energy of charged or neutral particles, while about 10% of the beam energy is reflected on the surface of a metal target. Other following processes can be neglected as compared with the conversion to the kinetic energy; the radiation from a spouting plasma, the ionization of the metal vapor, the thermal conduction in the metal target and so on. However, the reflection on the insulator can be neglected in this experiment because the insulator is made of porcelain which absorbs the far-infrared radiation so much. Therefore, only the kinetic energy of the spouting particles and the energy required to change the phase of material in the spot

area on the insulator are considered, and it is assumed that the whole laser beam energy is absorbed on the surface of the insulator.

The following equation expresses E_t, the energy used to change from a solid phase to a gas phase, using l which is the thermal diffusion length of the insulator:

$$E_t = \frac{(f-d)^2 S_0 l \rho}{M f^2} [C(\Delta T_{m-r} + \Delta T_{b-m}) + C_m] + \frac{m}{M} C_b \quad , \qquad (4-3)$$

$$l = (4MK\tau/\rho C)^{1/2} \quad ,$$

where f is the focal length of the germanium lens, d is the distance between the germanium lens and the surface of the insulator, S_0 is the area of the laser beam before the incidence into the germanium lens, ΔT_{m-r} is the temperature difference between the room temperature and the melting point of the insulator, ΔT_{b-m} is the temperature difference between the melting point and the boiling point of the insulator, C_m and C_b are the latent heat of fusion and evaporization, respectively, K is the heat conductivity and ρ, C, M, τ are described in eqs.(4-1) and (4-2).

The acceleration of the insulator, a, is expressed by[4-6]

$$a = \frac{2}{u \cdot m_0} \cdot \frac{dE_a}{dt} \quad , \qquad (4-4)$$

where u is the expansion velocity of the spouting particles, m_0 is the mass of the insulator, E_a is the energy used to accelerate the spouting particles. Letting E_a be $E_L - E_t$, the force F_2 as the reaction of the spouting particles is expressed by

$$F_2 = \frac{2}{u} \cdot \frac{E_L - E_t}{\tau} \quad . \qquad (4-5)$$

(3)Deduction of force F_3 in region 3

The intensive air breakdown plasma is observed in front of the surface of the insulator besides the plasma spouting from the surface of the insulator in this region. Therefore both the reaction of the spouting particles and the shock wave from the air breakdown plasma are considered as the vibration force of the insulator. Only the latter process is estimated here.

Assuming that the air breakdown plasma is momentarily generated at one special point in air where the whole laser beam energy is absorbed, the following equation expresses R_B which represents the radius of the spherical shock wave at the time t after the irradiation of the laser beam[4-7]:

$$R_B = \xi_0 \left[\frac{E_L t^2}{\rho_0} \right]^{1/5} \quad , \qquad (4-6)$$

where $\xi_0 = [75(\gamma-1)(\gamma+1)/16\pi(3\gamma-1)]^{1/5}$, γ is the ratio of specific heat of the gas(=1.3 in air at atmospheric pressure), and ρ_0 is the density of air. The front pressure of the shock wave, P_3, is

expressed by(4-7)

$$P_3 = \frac{2\rho_0}{\gamma+1}\left(\frac{dR_B}{dt}\right)^2 = \frac{8}{25(\gamma+1)}\,\xi_0^2(\rho_0^3\,E_L^2\,t^{-6})^{1/5} \quad . \quad (4-7)$$

The variable t is eliminated using eqs.(4-6) and (4-7), then the force F_3 on the surface is expressed by the following equation, integrating the normal line component in the pressure applied on the infinitely small ringed area, x in diameter and Δ x in width, as shown in Fig.4-7:

$$F_3 = \frac{8\xi_0 E_L}{25(\gamma+1)}\int_0^{x'}\frac{2\pi r x}{(r+x^2)^2}\,dx \quad , \quad (4-8)$$

where r is the distance between the air breakdown plasma and the surface of the insulator.

The relation between r and d is experimentally expressed by the following equation from the figure of the photographs as shown in Fig.4-2:

$$r \doteqdot \frac{d_{opt}+d-f}{2} \quad . \quad (4-9)$$

Therefore, letting x' be infinite and substituting eq.(4-9) into eq.(4-8), the force F_3 is expressed by

$$F_3 = \frac{16\pi\xi_0 E_L}{25(\gamma+1)(d_{opt}+d-f)} \quad . \quad (4-10)$$

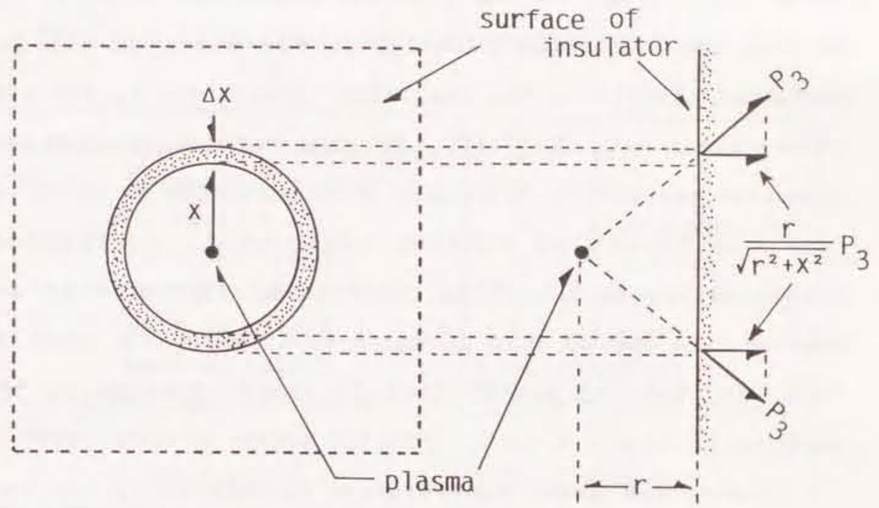

Fig.4-7.Relationship between location of laser-produced plasma and pressure P_3 on the surface of insulator.

(4)Relative comparison of calculated forces with observed values of a_{rms}

Table 4-1 shows the material constants of the insulator used for the calculation. The symbol '*' in Table 4-1 is added to an unknown material constants, and the unknown constants are assumed to be the average of the material constants of Al_2O_3 and SiO_2. Quoting the expansion velocity of the atoms of Al, Si and O, contained chiefly in the insulator, from ref.4-5, the average of these velocities, 3×10^6cm/s, is used for the calculation as the expansion velocity u. The mass m is estimated as about 2μg/shot from the result of another experiment, corresponding to approximately to the value reported by Shimomura et al.(4-5). However, the second term in eq.(4-3) is much less than the first term, so that the energy loss E_t almost depends on the first term.

Figure 4-8 shows the relative variations of the calculated value F_2 and the observed value of a_{rms} at $d=d_{opt}$ with the change of the laser beam energy E_L as the standard that the relative values of a_{rms} and F_2 at E_L=5.9J are 10. The variation of a_{rms} considerably agrees with the variation of F_2, and F_2 is nearly proportional to E_L because E_t is small compared with E_L. The same tendency is obtained in the variations of F_1 and F_3 with E_L. Therefore it is found that the dependence of a_{rms} on E_L can be explained using this model.

Figure 4-9 shows the relative variations of the observed value of a_{rms} and the calculated values of F_1, F_2 and F_3 with the change of d as the standard that the relative values of a_{rms} and

Table.4-1 Material constants for calculation

thermal expansion coefficient	β = 5×10^{-6}(1/℃)
molecular weight*	M = 81
density	ρ = 2700(kg/m³)
specific heat	C = 54.4(J/mol)
modulus of elasticity	ε = 1.0×10^{11}(N/m²)
melting point*	T_m = 2000(K)
boiling point*	T_b = 3250(K)
latent heat of fusion*	C_m = 1.0×10^5(J/mol)
latent heat of evaporization*	C_b = 1.2×10^6(J/mol)
heat conductivity	K = 20(W/m·℃)

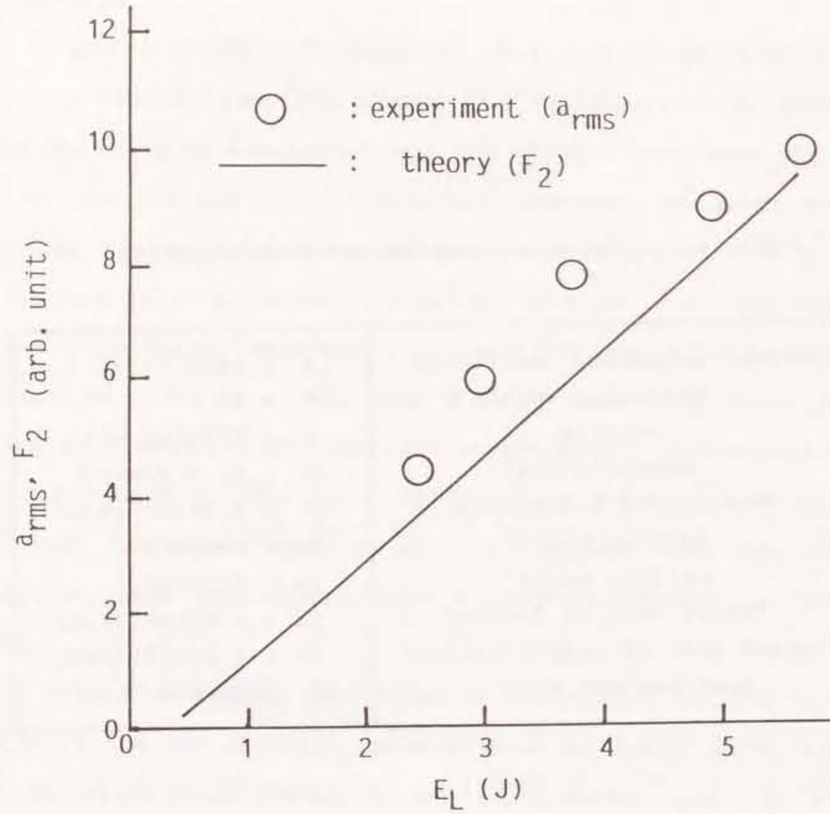

Fig.4-8.Relative variations of acceleration a_{rms} and force F_2 at $d=d_{opt}$ with laser energy E_L.

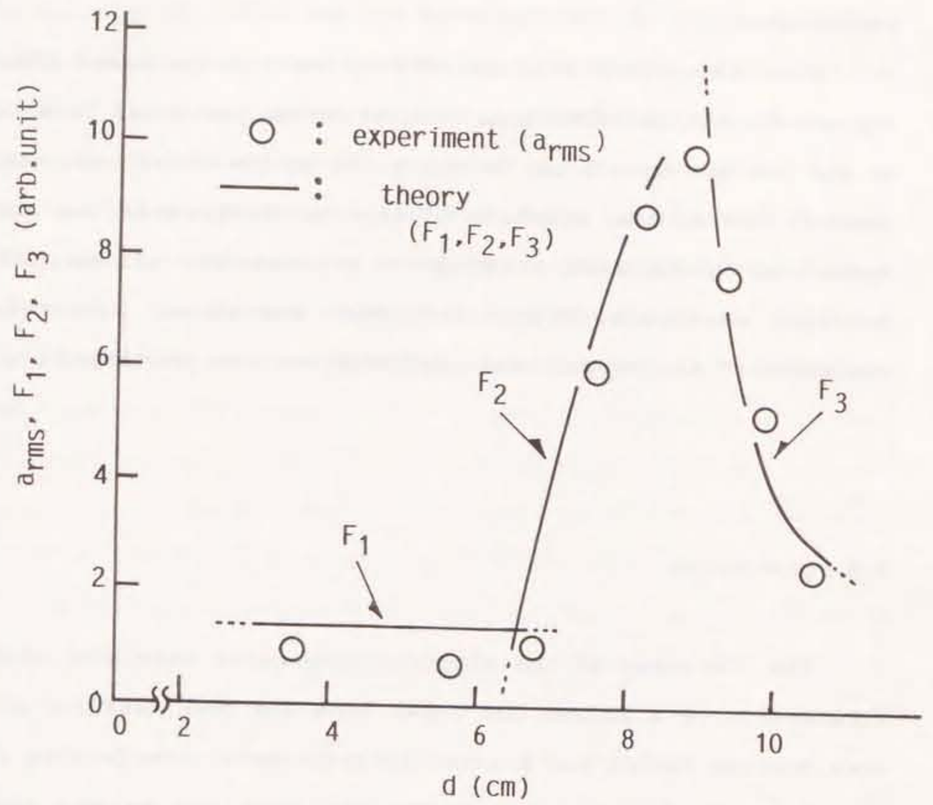

Fig.4-9.Relative variations of acceleration a_{rms} and forces F_1, F_2 and F_3 with d.

F_2 at $d=d_{opt}$ are 10. The variation of a_{rms} with d in the three regions are found to be similar to those of F_1, F_2 and F_3, respectively.

From the above calculated results, it is found that the dependence of the vibrational amplitude on the laser beam energy E_L and the distance d can be explained by the model combining the thermal shock, the reaction of the spouting particles and the spherical shock wave from the air breakdown plasma. If the material constants of the insulator are known, the relative variation of the vibrational amplitude will be predicted.

4-5. Conclusion

The vibration of the electric suspension insulator with the irradiation of a pulsed CO_2 laser beam has been measured with an acceleration sensor and a laser interferometer. Performing FFT to the vibrational signals of the acceleration sensor and the interferometer, it was clear that the vibration includes various frequency components immediately after the irradiation of the laser beam and that the insulator is vibrated in a natural mode with the passing of time.

The variation of the vibrational amplitude with the irradiation intensity of the laser beam consisted of three regions. The vibrational amplitude was independent of the irradiation intensity in the first region. As the irradiation

intensity was increased more, a plasma spouted from the surface of the insulator and the vibrational amplitude was increased in the second region. With the far more increase of the irradiation intensity, an air breakdown plasma was generated in front of the surface of the insulator, and the vibrational amplitude was decreased in the third region.

It was also shown that the variation of the vibrational amplitude can be explained by the model combining the vibrational principles of the thermal shock, the reaction of the spouting particles and the spherical shock wave from the air breakdown plasma.

References

4-1)A.C.Tam : "Applications of photoacoustic sensing techniques", Rev. Mod. Phys. 58(1986) 381.

4-2)D.A.Hutchins:"Mechanisms of pulsed photoacoustic generation", Can. J. Phys. 64(1986) 1247.

4-3)V.S.Teslenko : Sov. J. Quantum. Electron. 7(1977) 981.

4-4)L.S.Gournay : "Conversion of electromagnetic to acoustic energy by surface heating", J. Acoust. Soc. Am. 40(1966) 1322.

4-5)T.Shimomura, M.Yano, T.Noguchi and K.Horii : "Laser-produced metal plasma", Bulletin of the Electro-technical Laboratory, 36(1972) 264, in Japanese.

4-6)C.Yamanaka : REZA-KOGAKU p163(Denki denshi kogaku taikei, No.20, 1981, CORONA-sha), in Japanese.

4-7)Y.B.Zel'dovich and Y.P.Raizer : Physics of Shock Waves and High-Temperature Hydrodynamic Phenomena, p99 (Academic Press, New York and London, 1966)

CHAPTER 5 STUDY ON NON-DESTRUCTIVE AND REMOTE INSPECTION OF ELECTRIC SUSPENSION INSULATOR BY MEANS OF LASER BEAM

5-1. Introduction

In generally, when the electric insulator is slightly struck with a rigid rod, the crack in the insulator causes the pitch and the reverberation of the sound to change. As described in the previous chapter, it was confirmed that the natural vibration, which corresponds to the sound, can be remotely detected with a laser interferometer. Therefore, it is probable to distinguish a cracked insulator from a normal one by remotely detecting the natural vibration using laser beam.

For the non-destructive inspection using laser beam, it has been reported that the surface of the cracked solid sample is periodically heated by a weak laser beam so as not to damage the surface and that the weak acoustic signal generated by the effect of thermal shock informs on the location and the size of the crack in the solid sample(5-1),(5-2). It has been also reported that the crack or slot on the solid sample can be detected by measuring the transmissive and reflective pressure waves generated by the laser-produced plasma(5-3),(5-4). However, for the former method the use of a lock-in amplifier to improve a S/N

ratio and the scanning of the irradiating point on the surface of the sample are inconvenient because it takes long time to inspect the sample. For the latter method there are two problems in observing those pressure waves. One is to require the instrument with a very high upper-limit frequency because the pressure wave involves many high frequency components over several mega-hertz. The other is the difficulty of the recognization of the pressure wave reflected on the cracks in the sample with a complicated shape.

The method to detect the natural vibration has the following advantages:

(1)A cracked insulator can be detected with a single laser operation using an interferometer because the efficient energy conversion from the laser beam to the vibration of the insulator makes the acoustic signal generated clearly. Therefore it is expected to inspect the insulator without a lock-in amplifier and to save the inspecting time.

(2)There are no particular restrictions for the shape and the size of the insulator because the cracked insulator can be distinguished by detecting the change of the natural vibration for the frequency components or the duration of the natural vibration.

A lineman has to go up over several-ten meters above the ground and directly touches the insulators with a specific instrument as usual in order to test them on the practual high voltage transmission lines. However, it is necessary to check the insulators remotely in order both to improve the reliability and

the safety of the test and to save the working time. It is considered that the inspecting system described in this chapter is the effective method for such a demand because a laser beam has the characteristics of remote sensing with a good directivity and a long interferable length.

A procedure to inspect an electric suspension insulator by detecting the natural vibration is described, and the possibility of the non-destructive and remote inspection of a insulator is examined using the apparatus described in chapter 4. The irradiation intensity of a pulsed CO_2 laser beam required to inspect the insulator is experimentally examined, and the conditions of the incident laser beam and the germanium lens to inspect the insulator from a long distance are also discussed.

5-2. Experimental Apparatus and Procedure

The vibration of an electric suspension insulator made of ceramics is measured using the apparatus shown in Fig.4-1, and the difference of the natural vibration between a normal insulator and a cracked one is observed for three kinds of the insulators whose diameters are about 26cm, 28cm and 30cm, performing FFT to the vibrational signals. The estimation of the vibrational difference described in 5-3-2 is performed for several insulators 26cm in diameter.

5-3. Experimental Results

5-3-1. Influence of Crack on Vibrational Spectrum of Electric Suspension Insulator

Here is observed the vibrational difference between normal and cracked insulators for three kinds of the insulators with the diameters of about 26cm, 28cm and 30cm. The artificial cracking of the insulator is performed by striking with a chisel, and the cracked insulator has one crack from the most inner rib to the periphery through the thickness of the whole shed. The typical crack found in an actual transmission line is obtained in such a way.

Figure 5-1 shows the temporal variation of the frequency spectrum of the natural vibration detected by the He-Ne laser interferometer for the cracked insulator 26cm in diameter which is the same type as the insulator used in the chapter 4. The vibrational signal during 1-31msec includes many frequency components similarly to the spectrum for the normal insulator shown in Fig.4-4. However, the frequency components of the natural vibration are not observed because the natural vibration decays so fast to a degree of background noise within the duration of 70msec after the irradiation of the CO_2 laser beam. A similar tendency is observed for the insulator 28cm in diameter as shown in Fig.5-2. Figure 5-3 shows the temporal variations of

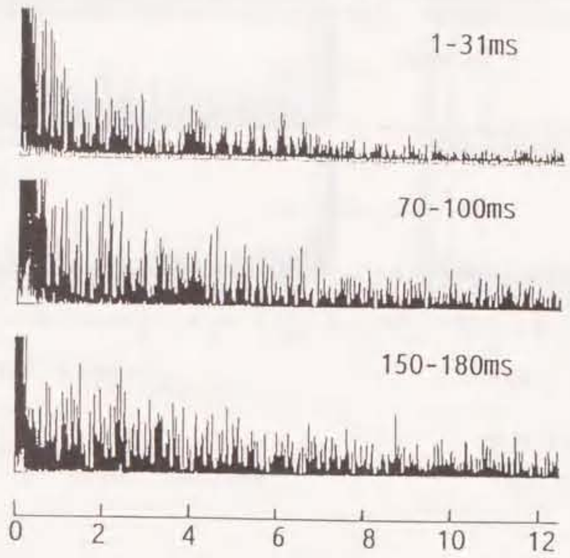

Fig.5-1.Temporal relative variation of vibrational frequency spectrum for a cracked insulator 26cm in diameter.

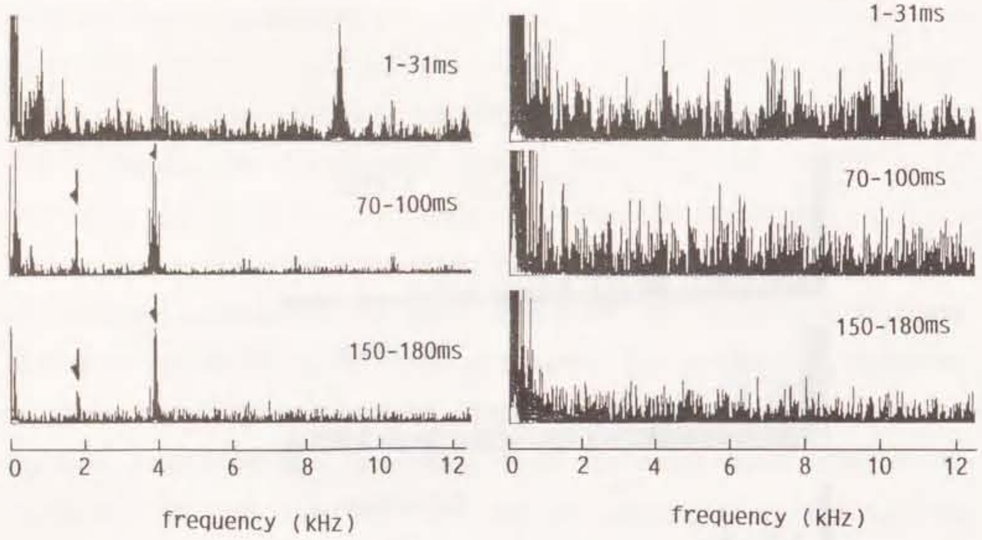

(a) normal insulator (b) cracked insulator

Fig.5-2.Temporal relative variations of vibrational frequency spectrums (a)for normal insulator and (b)for cracked insulator 28cm in diameter.

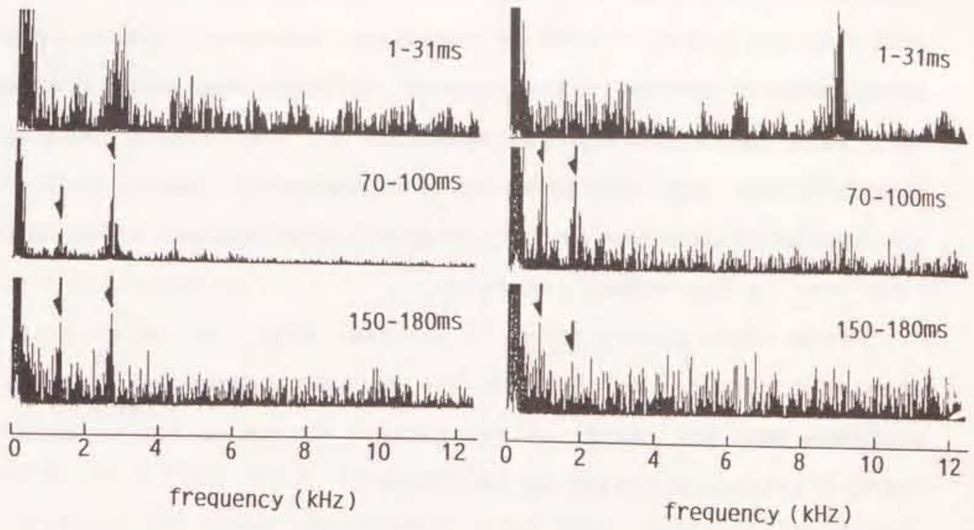

(a) normal insulator (b) cracked insulator

Fig.5-3.Temporal relative variations of vibrational frequency spectrums (a)for normal insulator and (b)for cracked insulator 30cm in diameter.

the frequency spectrums for the normal and cracked insualtors with the diameter of 30cm. In the spectrum of the normal insulator, the frequency components of the natural vibration are observed at about 1.3kHz and 2.6kHz. However, the frequency components of the natural vibration shifts to the lower frequency of 0.9kHz and 1.8kHz in the spectrum for the cracked insulator. Furthermore, the amplitude of the natural vibration in the cracked insulator decays to a degree of background noise faster than that in the normal insulator.

From these observation, it is clear that the cracking of the insulator results in changing the natural vibration, and it is probable that the change of the natural vibration can be detected using a frequency analyzing technique.

5-3-2. Inspection of Electric Suspension Insulator

The inspection of the electric suspension insulator 26cm in diameter is examined here. To distinguish a cracked insulator from a normal one, the detection of the vibrational changes is tried here by using frequency analyzing technique and by hearing the sound of the vibrational signal.

(1)Method to use frequency spectrum of natural vibration

It is tried to detect the cracked insulator by estimating the differences of vibrational frequency spectrum and the damping factor for the natural vibration at 4.4kHz shown in Fig.4-4.

First, the method to estimate the difference of vibrational

frequency spectrum is described. The difference is estimated in the spectrum during 150-180msec after the irradiation of the CO_2 laser beam when the insulator is sufficiently vibrated in the natural mode. The standard spectrum $S_0(f)$ is defined as the average of the spectrums of three normal insulators normalized with the peak value at 4.4kHz. As shown in Fig.5-4, the difference between the standard spectrum $S_0(f)$ and the spectrum $S(f)$ of the inspected insulator is estimated by the integrated value V expressed by

$$V = \int_{f_0}^{f_1} \{S_0(f)-S(f)\}^2 \, df \quad , \qquad (5-1)$$

where f_0 is 3.9kHz and f_1 is 4.9kHz.

Figure 5-5 shows the values V for the insulators with and without a crack. It is evident that the crack in the insulator causes the value of V to be increased, and the threshold for the distinction of a cracked insulator is estimated as the relative value of 12.

Next, the method to estimate the damping factor of the natural vibration is described. The damping factor k is defined by the following equation which expresses the intensity I of the natural vibration at the time t:

$$I = I_0 \cdot \exp(-kt) \quad , \qquad (5-2)$$

where I_0 is a constant value.

Figure 5-6 shows the values k for the insulators with and

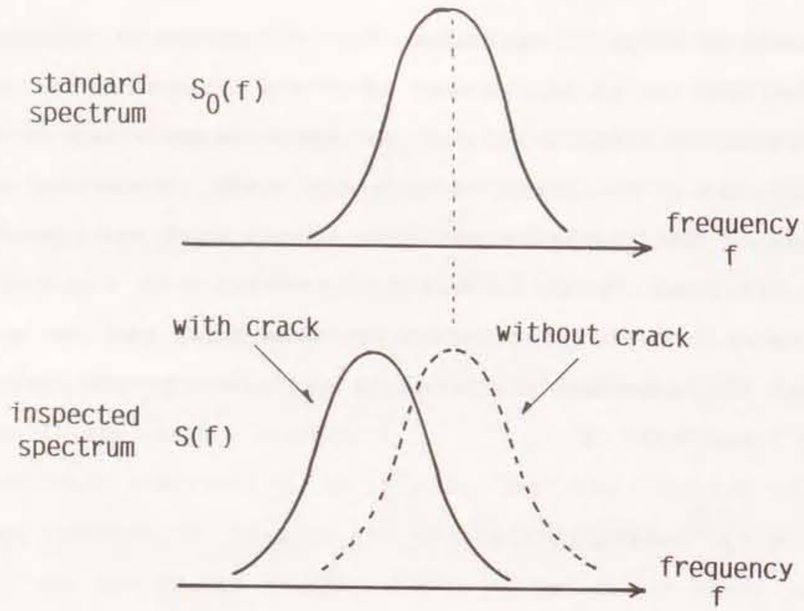

Fig.5-4.Estimation of spectrum difference.

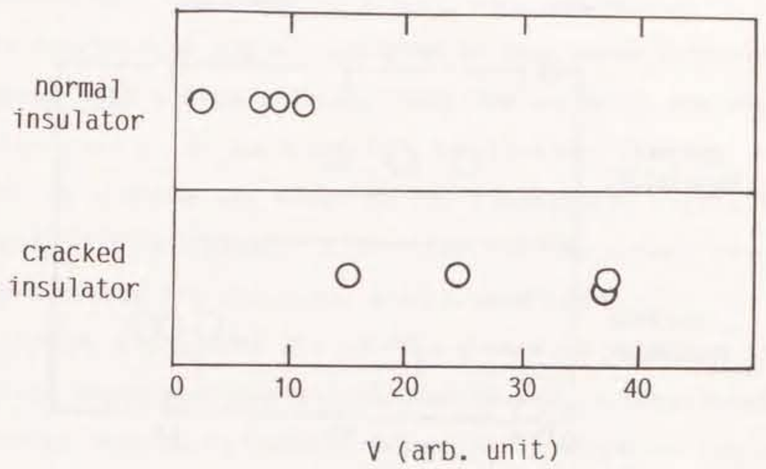

Fig.5-5.Change of difference to the standard spectrum due to crack.

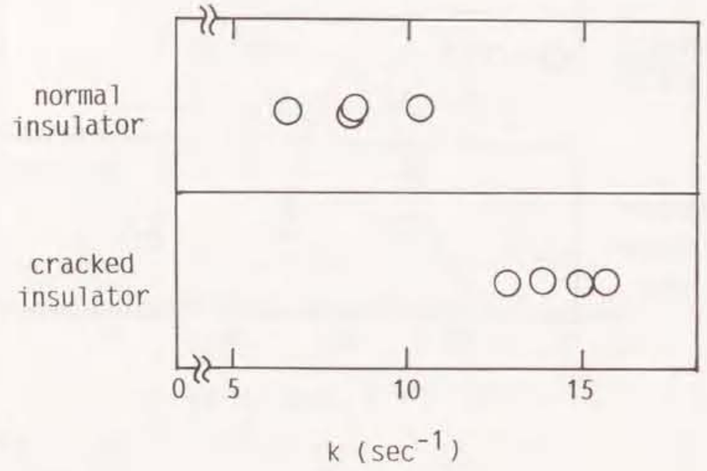

Fig.5-6.Change of damping factor k of vibration due to crack.

without a crack. It is apparent that the crack in the insulator causes the value of k to be increased, and the threshold of k for the distinction of a cracked insulator is estimated as about 11sec^{-1}.

(2)Method to hear the sound of vibrational signal

The vibrational signal detected by the laser interferometer is recorded with a tape recorder, and the sound of the signal is carefully heard. It is possible to distinguish the cracked insulator by hearing the sound of the vibrational signal because the sound of the signal is similar to the sound caused by slightly striking the insulator with a metal rod.

Although the obscurity of the judgment remains in this method, the hearing of the vibrational signal is considered to be an economic method because a human can recognize the slight difference of the sound for frequency and damping time without the expensive instruments like a FFT analyzer.

(3)Application of these methods to practical uses

Although it is necessary to examine the reliability, especially the accuracy of the judgment, by testing many various insulators, it is suggested that the cracked insulator can be distinguished by using the vibrational frequency spectrum and by hearing the sound of the vibrational signal detected with a laser interferometer. The combination of these methods is expected to make the inspection more reliable. Further these methods are properly used according to the inspecting conditions. It is considered that the method to hear the sound of vibrational signal is preferable for an inspection in an actual field spot

because of the needlessness of expensive instruments and that the method to use the vibrational spectrum is preferable for an automatic inspection in a production line or a field.

Although the inspection has been performed only for the insulator 26cm in diameter, it is considered that the insulators with different diameters of 28cm and 30cm can be also inspected because the change of the natural vibration is clearly observed.

5-3-3. Irradiation Intensity of Laser Beam to Inspect Electric Suspension Insulator

It is examined if the frequency spectrum of the natural vibration as shown in Fig.4-4 is observed with the change of the irradiation intensity of laser beam for the insulator 26cm in diameter. From the results shown in Fig.5-7, it is obvious that the frequency spectrum of the natural vibration is observed for the irradiation intensity over $2 \times 10^7 W/cm^2$. This value considerably agrees with the irradiation intensity where a plasma spouts from the surface of the insulator as shown in Fig.4-6. A similar tendency is also observed for the insulators 28cm and 30cm in diameter.

5-4. Discussion

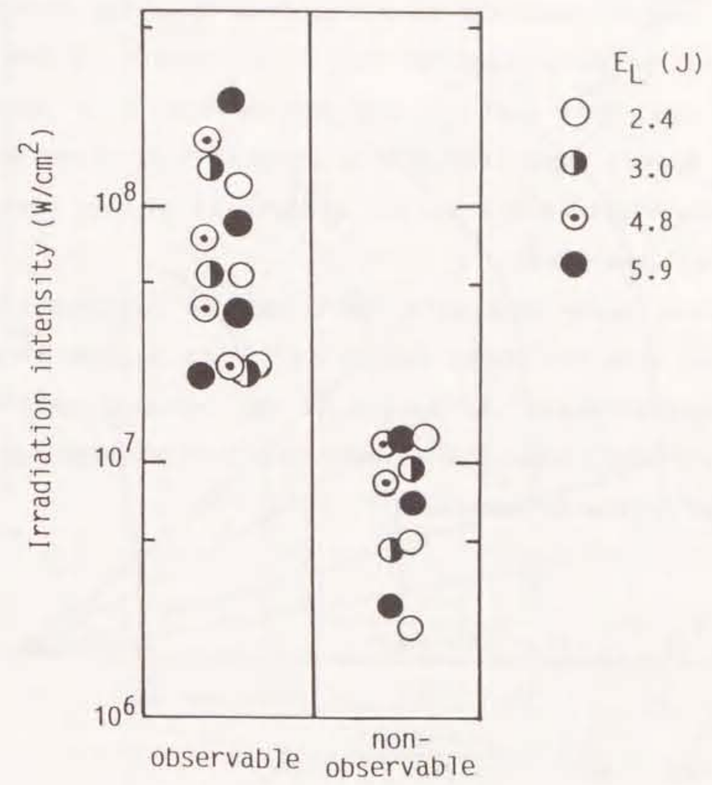

Fig.5-7. Observation of natural vibration with change of irradiation intensity of laser beam.

It is suggested from the results in 5-3-2 that the cracked insulator can be remotely distinguished from the distance of about 10cm, corresponding to the focal length of the convex germanium lens. Here are examined the conditions to inspect the insulator from a long distance of several-tens meter using the method described in 5-3-2 at the standpoint of the irradiation intensity of laser beam.

When the laser beam with TEM_{00} mode is focussed through a convex lens with the focal length of f, the beam radius w_{02} at the beam waist, where the radius of the focused laser beam is minimum, and the distance z between the lens and the beam waist satisfy the following equations[5-5]:

$$z = f - \frac{f^3}{f^2 + (\pi w_{01}/\lambda)^2} \quad , \qquad (5\text{-}3)$$

$$\frac{1}{w_{02}} = \frac{1}{w_{01}} + \frac{(\pi w_{01}/\lambda)^2}{f^2} \quad , \qquad (5\text{-}4)$$

where w_{01} is the beam radius before the incidence into the lens, and λ is the wavelength of CO_2 laser beam. Figure 5-8 shows the contour lines of f and w_{01} as functions of W_{02} and z, resolving eqs.(5-3) and (5-4).

Figure 5-9 shows the relationship between the laser beam energy E_L and the beam radius W_{02} at the beam waist, assuming that the pulse width of the laser beam is 400nsec.

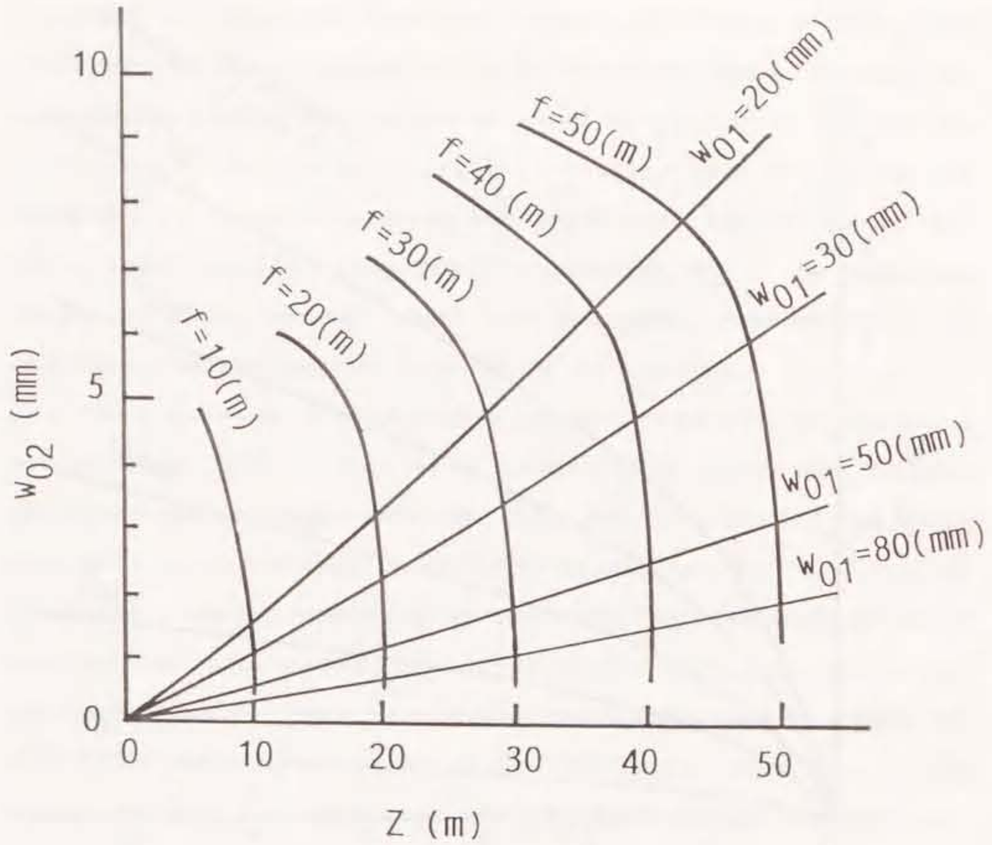

Fig.5-8. Contour lines of focal length f and incident beam radius w_{01} as function of distance z and beam radius w_{02} at beam waist.

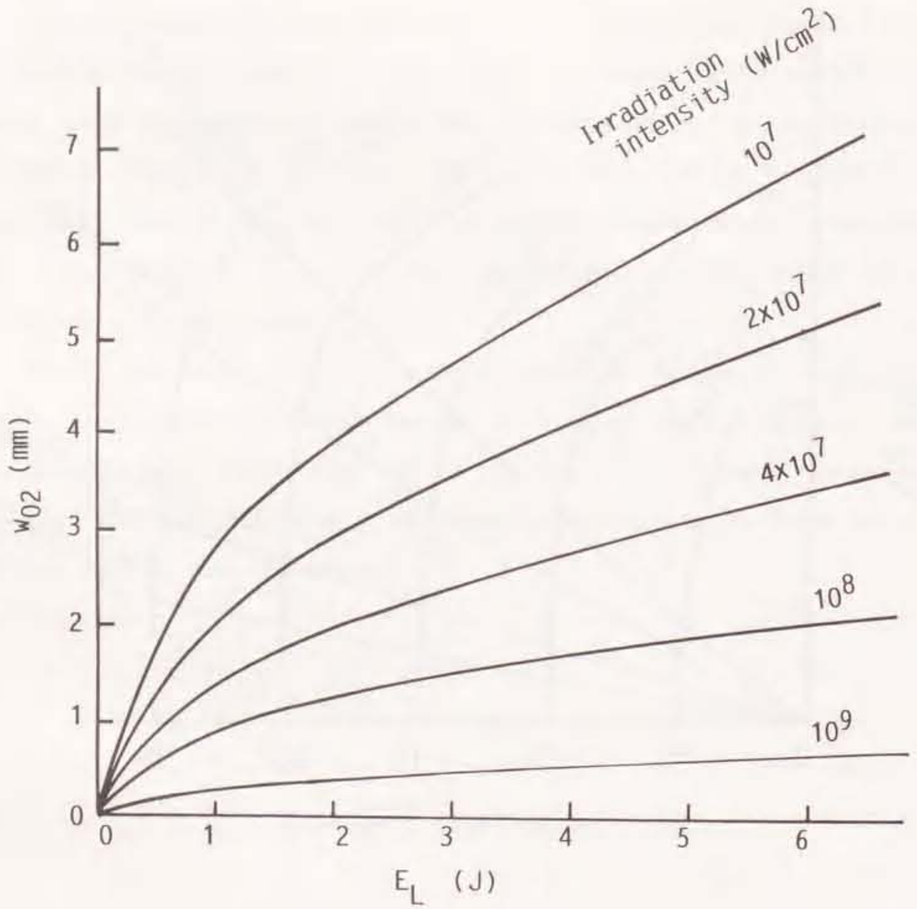

Fig.5-9. Relationship between laser beam energy E_L and beam radius w_{02} at beam waist as a parameter of irradiation intensity of laser beam.

The procedure to determine w_{01} and f in the case that the insulator is inspected from the distance of z using a pulsed CO_2 laser beam with the energy of E_L is described below. To make the explanation simple, the values of z and E_L are let be 40m and 2J, respectively. As the irradiation intensity over $2\times10^7 W/cm^2$ is necessary at least to inspect the insulator, the radius w_{02} has to be less than 3mm from Fig.5-9. Letting w_{02} to be 3mm, the values of f and w_{02} are about 40m and 45mm, respectively, in accordance to the contour lines shown in Fig.5-8.

Such a laser device and a convex lens can be produced technically, and it has been reported to generate the air breakdown plasma longer than 20m along the direction of the laser beam with a convex lens whose focal length is 30m[5-6]. Further the interferometer measuring system with the resolving power of several-ten nano-meter from a 100m distance has been also reported[5-7]-[5-12], and this system has a good ability enough to detect the natural vibration of the insulator. Therefore, it is suggested that the insulator can be inspected from a several-tens-meter distance.

In a field inspection, it is necessary to avoid the influence of wind on the measuring system. As the swing of the insulator due to wind induces a continuous change in the output signal of the interferometer, the choice of the natural vibration not to overlap on the continuous change in frequency region leads to the avoidance of the influence of the swing. Further a pulsive disturbance can be avoided by operating the pulsed laser in a proper timing.

5-5. Conclusion

The non-destructive and remote inspection of an electric suspension insulator by detecting the natural vibration of the insulator has been examined.

It was confirmed that the change of the natural vibration due to a crack can be detected with a laser interferometer, and it was also suggested that a cracked insulator can be distinguished from a normal one by using the frequency spectrum of the detected vibrational signal and by hearing the sound of the vibrational signal.

In this experiment, the irradiation intensity of laser beam of about $2 \times 10^7 W/cm^2$ was necessary at least to inspect the insulator, and it was predicted that the insulator can be remotely inspected from a several-ten meter distance using the present laser technology.

References

5-1)P.Hess and J.Pelzl : Photo Acoustic and Photo Thermal Phenomena p400 (Springer Series in Optical Sciences vol.58, Springer-Verlag, Berlin, Heidelberg, New York, London, Paris, Tokyo).

5-2)I.Tomeno and H.Ohzu : "Photosignal from subsurface defects in ceramics", Jpn. J. Appl. Phys. 24(1985) 1445.

5-3)J.A.Cooper, R.A.Crosbie, R.J.Dewhurst, A.D.W.Mckie and S.B.Palmer : "Surface acoustic wave interactions with cracks and slots: A noncontacting study using lasers", IEEE Trans. on Ultra., Ferro., and Freq. Cont. UFFC-33(1986) 462.

5-4)F.Nadeau and D.A.Hutchins : "Interaction of surface waves with slots using noncontact laser-generation and interferometric detection", Proc. 1984 IEEE Ultrason. Symp. p921-925(1984).

5-5)T.Takaoka and T.Takahashi : REZA-GIJUTSU-NYUMON p87(1986, AKIBA-shuppan), in Japanese.

5-6)W.F.Hagen : "Diffraction-limitted high-radiance Nd-glass laser system", J. Appl. Phys. 40(1969) 511.

5-7)K.M.Baird : "The role of interferometry in long distance measurement", Metrologia, 4(1968) 135.

5-8)G.L.Bouldet and A.G.Orszag : "Absolute distance measurements by CO_2 laser multiwavelength interferometry", Appl. Opt. 18(1979) 225.

5-9)C.W.Gillard, N.E.Buholz and D.W.Ridder : "Absolute distance interferometry", Opt. Eng. 20(1981) 129.

5-10)H.Matsumoto and S.Seino : "Infrared two-wavelength

interferometry for measuring long length", Ann. CIRP, 31(1982) 401.

5-11)H.Matsumoto : "Synthetic millimeter-wave signal generation for length measurement", Appl. Opt. 23(1984) 973.

5-12)H.Matsumoto : JIDOKA-GIJUTSU p26, vol.17, No.10 (1985), in Japanese.

CHAPTER 6 CONCLUSION

6-1. Principal Results

Discharge-pumped pulsed CO_2 lasers are powerful far-infrared coherent sources and have the various potential applications in science and industry. From a practical point of view, it is desirable to increase the extractable energy in a corona-preionized compact TEA-CO_2 laser, because an efficient laser operation is possible with an easy maintenance. In this thesis, the superposition of a high frequency corona discharge (called as HFCD) on a main discharge was focussed on in order to increase the laser output. Additionally, the non-destructive and remote inspection of electric suspension insulators was tried as an application of pulsed CO_2 laser.

First of all, the superposition of the HFCD on the main discharge was examined in order to increase the preionization intensity in a corona-preionized TEA-CO_2 laser. The laser output was increased by this method for the input energy density up to about 220J/l, where the laser output was saturated due to the glow-to-arc transition in an ordinary corona-preionized TEA-CO_2 laser, and the maximum laser output density of about 14J/l was obtained. When the HFCD current was characterized by the triggering time ($t_{G3\text{-}BD}$), the peak value (I_p), the half period (T) and the duration (t_e), the optimization of $t_{G3\text{-}BD}$, the

increase of I_p and the decrease of T were necessary to increase the laser output, while t_e was required to be more than about 1μs. It was considered that homogeneous electron layers should be produced by the HFCD current while the discharge current flowed from the peaking capacitor C_2. On the other hand, it was also considered that the increase of the peak value and the decrease of the half period led to the suppression of the glow-to-arc transtion because the electron density of the layer was increased with the peak value of the HFCD current and the production rate of the layer was increased with the decrease of the half period. Furthermore, when the triggering time of the HFCD current was optimized to maximize the laser output, the delay time of the main discharge after flowing the HFCD current corresponded to the time required for the layer to propagate across the main electrodes. That suggested that the glow-to-arc transition was effectively suppressed after the whole discharge volume was sufficiently ionized by the electron layer. It was also suggested from the calculation using the equivalent circuit that the reductions of resistance and inductance in the HFCD circuit might result in increasing the laser output.

A new HFCD circuit without another power source (called as SC-HFCD circuit) was devised to miniaturize the laser device and to save the energy for the HFCD operation. In the SC-HFCD circuit, the HFCD operation was possible by recycling the residual energy not to be injected into the discharge volume. Both the main discharge and the laser output were improved due to the HFCD effect using the SC-HFCD circuit, and glow discharges

were produced for the input energy density up to 230J/l after the main discharge circuit and the laser gas mixture were optimized. Moreover, the maximum laser output of 17.5J/l was obtained with the SC-HFCD circuit at the input energy density of 250J/l. The output voltage of the SC-HFCD circuit was determined by the amounts of electrical charge flowing into and out of the SC-HFCD circuit, and the output voltage was maintained at a constant value when those two amounts of electrical charge were equal. The output voltage was decreased when the glow-to-arc transition occured, because the residual energy was not collected due to the rapid reduction of the voltage across the main electrodes. These charcteristics of the output voltage were predicted by the calculation using the equivalent circuit, and the observed and calculated results considerably agreed. The increase of the capacitance to collect the residual energy led to the insurance of the HFCD operation because the output voltage of the SC-HFCD circuit was maintained at a relatively high value even if the glow-to-arc transition should occur.

The vibration of the electric suspension insulator with the irradiation of a pulsed CO_2 laser beam was measured using an acceleration sensor and a laser interferometer. It was shown that the vibration included many various frequency components immidiately after the irradiation of the laser beam and that the insulator continued to be vibrated in the natural mode after passing time. The irradiation intensity had much effect on both the vibrational amplitude and the phenomena on the surface of the insulator. The change of the vibrational amplitude corresponded

to that of the phenomena. These changes with the irradiation intensity were composed of following three regions. In the region 1, the laser-produced plasma was seldom observed on the surface of the insulator and the vibrational amplitude was independent of the irradiation intensity. In the region 2, the intensive plasma spouting from the whole spot area was observed and the vibrational amplitude was increased with the irradiation intensity. In the region 3, the air-breakdown plasma was observed in front of the surface of the insulator other than the plasma spouting from the spot area, and the vibrational amplitude was decreased with the irradiation intensity. Assuming that the dominant vibration force in each region was the thermal shock, the reaction of the spouting particles and the spherical shock wave from the air-breakdown plasma, respectively, the calculated variation of the force applied on the surface of the insulator relatively agreed with the observed variation of the vibrational amplitude.

The non-destructive and remote inspection of an electric suspension insulator by measuring the natural vibration was described. Furthermore, the conditions to apply this technique to the actual field inspection on the transmission line tower was investigated. It was suggested from the results of the frequency analysis that the frequency components and the decay constant of the natural vibration changed due to a crack independently of the size of the insulator. Therefore the influences of cracks on the frequency components and the decay constant of the natural vibration were estimated by both the quantitative method using

the frequency analysis and the sensoring method using the human's auditory sense. It was shown that the cracked insulator was distinguished by these two methods under the condition of the irradiation intensity of the pulsed CO_2 laser over $2\times10^7 W/cm^2$, and that the condition of the irradiation intensity was attained with a comparative ease using the present laser technology evenwhen the pulsed CO_2 laser beam was irradiated on the surface of the insulator from the distance of several-tens meter. Therefore it was considered that the inspection described here will be applied to the actual field. Moreover, it was considered that the influence of wind on the inspection system can be avoided by operating the pulsed laser in a proper timing and by choosing the proper natural-mode spectrum.

6-2. Practical Significance of the Present Work

The HFCD method made the corona preionization intensified and led to the increase in the input energy density without the glow-to-arc transition to over 200J/l. This method can be easily applied to the corona-preionized TEA-CO_2 laser used in the practual field because the HFCD circuit is only added to the excitation circuit without any changes. Further the HFCD method can be also applied to other discharge-pumped molecular gas lasers with corona preionization, i.e. TEA-N_2 laser, excimer laser etc..

Although only the preionization intensity prior to the main discharge has been focussed on to suppress the glow-to-arc transition, it was suggested that the successive production of homogeneous electron layers even during the main discharge is important. The new guiding principle to inject more energies into the discharge volume has been given for all types of CO_2 lasers with the preionization.

A TEA-CO_2 laser was applied to a non-destructive and remote inspection as a tool to vibrate an electric suspension insulator, and it was suggested that a cracked insulator can be remotely distinguished from a normal one by detecting the vibration of the insulator with a laser interferometer. Although the inspection only for electric insulators was carried out, this technique will be applied to various articles because each article has its inherent natural vibration which depends on a crack as well as shape and material.

Although the remote inspection was performed from a only 10cm distance which corresponded to a focal length of a focussing germanium lens, it was suggested that the long-distant remote inspection using a convex lens with a long focal length is possible. At the present time when many large-scaled structures have been in the world, it is desirable to carry out the remote inspection of such a structure. This technique is one method to satisfy such a demand.

ACKNOWLEDGEMENTS

The author would like to express his great appreciation to Professor Toshio Goto, Faculty of Engineering, Nagoya University, for his encouragement and instructive suggessions in completing this dissertation.

The author is deeply grateful to Professor Kenji Horii, Faculty of Engineering, Nagoya University, for his constant and inspiring guidance throughout the course of this work.

The author is greatly indebted to Professor Hideo Sugai, Faculty of Engineering, Nagoya University, for his encouragement and helpful discussions in preparing this dissertation.

The author is deeply grateful to Associate Professor Chobei Yamabe, Faculty of Engineering, Nagoya University, for his encouragement and valuable discussions throughout the course of this work.

The author wishes to express his gratitude to teaching staffs, Assistant Professor Noriyuki Shimizu, Faculty of Engineering, Nagoya University, and Dr.Naotake Kitamura who is now Associate Professor in Department of Electronic Engineering, Aichi Technology College, for their valuable discussions and useful advices.

The author is grateful to the members of Professor Horii's laboratory for their helps and encouragements, especially to the author's co-workers, Mr.Hideyuki Ishimaru, Mr.Issei Kobayashi, Mr.Yasuharu Niwa, Mr.Keiichi Narita, Mr.Takeshi Yasuda and

Mr.Takamitsu Suzuki for their devoted helps and eager discussions.

The author wishes to express his gratitude to the members of NGK INSULATOR, LTD. for their cooperation and the supply of the samples.

Finally, but not least the author thanks to his parents, his brother and his friends for their encouragements.

List of Papers Concerned with this Dissertation

Title	Journal & Date	Coauthor
Improvement of a Corona-Preionized TEA-CO_2 Laser by means of High-Frequency Corona Discharge	Jpn. J. Appl. Phys., Vol.29, No.1, pp.95-100, January 1990	C. Yamabe K. Horii
Study on Remote Inspection of Electric Insulator with Crack by Laser Beam (in Japanese)	Trans. IEE of Japan, Vol.110-D, No.5, pp.561-569, May, 1990	C. Yamabe K. Horii
Development of Corona-Preionized TEA-CO_2 Laser with HFCD circuit Recycling Residual Energy	Rev. Laser Eng., submitted	C. Yamabe K. Horii
Study on Non-destructive and Remote Inspection of a Cracked Electric Insulator by means of a Laser Beam	CLEO(Conference on Lasers and Electro-Optics), May, 22, 1990 California, USA	C. Yamabe K. Horii